Dependence of Substrate-Water Binding on Protein and Inorganic Cofactors of Photosystem II

Garth S. Hendry

September, 2002

A thesis submitted for the degree of Doctor of Philosophy of

The Australian National University

Photobioenergetics, Research School of Biological Sciences,

The Australian National University, Canberra

This thesis represents research undertaken in the Photobioenergetics Group, Research School of Biological Sciences, The Australian National University, Canberra. This work was completed between March 1999 and September 2002 while I was the recipient of an Australian National University PhD scholarship.

Except where otherwise acknowledged, the work presented in this thesis is my own and was performed under the supervision of Dr Tom Wydrzynski.

Garth S. Hendry, September 2002

αριστου μευ υδωρ

'The noblest of elements is water'

Pindar

Acknowledgments

When the All Blacks take to the paddock and thump the Wallabies in the semi-final of the RWC 2003 at Stadium Australia late next year, the boys will know that the ensuing success of world cup victory is all about commitment, team work and knowing that everyone, on and off the field, gave it 110%.

The same mentality applies to many life situations. To mind, I acknowledge that my achievements are only made possible by family, friends and colleagues, who over the years, have invested their endless time, energy and resources into me and without hesitation. It is for this reason I wish to thank the following people:

Dr Tom Wydrzynski for adopting a no-fuss, open door attitude to talk up the finer points of water oxidation and for providing me with this great opportunity.

Drs Warwick Hillier and Karin Åhrling for their technical advice, moral support, and for knowing what it means to run 12+ hours of continuous measurements.

Dr Fred Chow and Professors Jan Anderson and Barry Osmond for providing a stimulating intellectual environment from which I have attained invaluable experience.

To fellow students, friends and colleagues: Abby, Emily, Kate, Mack, Damo, Nick, Jade, Vaughan, Brett, Luke, Sam, Patty, Joel, Reza, Spencer, Rob, Bart and Ossie-thanks for your continued friendship and support.

To Mum, Dad, Jenny and Gran- it is your love, vision and commitment that has driven me in my endeavor to attain the very best education- thank-you.

And to Anna, you have an amazing attitude towards life and I couldn't imagine a better person to share this journey of life with – thank-you for being my best friend, I love you.

Abstract

The photosynthetic water oxidation reaction is catalyzed by an inorganic $Mn_4O_xCaCl_yHCO_3^-{}_z$ cluster at the heart of the oxygen evolving complex (OEC) in photosystem II. In the absence of an atomic resolution crystal structure, the precise molecular organization of the OEC remains unresolved. Accordingly, the role of the protein and inorganic cofactors of PSII (Ca^{2+}, HCO_3^- and Cl^-) in the mechanism of O_2-evolution await clarification. In this study, rapid ^{18}O-isotope exchange measurements were applied to monitor the substrate-water binding kinetics as a function of the intermediate S-states of the catalytic site (i.e. S_3, S_2 and S_1) in Triton X-100 solubilized membrane preparations that are enriched in photosystem II activity and are routinely used to evaluate cofactor requirements. Consistent with the previous determinations of the ^{18}O exchange behavior in thylakoids, the initial ^{18}O exchange measurements of native PSII membranes at $m/e = 34$ (which is sensitive to the $^{16}O^{18}O$ product) show that the 'fast' and 'slowly' exchanging substrate-waters are bound to the catalytic site in the S_3 state, immediately prior to O_2 release. Although the slowly exchanging water is bound throughout the entire S-state cycle, the kinetics of the fast exchanging water remains too fast in the S_2, S_1 [and S_0] states to be resolved using the current instrumentation, and left open the possibility that the second substrate-water only binds to the active site after the formation of the S_3 state. Presented is the first direct evidence to show that fast exchanging water is already bound to the OEC in the S_2 state. Rapid ^{18}O-isotope exchange measurements for Ex-depleted PSII (depleted of the 17- and 23-kDa extrinsic proteins) in the S_2 state reveals a resolvable fast kinetic component of $^{34}k_2 = 120 \pm 14$ s^{-1}. The slowing down of the fast phase kinetics is discussed in terms of increased water permeation and the effect on the local dielectric following removal of the extrinsic subunits. In addition, the first direct evidence to show the involvement of calcium in substrate-water binding is also presented. Strontium replacement of the OEC Ca^{2+}-site reveals a factor of ~3-4 increase in the ^{18}O exchange of the slowly exchanging water across the S_3, S_2 and S_1 states while the kinetics of the fast exchanging water remain unchanged. Finally, a re-investigation of the proposed role for bicarbonate as an oxidizable electron donor to photosystem II was unable to discern any ^{18}O enrichment of the photosynthetically evolved O_2 in the presence of ^{18}O-bicarbonate. A working model for O_2-evolution in terms of these results is presented.

Publications

Arising from this work:

Hendry, G., and Wydrzynski, T. (2002) Substrate-water exchange kinetics in photosystem II reveal S-state dependent interactions with calcium. In preparation.

Hendry, G., and Wydrzynski, T. (2002) The two substrate-water molecules are already bound to the oxygen evolving complex in the S_2 state of photosystem II. *Biochemistry* in press.

Hillier, W., **Hendry, G**., Burnap, R. L., and Wydrzynski, T. (2001) Substrate water exchange in photosystem II depends on the peripheral proteins. *J. Biol. Chem.* **276,** 46917-46924.

Conference paper:

Hendry, G., and Wydrzynski, T. (2001) Evidence for the binding of two substrate water molecules in the S_2 state of photosystem II. PS2001 Proceedings. 12th International Congress on Photosynthesis, CSIRO Publishers. www.publish.csiro.au/PS2001, S10-017

Other publications:

Hendry, G., Freeman, J., and Wydrzynski, T. (2003) Extraction of the functional manganese and calcium cofactors from photosystem II preparations. *Photosynthesis Research Protocols* in preparation.

Clarke, S. M., Funk, C., **Hendry G. S**., Shand, J. A., Wydrzynski, T., and Eaton-Rye, J. J. (2002) Amino acid deletions in the cytosolic domains of the chlorophyll *a*-binding protein CP47 slow Q_A^- oxidation and/or prevent the assembly of photosystem II. *Plant Mol. Biol.* in press.

Contents

Chapter 1

General Introduction

Chapter 2

^{18}O Isotope Exchange Measurements

Chapter 3

Substrate-Water Binding in Extrinsic Protein Depleted Photosystem II

Figures

Tables

Equations

Schemes

Abbreviations

α	miss parameter
β	double hit parameter
^{o}C	degrees Celsius
μF	microFaraday
μg	microgram
μL	microliter
μM	micromolar
mA	milliampere
mL	milliliter
mM	millimolar
ADP	adenosine di-phosphate
ATP	adenosine tri-phosphate
bRC	bacterial photosynthetic reaction center
CA	carbonic anhydrase
Chl	chlorophyll
CW-EPR	continuous wave EPR
DCBQ	2,6-dichloro-p-benzoquinone
EGTA	ethyleneglycol-bis(β-aminoethylether)-N,N,N',N'-tetraacetic acid
ENDOR	electron nuclear double resonance
EPR	electron paramagnetic resonance
ESEEM	electron spin echo envelope modulation
EXAFS	extended X-ray absorption fine edge structure
Ex-depleted PSII	PSII depleted of the 17- and 23-kDa extrinsic proteins
FTIR	Fourier transform infrared spectroscopy
fwhh	full width half height
GlAc	glacial acetic acid
K	Kelvin
kDa	kiloDalton
kJ	kiloJoules
kV	kilovolt
LED	light emitting diode
LHCII	light harvesting complex, type II protein

LMW	low molecular weight protein
m/e	mass per charge
MeOH	methanol
MES	4-morpholinoethanesulfonic acid
MIL	0.001 inches
MLS	S_2 state EPR multiline signal
NADP	nicotinamide adenine di-phosphate
NMR	nuclear magnetic resonance
OEC	oxygen evolving complex
PAGE	polyacrylamide gel electrophoresis
PCET	proton coupled electron transfer
pH	$-\log_{10}[H_3O^+]$
Pheo	primary electron acceptor molecule, pheophytin
P_i	inorganic phosphate
PSI	photosystem I
PSII	photosystem II
PPBQ	phenyl-p-benzoquinone
P_{680}	primary electron donor in PSII
Q_A	primary quinone electron acceptor molecule in PSII
Q_B	secondary quinone electron acceptor molecule in PSII
SDS	sodium dodecyl-sulfate
TL	thermoluminescence
UV	ultra-violet
(*v/v*)	volume per volume
(*w/v*)	weight per volume
WOC	water oxidizing complex
XANES	X-ray absorption near edge spectroscopy
XAS	X-ray absorption spectroscopy
XES	X-ray emission spectroscopy
Y_D	redox active tyrosine-161 of the D_2 protein
Y_{inj}	oxygen yield from the $H_2^{18}O$ injection
Y_Z	redox active tyrosine-161 of the D_1 protein
Y_{2x}	oxygen yield due to a double hit
Y_{3N}	normalized oxygen yield on the third flash
Y_{3C}	corrected oxygen yield on the third flash

Chapter 1   General Introduction

1.1 WHY PHOTOSYNTHESIS RESEARCH?

The interaction of sunlight with living matter is perhaps the most fundamental natural phenomenon and yields an abundant energy resource on which the pyramid of life has evolved. This energy conversion process is termed photosynthesis and can be principally derived into two distinct 'reactions'- the capture and conversion of solar energy into chemical potential *and* the mediation of this potential for the reduction of CO_2 to sugar. The former process is coined the 'light reactions' of photosynthesis and involves an integrated network of pigment-protein molecules which have evolved to exploit the energy potential of sunlight. The light-driven molecular machinery affords the efficient (>97%) conversion of solar energy to a stable charge separated state. Based on the principles of this mechanism, efforts to develop (bio)mimetic applications as renewable energy strategies are under-way. The bio- and nano-technology revolutions are shaping the design of simple, yet energy efficient biological and synthetic analogues to their more convoluted functional plant equivalents. Recent examples include artificial membranes (Steinberg-Yfrach et al., 1998) and photovoltaic devices (Grätzel, 2001). Indeed, a new research direction is in the design and (recombinant) synthesis of minimalistic protein maquettes that incorporate redox cofactors for light induced charge separation (currently being undertaken in this laboratory). The ultimate vision for this project is to mimic the photoreactions of the water oxidase enzyme, photosystem II. Independent of the approach, it is hoped that these strategies will afford clean, environmentally safe and cost-effective solution(s) to replace existing (non-renewable, e.g., coal, natural gas, oil) energy portfolios. It is our underlying knowledge of natural photosynthesis that facilitates the design of these artificial systems, so understanding the functional dynamics of solar energy conversion is critical in defining the success of artificial photosynthesis. In the words of the late Sir Rutherford Robertson: 'Dare to Dream'.

1.2 OXYGENIC PHOTOSYNTHESIS: THE LIGHT REACTIONS

1.2.1 O_2-Evolution: A Contemporary Perspective

The evolution of O_2 producing cyanobacteria that use water as a terminal reductant transformed the earth's atmosphere to one suitable for the evolution of aerobic metabolism (Dismukes et al., 2001). The transition toward the modern global environment was paced by a decline in volcanic and hydrothermal activity (Des Marais, 1998) that allowed the expanded colonization of O_2 producing organisms- namely

cyanobacterial precursors and which ultimately enabled the evolution of all aerobic life forms. The enzyme responsible for generating O_2 is called photosystem II (PSII) and uses water as its substrate to source electrons for light-activated energy conversion reactions, releasing O_2 as a waste product. The thermodynamics of this redox process are energetically demanding; the energy potential for the forward reaction:

$$2H_2O \ \rightarrow \ \ O_2 \ + \ 4H^+ \ + \ 4e^-$$
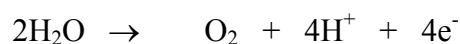
<div align="right">Equation 1-1</div>

is +0.82 V at pH 7.0. Thus to split water into its constituent elements requires an even stronger oxidant; light excitation of the photosystem II reaction center chlorophyll complex (forming the cation radical P_{680}^+) generates redox potentials of > +1 V. This potential is then coupled *via* a redox active tyrosine residue (Y_Z: Y161 of the D1 protein, *Synechocystis* numbering) to the oxygen-evolving complex (OEC), a unique protein motif containing an inorganic $Mn_4O_xCa_1Cl_yHCO_{3\ z}^-$ cluster and in a sequential series of light-activated steps, drives the water oxidation chemistry. The photosystem II enzyme is unique in that it does not perform sequential one-electron oxidations of its physiological substrate, rather it extracts four electrons from the OEC and then reacts with two water molecules to generate O_2 (Dismukes, 2001).

The innovation of oxygenic photosynthesis was facilitated by two essential evolutionary developments at the molecular level: (1) an increase in the redox potential generated following light excitation of the principle photopigment; and (2) the acquisition of a charge accumulating entity (Blankenship, 2002). The first of these requirements is based on the energy coupling in which photoexcitation of the reaction center generates a sufficiently strong oxidant capable of splitting water. Early evolution of a chlorophyll-containing reaction center satisfied this requirement (E_0 [Chl a] = +1.12 V; Klimov et al., 1979). The substitution of bacteriochlorophyll (the predominant pigment found in anoxygenic phototrophic organisms) for chlorophyll was likely to have occurred through a series of gene deletion events that prevented the chemical reduction of the porphyrin ring B and conversion of the C3 vinyl to an acetyl group (Blankenship and Hartmann, 1998).

The second evolutionary development was the acquisition of a catalyst that could access lower potential, multi-electron, oxidation processes such as the four-electron oxidation

of H_2O to O_2 (Dismukes et al., 2001). This is necessary because the redox chemistry of water is a concerted four-electron process whereas photochemistry is a one-electron event. The incorporation of manganese at the active site of water oxidation facilitated this requirement; the inherent nature of transition metals enables redox cycling through to high-valence oxidation states, and in the case of the OEC, it is variously suggested that the Mn ion(s) cycle from the Mn (II) up to the Mn(V) oxidation state following successive turnovers of the PSII reaction center (reviewed in BBA-Bioenergetics: special issue 'Photosynthetic Water Oxidation', [Nugent, J. H. A., Ed.] *volume* 1503, 2001).

Despite this, the evolutionary events that gave rise to the OEC are still unclear. Blankenship and Hartmann (1998) proposed an evolutionary path for oxygenic photosynthesis that involves hydrogen peroxide as a transient electron donor in a two electron reaction to produce O_2. In contrast, Dismukes and co-workers use thermodynamic arguments based on geochemical evidence to propose that manganese-bicarbonate complexes served as the primordial source of the functional Mn (and electrons) for the OEC (Dismukes et al., 2001). Interestingly, the same group showed that bicarbonate accelerates the assembly of the tetramanganese-oxide core during photoactivation of preparations depleted of the functional Mn and Ca^{2+} ions (Baranov et al., 2000). Despite the inherent evolutionary and functional complexity of oxygenic photosynthesis, the creation of a photosynthetic apparatus capable of splitting water into O_2, protons and electrons was instrumental in the evolution of life.

1.2.2 Photosynthetic Electron Transport

The light driven oxidation of water by PSII is the initial step in oxygenic photosynthesis that ultimately provides electrons for the reduction of $NADP^+$. The components of the photosynthetic electron transport chain are illustrated in Figure 1-1 and include the membrane bound protein-cofactor complexes photosystem II, cytochrome b_6f, and photosystem I (PSI). In addition, the two pools of mobile electron carriers (plastoquinone and plastocyanin) mediate electron transfer between PSII and cytochrome b_6f, and, cytochrome b_6f and PSI, respectively. The light energy captured by each photosystem drives the (linear) proton-coupled electron transfer (PCET) reactions that ultimately produce O_2, reduced $NADP^+$ (NADPH) and ATP. The incorporation of two photoreactions in series relaxes the energy requirement for shorter wavelength photons (i.e., photons of sufficient energy to span the redox-potential

between O_2 and NADPH) and as such, photons in the longer wavelength region (i.e., 680 nm for PSII and 700 nm for PSI) become useful (Hillier and Babcock, 2001). The protons that are pumped into the lumen as a result of PCET (through oxidation of two water molecules at PSII and reduction of the plastoquinol pool at the cytochrome b_6f binding site) generate an electrochemical gradient across the thylakoid membrane. This energy potential is then harnessed *via* chemiosmotic coupling through the rotary motion of the ATP synthase in the regeneration of cellular energy (ATP) from ADP and inorganic phosphate (P_i). Ultimately, the ATP and NADPH produced during the light reactions of photosynthesis are consumed (as enzymatic cofactors) during the assimilation of CO_2 in the stroma of the cell.
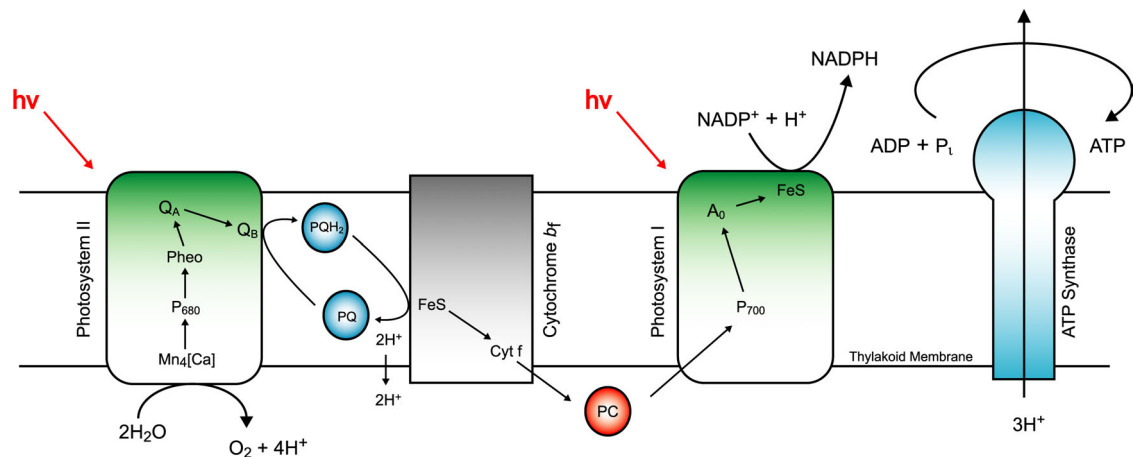
Figure 1-2 **Photosynthetic electron transport chain in higher plants.**

1.3 PHOTOSYSTEM II

Photosystem II (PSII) is the multi-subunit protein complex embedded in the thylakoid membranes of green plants, algae and cyanobacteria that catalyzes the oxidation of water and reduction of plastoquinone. The PSII complex consists of approximately 25 protein subunits *in vivo*, encoded for by the *psb*A-Z genes (reviewed in Hankamer et al., 2001a) with the exception of the *psb*G gene which was found to encode a component of the chloroplast located NADPH/quinone oxidoreductase (Nixon et al., 1989). Table 1-1 lists the properties of the various PSII proteins. Essential to the structure and function of PSII is the D1/D2 heterodimer which binds the complement of pigment and cofactor molecules involved in the charge separation and electron transfer reactions. These include 6 chlorophyll *a*, 2 pheophytin *a*, 2 β-carotene (Eijckelhoff et al., 1996; Gounaris et al., 1990), the redox active tyrosine residues Y_Z (Debus et al., 1988a; Metz et al., 1989) and Y_D (Debus et al., 1988b; Vermass et al., 1988) and the plastoquinone molecules Q_A and Q_B (Figure 1-3).

Table 1-1   **The proteins of Photosystem II**

Gene Name	Protein Name	M.W.[1] (kDa) mature peptide	Transmembrane α-helices	Location
*psb*A	D1	38.0 (32)[2]	5	RCP[3]
*psb*B	CP47	56.3 (47)	6	Proximal Antenna
*psb*C	CP43	50.0 (43)	6	Proximal Antenna
*psb*D	D2	39.4 (34)	5	RCP
*psb*E	Cyt b559(α)	9.3	1	RCP
*psb*F	Cyt b559(β)	4.4	1	RCP
*psb*H	PsbH	7.7	1	LMW[4]
*psb*I	PsbI	4.2	1	LMW
*psb*J	PsbJ	4.1	1	LMW
*psb*K	PsbK	4.3	1	LMW
*psb*L	PsbL	4.4	1	LMW
*psb*M	PsbM	3.7	1	LMW
*psb*N	PsbN	4.7	1	LMW
*psb*O	33 kDa	26.5 (33)	0	Extrinsic
*psb*P[5]	23 kDa	20.2 (23)	0	Extrinsic
*psb*Q[5]	17 kDa	16.5 (17)	0	Extrinsic
*psb*R	10 kDa	10.2	0	Extrinsic
*psb*S	PsbS	21.7	4	Peripheral
psbT_n	5 kDa	3.3	0	Extrinsic
psbT_c	PsbT_c	3.9	1	LMW
*psb*U[6]	PsbU	9-12	0	Extrinsic
*psb*V[6]	Cyt. c-550	15.6	0	Extrinsic
*psb*W	PsbW	6.1	1	LMW
*psb*X	PsbX	4.1	1	LMW
*psb*Y	PsbY	?	?	LMW
*psb*Z	PsbZ	6.5	1	LMW
Lhcb1	LHCII[7]	28	3	CAB/C Antenna[8]
Lhcb2	LHCII	27	3	CAB/C Antenna
Lhcb3	LHCII	25	3	CAB/C Antenna
Lhcb4	CP29	31 (29)	3	CAB/C Antenna
Lhcb5	CP26	28 (26)	3	CAB/C Antenna
*Lhcb*6	CP24	21 (24)	3	CAB/C Antenna

[1]molecular weight (M.W.) predicted from DNA sequence information, [2]values in the parentheses indicate the apparent molecular weight to which the protein migrates during SDS-PAGE, [3]reaction centre protein, [4]low molecular weight protein, [5]genes encoding proteins only associated with higher plant PSII, [6]genes encoding proteins only associated with cyanobacterial PSII, [7]light harvesting complex protein (type II), [8]chlorophyll *a/b* and carotenoid binding antenna proteins. [The information contained within this table was reproduced from Hankamer et al., (2001a)].

The proximal antenna proteins, CP43 and CP47 are located on opposite sides of the D1/D2 heterodimer and in addition to their structural role are involved in excitation energy transfer from the peripheral light-harvesting antenna proteins to the PSII reaction center (P_{680}). A diagram of a PSII core complex from spinach is illustrated below in Figure 1-3.
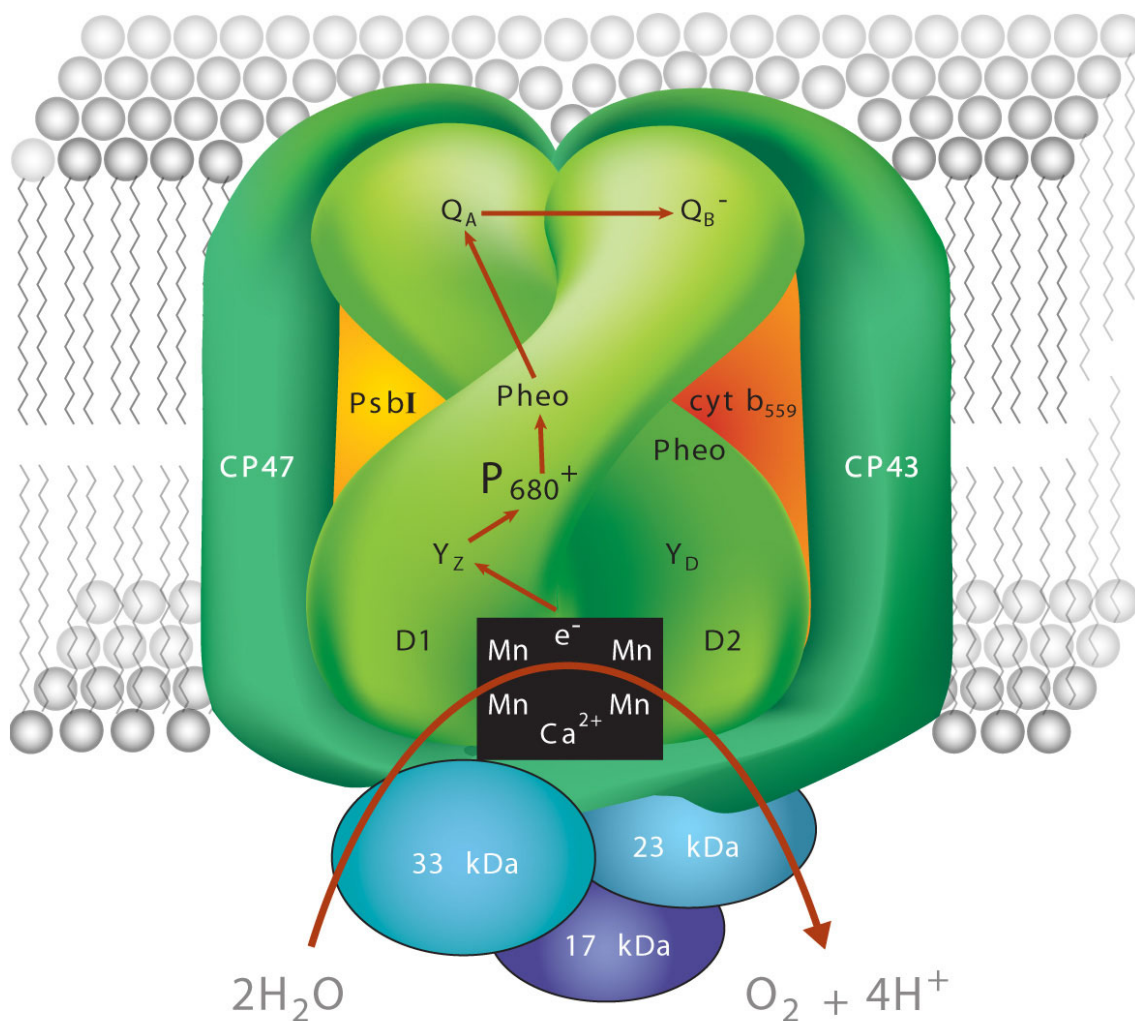
Figure 1-3 **Diagram of a PSII core complex from spinach. The red arrows indicate electron flow from H_2O to Q_B^-.**

Structural information obtained from cyanobacterial (Zouni et al., 2001) and higher plant (Hankamer et al., 2001b) O_2 evolving core preparations has provided a 3-dimensional spatial assignment of the major PSII proteins within the thylakoid membrane. The secondary structure elements of these proteins including cofactor positions were modeled into the electron density maps using C_α traces and porphyrin

rings (of which chlorophyll is a derivative). The results show that the D1/CP43 and D2/CP47 α-helical domains are arranged with a local two-fold rotation symmetry (a pseudo C2-axis around which the D1/D2 heterodimer is organized). This type of structural design is also apparent for the L- and M-subunits of the purple bacterial reaction center (bRC) and for the PsaA/PsaB heterodimer from PSI. Indeed, the overall similarity in protein architecture of PSII, PSI and the bRC supports the hypothesis of a common evolutionary origin for all photosynthetic reaction center complexes (Rhee et al., 1998; Schubert et al., 1998).

1.3.1 Low Molecular Weight Proteins

A number of low molecular weight proteins (LMW) are also bound to PSII and each protein is predicted to contain a single transmembrane α-helical domain (Hankamer et al., 2001a). Efforts to identify the location of these helices have been limited by the resolution of the PSII crystal structures. Furthermore, the LMW proteins lack homology with proteins from other photosynthetic reaction centers where the more refined resolution of these structures has enabled identification of specific side chains. Despite these limitations, results from other studies have been used to piece together tentative positions for these proteins within the PSII enzyme (e.g. Tomo et al., 1993; Shi et al., 1999). Although the precise function of each LMW protein is not well understood, gene deletion experiments have been employed to determine the effect (if any) on structure and/or function relationships within PSII (reviewed in Hankamer et al., 2001a).

1.3.2 The Extrinsic Proteins

The water soluble extrinsic proteins are peripherally bound to the lumenal face of PSII and function to optimize the water splitting activity (Seidler, 1996). In higher plants, the 33-, 23- and 17-kDa extrinsic proteins are named according to the apparent molecular weight to which they migrate during SDS-PAGE. The 33-kDa manganese stabilizing protein (MSP) is required to stabilize the ligation of the Mn cluster in the dark, and to promote efficient redox cycling in the light (Vander Meulen et al., 2002) while the 23- and 17-kDa extrinsic proteins have been implicated in maintaining the concentration of Ca^{2+} and Cl^- within the OEC, cofactors essential for optimal O_2-evolution. The functional significance of the extrinsic proteins is addressed later (Section 3.1.2.) Interestingly, the 33-kDa extrinsic protein has been conserved throughout evolution and is found associated with all known oxygenic photosynthetic

organisms. However, the genetic character of the other two subunits differs between higher plant and cyanobacterial photosystem II. The *psb*U and *psb*V genes found in the cyanobacterial genome (encoding a 12 kDa and cytochrome *c*-550 protein, respectively) have been replaced in higher plant PSII by the *psb*P and *psb*Q genes (encoding the 23- and 17-kDa extrinsic proteins, respectively). In the absence of the PsbU and PsbV proteins, the rate of O_2-evolution was found to be strongly dependent on both Ca^{2+} and Cl^- suggesting that these proteins perform a similar function to the 17- and 23-kDa extrinsic subunits in higher plants (Enami et al., 1998).

1.3.3   Light-Harvesting Antenna

The other principle distinction between higher plant and cyanobacterial PSII can be made according to the type of pigments (and the proteins to which these cofactors are ligated) that make up the light-harvesting antenna. The role of the light-harvesting antenna is to absorb light in the visible spectrum and efficiently transfer its energy to the photoactive reaction center (P_{680}). In higher plant photosystem II, solar energy is captured by the light-harvesting Chl *a/b* and carotenoid proteins of PSII and PSI (Table 1-1). These membrane bound proteins contain mainly chlorophyll *a* (200-300 per reaction center), but the absorption spectra of chlorophyll *a* is supplemented by that of the accessory pigments (carotenoid and chlorophyll *b*) thereby allowing the antenna to absorb light of a relatively broad spectral range. The Chl *a/b* and carotenoid pigment molecules are bound non-covalently to the light-harvesting proteins, as seen in the X-ray structure of LHCII protein (Kühlbrandt et al., 1994). In contrast, cyanobacteria use a different light-harvesting antenna system known as the phycobilisome complex (PBS), a water soluble structure bound to the cytosolic face of photosystem II (reviewed in Ke, 2001). The PBS complex is composed of four different (bilin) pigment types: allophycocyanin (APC), phycocyanin (PC), phycoerythrin (PE) and phycoerythrocyanin (PEC) where the absorption maxima of these pigment molecules range from 570 nm (PE) to 650 nm (APC). The diversity between the prokaryotic and eukaryotic light harvesting systems is primarily attributed to the niche in which the organism resides; the absorption spectra of the predominant pigment reflects the type of light found in that environment.

1.3.4   Primary Photochemistry and Energy Transfer Reactions

Following light energy capture and equilibration within the light-harvesting antenna, the excitation energy is then funnelled to the reaction center and site of photochemistry *via*

coupled resonance transfer. These energy transfer reactions are mediated through the chlorophyll *a* molecules bound to the proximal antenna proteins (CP43 and/or CP47) where the quantum efficiency of this process approaches unity (Hillier and Babcock, 2001). The incident excitation energy induces a charge-separated state between the reaction center chlorophyll(s) and the primary electron acceptor (pheophytin *a*) generating $P_{680}^+Pheo^-$. Thus, the overall energy-transfer and trapping process can be represented by the following equation:

$$(antenna\text{-}P_{680})^* \leftrightarrow (P_{680}\text{-}Pheo)^* \leftrightarrow P_{680}^+Pheo^-$$
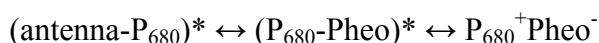
<div align="right">Equation 1-2</div>

where * represents the transient excited state configuration. Equilibration of the excitation energy within the antenna complex (≤ 5 ps; Dau and Sauer, 1996) and within the reaction center (≤ 400 fs; Durrant et al., 1992; Merry et al., 1998) is considered to be rapid and non rate-limiting. However, the kinetics of energy transfer from the antenna to the reaction center is principally divided into two models: (1) the reversible radical pair model and (2) energy transfer to the trap-limited model (reviewed in Diner and Rappaport, 2002). In the radical pair model, there is rapid equilibration of the excitation energy between the antenna and the reaction center and thus the energy transfer is rate-limited by the electron transfer reactions within the reaction center. In contrast, the energy transfer to the trap-limited model proposes that energy transfer between the antenna complex and reaction center is slow and rate-limiting.

The actual rate of charge separation has been determined using transient absorption spectroscopy and ultra-fast fluorescence decay measurements where the time course for this reaction is estimated at between 1 and 20 ps (Roelofs et al., 1992; Schelvis et al., 1994; Visser et al., 1995; Klug et al., 1995; Donovan et al., 1997; and Greenfield et al., 1997). Indeed, the rapid kinetics are necessary to ensure high quantum efficiency for the energy-conserving forward reaction (van Gorkom and Schelvis, 1993). The recombination of $P_{680}^+Pheo^-$ to $P_{680}Pheo$, heat, and potentially damaging triplet states (i.e., through formation of singlet oxygen) is prevented by further electron transfer from pheophytin *a* to the one-electron acceptor (Q_A) resulting in the formation of $P_{680}^+PheoQ_A^-$. Re-reduction of P_{680}^+ proceeds *via* electron donation from Y_Z typically in the (10-100) nanosecond time domain (Schilstra et al., 1998; Christen et al., 1999), although on the $S_0 \rightarrow S_1$ (and possibly the $S_3 \rightarrow S_0$) transition, the authors report a slower

μs kinetic component that they assign to intraprotein proton/hydrogen transfer. Finally, Y_Z^+ (or $Y_Z^\bullet$ in the case of H-abstraction models) is reduced by the OEC with S-state dependent kinetics in the range of 30-1300 μs (Razeghifard et al., 1997 and references therein) and on the acceptor side, the electron at the Q_A site is passed to Q_B within 0.2-3.0 ms (de Wijn and van Gorkom, 2001). The rate of Q_A^- oxidation by Q_B depends on the occupancy of the Q_B site *and* as Q_B is a two-electron gate its redox-state, i.e., Q_B (full quinone) or Q_B^- (semiquinone).

1.4   THE CHEMISTRY OF WATER OXIDATION

1.4.1   S-State Cycling

Our understanding of the mechanism of water oxidation was predominantly shaped by the experiments of Joliot and co-workers who measured fast O_2 release kinetics in dark-adapted Chlorella after a series of short (10 μs) saturating preflashes (Joliot et al., 1969). The resulting O_2 flash yield pattern revealed a distinct damped periodicity of four with maxima on the third and then every subsequent fourth flash (i.e., flash 3, 7, 11, 15 and so on) until a steady state value is eventually reached. To explain this phenomenon, Kok and co-workers proposed that the OEC cycled through 5 intermediary oxidation states (termed S-states; S_n where n = 0, 1, 2, 3 or 4 and denotes the number of charge equivalents accumulated) during sequential photoactivations of the PSII enzyme (Kok et al., 1970). Beginning in the most reduced S_0 state, each S-state transition is driven forward by the absorption of a light quantum at P_{680}. Upon reaching the S_4 state, the OEC then reacts to produce O_2. Concomitant with the release of O_2 is the regeneration of the S_0 state and the cycle begins anew. The S-state cycle is illustrated in Figure 1-4:
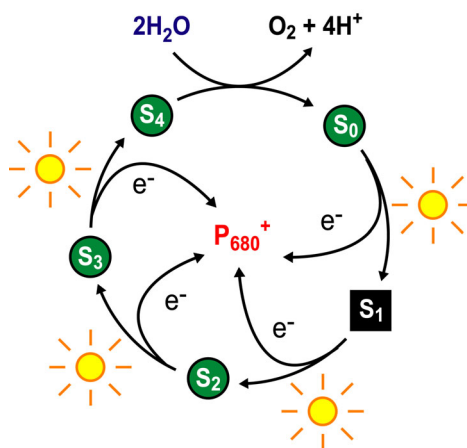
Figure 1-4   The S-state cycle.

To account for maximum O_2 release on the third flash, it was concluded that the S_1 state must be dark stable while the effective damping in the O_2 flash yield oscillation pattern was explained by a miss (α) and double hit (β) parameter (Forbush et al., 1971). On any given flash, there is a finite probability that the enzyme will fail to advance oxidation state (miss parameter, α) or will undergo a double excitation event (double hit parameter, β) and this will inevitably lead to a mixing in the S-state distributions (i.e., steady state O_2-evolution). Despite the ~30 years since its inception, the S-state model still provides the kinetic framework to explain the photoreactions of the OEC.

1.4.2   Atomic Structure of the Mn_4 Cluster

The atomic structure of the Mn cluster has been largely derived from spectroscopic and/or crystallographic information while several lines of evidence indicate a stoichiometry of four Mn ions per reaction center (Debus, 1992; Ananyev and Dismukes, 1996).

1.4.2.1   *X-ray Absorption Spectroscopy*

The application of X-ray spectroscopy has provided a powerful tool for probing the structural and electronic properties of the Mn complex as the OEC is stepped through the S-state cycle. The specificity of this technique has allowed the direct investigation of the Mn properties without interference from surrounding pigment molecules, the protein matrix or from other metals such as Ca^{2+}, Mg^{2+}, Cu and Fe which are present in active PSII preparations (Robblee et al., 2001).

1.4.2.1.1   *Mn Oxidation State Transitions*

X-ray absorption near-edge spectroscopy (XANES) is used to determine changes in Mn oxidation state. The spectra reveal a shift in the inflection point energies for $S_0{\rightarrow}S_1$ and $S_1{\rightarrow}S_2$ under both physiological (Roelofs et al., 1996) and low temperature conditions (Goodin et al., 1984; McDermott et al., 1988) and is taken to indicate a formal increase in Mn oxidation state during these transitions. In contrast, the nature of the $S_2{\rightarrow}S_3$ transition remains controversial with several groups reporting conflicting Mn XANES spectra (i.e., Roelofs et al., 1996 *versus* Ono et al., 1992 and supported by Iuzzolino et al., 1998). With this in mind, the Berkeley group recently initiated Mn Kβ X-ray emission spectroscopy measurements (XES) as an independent means to probe the Mn oxidation states (summarized in Robblee et al., 2001). The results of this study

concluded no Mn centered oxidation during the $S_2 \rightarrow S_3$ transition. Based on the XANES and Mn Kβ XES measurements, the proposed assignment for the Mn oxidation states are: S_0 (Mn II, III, IV, IV) or (Mn III, III, III, IV); S_1 (Mn III, III, IV, IV); S_2 (Mn III, IV, IV, IV); S_3 (Mn III, IV, IV, IV) [or (Mn IV, IV, IV, IV) for models that invoke Mn centered oxidation during the $S_2 \rightarrow S_3$ transition; e.g., Dau et al., 2001].

1.4.2.1.2 EXAFS Measurements

In contrast to the edge spectra, the EXAFS spectra (or extended X-ray absorption fine structure) is sensitive to the coordination number and ligand environment of the catalytic Mn. Using this technique, the interatomic distance between the absorbing Mn atom and (back-scattering) atoms in the first and second coordination spheres can be determined to within 0.01-0.03 Å accuracy (Dau et al., 2001). Analysis of the S_1 and S_2 state EXAFS spectra revealed three Fourier peaks at 1.8, 2.7 and 3.3 Å that have been assigned to Mn-O (or Mn-N), Mn-Mn and a mixed shell of Mn-Mn and Mn-Ca interactions, respectively (Penner-Hahn et al., 1990; Mn-N; DeRose et al., 1991; MacLachlan et al., 1992; Yachandra et al., 1993; Kusunoki et al., 1995; Iuzzolino et al., 1998). The 2.7 Å Mn-Mn distance is characteristic of di-μ-oxo bridged models while the 3.3 Å distance is characteristic of mono-μ-oxo bridged complexes (DeRose et al., 1994). These observations led to the original proposal that the Mn_4 cluster consists of two di-μ-oxo bridges linked by a single mono-μ-oxo bridge.

Study of the Mn EXAFS in the S_3 state (Liang et al., 2000) indicates a significant structural rearrangement during the $S_2 \rightarrow S_3$ transition and is thought to reflect the onset of substrate-water oxidation. The 2.7 Å Mn-Mn vector splits into a ~2.8 and 3.0 Å vector while the fate of the 3.3 Å mono-μ-oxo bridge remains divided. The Berkeley group invokes a lengthening in 3.3 Å vector to 3.4 Å while in contrast, the EXAFS work from Dau's laboratory would suggest the mono-μ-oxo bridge is oxidized on the $S_2 \rightarrow S_3$ transition (creating an additional ~2.7 Å $Mn_2(\mu\text{-}O)_2$ vector). It is hypothesized that the μ-oxo bridge oxidation involves deprotonation of a terminally ligated hydroxide or water molecule and that it is facilitated by the transition from five-coordinated Mn(III) to six-coordinated Mn(IV) (Dau et al., 2001). Indeed, this proposal is supported by the XANES data (i.e., Mn centered oxidation on the $S_2 \rightarrow S_3$) also from the same laboratory.

Geometric information obtained from dichroism measurements has revealed that the overall structure of the Mn_4 cluster is asymmetric (George et al., 1989; Robblee et al., 2001). In conjunction with the EXAFS measurements, these data place constraints on the structural alternatives that are possible. Some structural models for the Mn_4 cluster are depicted in Figure 1-5.
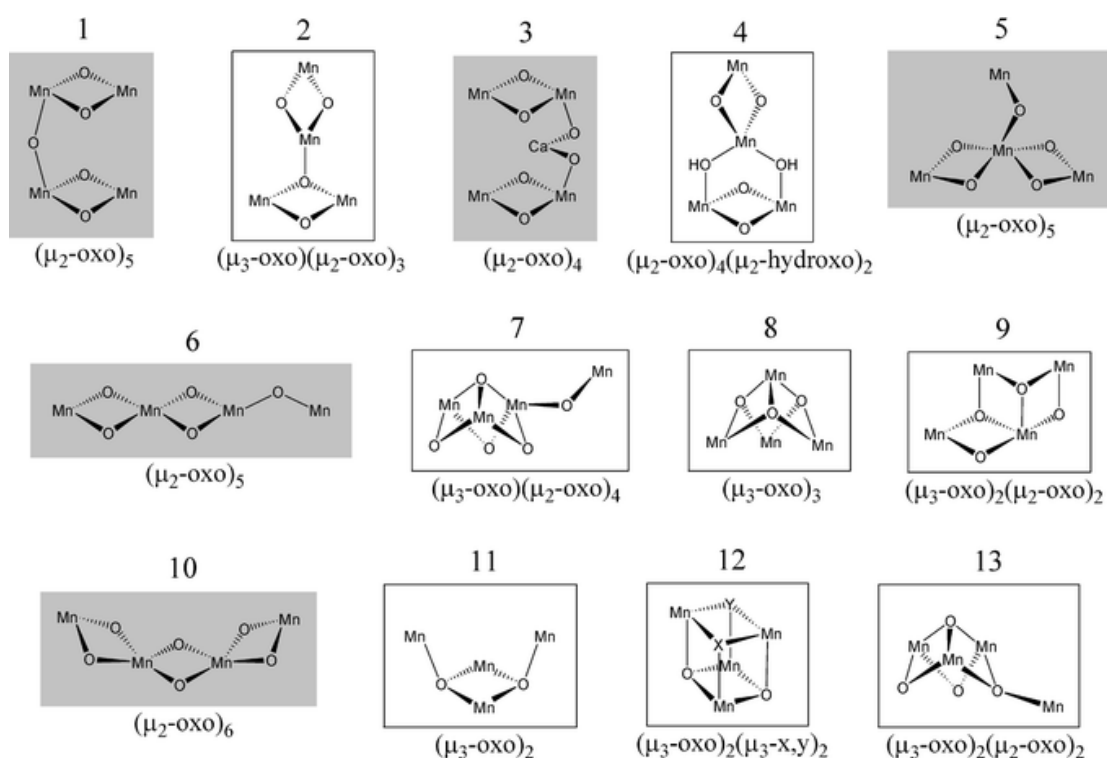
Figure 1-5 **Structural models for the Mn_4O_x cluster. The unshaded structures are compatible with both Mn EXAFS and EPR data (see below). [This figure was reproduced from Carrell et al., 2001].**

The proximity of Ca^{2+} to the Mn complex has been estimated through Mn EXAFS and more recently, Sr^{2+} EXAFS of Sr^{2+}-reconstituted preparations (Latimer et al., 1995; Cinco et al., 1998). Based on changes in the phase and amplitude of the second Fourier peak, the data provide evidence for the structural proximity of the Ca^{2+}-site to the Mn_4 cluster at ~3.5 Å. This result is in contradiction with data obtained by Riggs-Gelasco et al. (1996) who reported no EXAFS-detectable Mn-Ca contribution in the 3.3 Å Fourier peak of Sr^{2+} and Dy^{3+} substituted PSII. It is anticipated that Ca EXAFS will clarify the nature of the Mn-Ca interaction, although these measurements remain problematic due

to lower X-ray fluorescence yields and extraneous Ca^{2+} contamination. The functional significance of Ca^{2+} in O_2-evolution is discussed later (sections 1.4.5.1 and 4.1).

1.4.2.2 EPR and ENDOR Spectroscopy

Electron paramagnetic resonance (EPR) is largely complementary to the XANES and EXAFS techniques and has also been extensively used to probe the physical and electronic properties of the OEC Mn_4 cluster in the various intermediate S-states. This technique measures transitions between the electromagnetic energy states associated with magnetic moments of atomic or molecular systems. The S_2 state multiline signal (MLS) spanning 1500 G with > 18 lines (Dismukes and Siderer, 1981) is proposed to originate from a group of 2-4 Mn atoms in a mixed valence that contains Mn(III) and Mn(IV), (Dismukes and Siderer, 1981; Brudvig and Crabtree, 1986; Kusunoki, 1992). Anisotropic simulations of the S_2 state EPR signal have been performed by various groups to predict the structure and oxidation states of the Mn_4 cluster (e.g., Åhrling and Pace, 1995; Zheng and Dismukes, 1996; Hasegawa et al., 1999). The results of these studies are somewhat conflicting with no two groups reporting the same set of ^{55}Mn hyperfine tensors (see Table 1 of Peloquin and Britt, 2001). Peloquin and Britt argued that this inconsistency was due to the number of possible (CW) EPR transitions (1296 for a tetranuclear Mn cluster) and initiated a similar experimental approach using the pulsed EPR technique of ESE-ENDOR (electron spin echo ENDOR) which restricts the number of transitions to 40 (Peloquin et al., 2000). The ESE-ENDOR spectra were best simulated by a 'trimer-monomer' coupling model using a Mn (III, IV, IV, IV) valence assignment (see Figure 5 of Peloquin and Britt, 2001). In contrast, Dismukes and co-workers promote a Mn (III, III, III, IV) valence assignment for the S_2 state (Zheng et al., 1994) and argue that the different interpretations of these data arise from the physical origin of the hyperfine anisotropy (discussed in Carrell et al., 2001). In considering both the EPR and XAS constraints, Carrell et al. proposed eight Mn_4O_X core types allowed by the current spectroscopic data (see the unshaded structures in Figure 1-5).

1.4.3 Structural Insights from X-ray Crystallography

The most definitive information regarding the *position, size and shape* of the Mn_4 cluster has come from the X-ray crystal structure of *Synechococcus elongatus* at 3.8 Å resolution (Zouni et al., 2001). The dimensions of the electron density map were determined to be $6.8 \times 4.9 \times 3.3$ Å where the long axis is tilted at 23° to the membrane normal (Figure 1-6). The Mn cluster is located 7.0 Å from Y_Z which protrudes from the lumenal side of the CD helix of the D1 protein (see Figure 3a of Zouni et al., 2001).
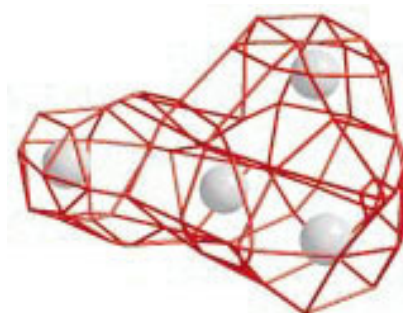
Figure 1-6　　**Electron density map of the Mn_4 cluster from the 3.8 Å X-ray crystal structure of *Synechococcus elongatus*. The tentative positions assigned to the Mn ions are indicated. [This figure was reproduced from Zouni et al., 2001].**

1.4.4 Mutagenesis Studies

Evidence from site-directed mutagenesis studies using the cyanobacterium *Synechocystis* sp. PCC 6803 indicates that the Mn and Ca^{2+} ion(s) are coordinated primarily or exclusively by residues of the D1 protein (see Diner, 2001; and Debus, 2001 for comprehensive reviews). The residues Asp-170, His-190, His-332, Glu-333, His-337, Asp-342 and Ala-344 have been identified as the most likely Mn coordination sites with photoautotrophic growth either retarded or abolished in strains carrying mutations at these sites (Nixon and Diner, 1992; Chu et al., 1995a,b). In addition, mutations at His-190, Glu-333 and Asp-342 resulted in PSII complexes that lack photooxidizable Mn ions and/or an increased sensitivity to photooxidative damage (Nixon and Diner, 1994; Tang et al., 1994; Chu et al., 1995a,b). Furthermore, mutants at Asp-59 and Asp-61 in the A-B loop of the D1 protein require higher concentrations of Ca^{2+} in the culture medium for photoautotrophic growth, suggesting that these residues are involved in Ca^{2+} binding. Indeed, experimental evidence showed that electron transfer from Y_Z to $P680^+$ was slowed in strains carrying mutations at these sites when grown in the absence of Ca^{2+} (Chu et al., 1995a,b).

1.4.5 Cofactor Requirements

1.4.5.1 Calcium

Calcium is an essential cofactor for water oxidation (Debus, 1992). The exact number of intrinsic Ca^{2+}-sites has been determined using a number of different experimental approaches [namely steady state activity measurements (Han and Katoh, 1995); $^{45}Ca^{2+}$ labeling (Ädelroth et al., 1995); atomic absorption (Kalosaka et al., 1990); and equilibrium analyses using a Ca^{2+} sensitive electrode (Grove and Brudvig, 1998)]. There is general agreement for 2 Ca^{2+}-sites per reaction center: a high-affinity binding site located within the light-harvesting complex which requires extreme conditions for removal (Han and Katoh, 1993; Chen and Cheniae, 1995); and a second, lower-affinity site from which Ca^{2+} can be removed by incubation in ≥ 1 M NaCl (in the presence of chelator(s)) or by low pH/citrate treatment of PSII membrane fragments (Kuwabara and Murata, 1983; Ono and Inoue, 1988). Indeed, the affinity of Ca^{2+} for the OEC site is thought to depend on both the redox state of the Mn_4 cluster and the presence of the extrinsic proteins (Boussac et al., 1985; Boussac and Rutherford, 1988b; Ghanotakis et al., 1984; Miyao and Murata, 1984). Removal of the lower affinity Ca^{2+} largely inhibits the O_2-evolving activity which can be partially restored by the addition of non-physiological concentrations of Ca^{2+} or, to a lesser extent, Sr^{2+}, (Ghanotakis et al., 1984; Ono and Inoue, 1988; Boussac and Rutherford, 1988a; Yocum, 1991). Spectroscopic evidence indicates that Ca^{2+} is closely associated with the Mn_4 cluster. In addition to the EXAFS spectra (section 1.4.2.1.2), Matysik et al. (2000) have recently demonstrated the proximity of the Mn complex to the ^{113}Cd-bound Ca^{2+} site using ^{113}CdNMR. The results also showed that $^{113}Cd^{2+}$ was located in a symmetrical six-coordinate sphere of oxygen, nitrogen and chlorine (Matysik et al., 2000). Moreover, Ca^{2+} is known to modulate the redox and magnetic properties of the OEC. Electron paramagnetic resonance measurements of Ca^{2+}-depleted preparations revealed the formation of novel S_2 and S_3 state spectra that disappeared upon reconstitution with Ca^{2+} (Boussac and Rutherford, 1988a; Boussac et al., 1989; Sivaraja et al., 1989; Ono and Inoue, 1990). In addition, reconstitution with Sr^{2+} induced the formation of the S_2 state $g = 4.1$ split signal concomitant with a decrease in the overall intensity of the multiline signal (Boussac and Rutherford, 1988a; Ono and Inoue, 1989). The results clearly indicate that the electronic structure of the Mn_4 cluster is somehow modified by Sr^{2+} occupation of the Ca^{2+}-site. Further discussion regarding the nature of the Ca^{2+}-site and the proposed roles for Ca^{2+} in O_2-evolution is found in Chapter 4.

1.4.5.2 Chloride

The chloride requirement has also been extensively studied through extraction and reconstitution experiments while quantitative binding measurements using ^{36}Cl$^-$ revealed that a single Cl$^-$ atom is bound to the OEC (Lindberg et al., 1993). Chloride-depletion largely inhibits the O$_2$-evolving activity which can then be (partially) restored by the addition of Cl$^-$ > Br$^-$ > NO$_3^-$(NO$_2^-$) > I$^-$ (Kelly and Izawa, 1978; Wincencjusz et al., 1999). In Cl$^-$-depleted PSII, the donor side reactions were blocked following formation of the S$_2$ state, and which does not give rise to the characteristic g = 2 EPR signal. Moreover, the modified S$_2$ state exhibited decay kinetics ~20 times slower than that of the normal S$_2$ state (Ono et al., 1986). It was recently shown by flash-induced UV absorption changes that Cl$^-$ is only required for S$_2 \rightarrow$ S$_3$ and S$_3 \rightarrow$ S$_0$, and not the S$_0 \rightarrow$ S$_1$ and S$_1 \rightarrow$ S$_2$ transitions (Wincencjusz et al., 1997). Indeed the rate of O$_2$-evolution in anion substituted PSII samples was found to be correlated with the instability of these higher oxidation states rather than associated with the kinetics of the S$_3 \rightarrow$[S$_4$]$\rightarrow$S$_0$ transition (Wincencjusz et al., 1999).

The position of Cl$^-$ relative to the Mn$_4$ cluster has been probed by Mn EXAFS using Br$^-$ substituted (Yachandra et al., 1991; Klein et al., 1993) and F$^-$ inhibited (DeRose et al., 1995) preparations. The results of these studies were consistent with a Mn associated halide ligand although the effects were too subtle to provide strong evidence concerning the identity of the Cl$^-$ binding site (Wincencjusz et al., 1998). Other groups have suggested the involvement of CP47 (Bricker et al., 2001; Clarke and Eaton-Rye, 2000) in coordinating Cl$^-$ binding in the vicinity of the Mn$_4$ cluster. Whether Cl$^-$ plays a purely structural role within the OEC or, is directly involved in the chemistry of water oxidation (e.g., Sandusky and Yocum, 1984; Limburg et al., 1999) remains to be clarified.

1.4.5.3 Bicarbonate

It is well established that bicarbonate is required on the acceptor side for optimal activity by photosystem II (reviewed in Van Rensen et al., 1999) although its precise role on the donor side reactions remained enigmatic until the recent work of Klimov and co-workers (reviewed in Klimov and Baranov, 2001). Their experiments provide compelling evidence to show that (1) bicarbonate stimulates electron flow on the donor side of photosystem II, (Klimov et al., 1995a,b; Wincencjusz et al., 1996; Allakhverdiev

et al., 1997), (2) bicarbonate stabilizes the Mn$_4$ cluster during photo- and thermoinactivation of PSII, (Klimov et al., 1997b) and (3) bicarbonate accelerates the assembly of the inorganic core of the OEC in Mn-depleted PSII, (Klimov et al., 1995a,b; Allakhverdiev et al., 1997; Klimov et al., 1997a,b; Hulsebosch et al., 1998; Baranov et al., 2000). In interpreting these data, Klimov and co-workers have proposed a number of functional roles for bicarbonate within the OEC which include a possible ligand to the first Mn ion, and as an intermediate (or alternative) electron donor to PSII. The significance of the latter proposal is addressed in Chapter 5.

1.5   SUBSTRATE-WATER INTERACTIONS

Important questions are at what point during the S-state cycle do the two substrate-water molecules bind to the catalytic site and how does this influence the formation of the O-O bond. In the original Kok hypothesis (Kok et al., 1970), it was implied that the substrate-water only enters the reaction sequence during the last transition ($S_3 \rightarrow [S_4] \rightarrow S_0$) immediately prior to the release of O_2. However, current mechanistic models invoke the binding of substrate-water to the Mn$_4$[Ca] cluster at the beginning of the S-state cycle, in the S_0 state (Hoganson and Babcock, 1997; Pecoraro et al., 1998; Limburg et al., 1999; Haumann and Junge, 1999; Schlodder and Witt, 1999; Siegbahn, 2000; and Messinger et al., 2001).

Many attempts have been made to probe substrate-water interactions at the catalytic site and these include measurements of proton release, magnetic resonance, FTIR spectroscopy and oxygen isotope exchange.

1.5.1   Proton Release Measurements

Since protons are the other product of water oxidation, measurement of the extent and rate of proton release from PSII has been an active area of research for several decades. The initial experimental evidence revealed a 1:0:1:2 pattern for the $S_0 \rightarrow S_1 \rightarrow S_2 \rightarrow S_3 \rightarrow S_0$ transitions (Fowler, 1977; Saphon and Crofts, 1977; Förster and Junge, 1985; Saygin and Witt, 1985) and is thought to reflect the intermediate oxidation reactions of water as a function of S-state (i.e. most recently proposed by Schlodder and Witt, 1999). Others argue that the stoichiometry of proton release is generally non-integer and depends strongly on the pH and the protein environment surrounding the catalytic site (Rappaport and Lavergne, 1991; Haumann and Junge, 1994; Rappaport and Lavergne, 2001). It is noted that the extent of proton release differed significantly

between thylakoids and PSII membrane fragments over the pH range of 5.5-8.5, while for PSII core samples, a pH-independent 1:1:1:1 proton release pattern was observed (see Figure 2 of Lavergne and Junge, 1993 and references therein). Interestingly, measurements of the rate of proton release revealed kinetic values similar to that observed for the oxidation of Y_Z (Haumann and Junge, 1994). This finding has been interpreted by some groups to indicate that proton release is directly derived from the oxidation of Y_Z (i.e., through hydrogen atom abstraction from the substrate-water bound to the OEC [Hoganson and Babcock, 1997; Gilchrist et al., 1995]). In contrast, Junge and co-workers argue that proton release is a composite of the chemical production *and* more indirect reactions such as the electrostatically induced pK shifts of peripheral amino acids in response to charge deposition within the OEC (Haumann and Junge, 1996; Ahlbrink et al., 1998).

1.5.2 Magnetic Resonance

In an attempt to probe the interaction of substrate-water directly with the Mn complex, Evans and co-workers have used the pulsed EPR technique of electron spin echo envelope modulation (or ESEEM). This approach involves the investigation of magnetic hyperfine interactions between complexes giving rise to the S_2 or S_0 EPR signals and ^2H_2O or $H_2^{17}O$. The initial ESEEM measurements were unable to detect any interaction that could be attributed to either specific binding of water to the Mn complex or to interaction between the complex giving rise to the S_2 state signal and the aqueous environment (Turconi et al., 1997). However, in the presence of deuterated methanol and following illumination of the S_1 state at 200K, weak modulation of the S_2 state spectra was observed at the Larmour frequency of deuterium indicating a Mn-deuterium distance of approximately 3-5 Å (Evans et al., 1999). This result was also observed in an independent study by Force and co-workers using methyl deuterated methanol (Force et al., 1998). Interestingly, the modulated ESEEM spectra had completely decayed over a period of 1-4 weeks at 77K, while no significant change in the intensity of the 'classical' S_2 state multiline signal was evident under the same conditions. The authors interpreted this result in terms of separate Mn environments, in which the metastable component of the S_2 state signal (also centered at $g = 2$) is accessible to the aqueous environment. In light of these observations, Evans and co-workers re-measured the three pulse ESEEM spectra of samples in the S_1 and S_2 states in the presence of ^1H_2O and ^2H_2O (Evans et al., 2000). The results revealed a similar phenomenon in which a weak magnetic interaction between ^2H in water and a

component of the PSII reaction center was detected in the S_2 state immediately following illumination at 200K. As with the [^{2}H]methanol study, the signal decayed over a period of 1-4 weeks at 77K. The results are explained in terms of two models: (1) the Mn complex exhibits two different conformations in which one conformation is accessible to the aqueous environment or (2) the Mn complex has two distinct (magnetic) components (see Evans et al., 2000 for a discussion). Although these experiments do not provide direct evidence for water binding to Mn, the spectra clearly indicates a specific interaction of the aqueous environment with the Mn complex (at 3-5 Å distance) in the S_2 and, *vide infra*, the S_1 state. The results provide strong evidence to support the involvement of Mn in the chemistry of water oxidation.

Similar experimental approaches have also been adopted using CW-EPR to detect hyperfine interactions between the Mn complex and the substrate-water. However, the results of these studies provide inconclusive evidence in support of such interactions. In the presence of ^{17}O labeled water, Hansson et al. (1986) demonstrated a weak hyperfine broadening (< 0.5 mT) of the MLS, but due to the prolonged incubation times used in this study, isotope exchange at non-substrate oxygen ligands may have occurred. Furthermore, a distinct hyperfine narrowing of the MLS was observed for samples suspended in ^{2}H labeled water (Nugent, 1987) while the same effect could not be demonstrated in two other studies (Yachandra et al., 1986; Haddy et al., 1989). Indeed, a problem in using the continuous wave magnetic resonance approach to identify Mn-substrate interactions is the difficulty in discriminating between the bound substrate-water and other water, oxygen and hydrogen ligands in the coordination sphere of the Mn that may be subject to isotope exchange.

1.5.3 FTIR Spectroscopy

In the most recent attempt to probe substrate-water interactions, the FTIR work by Noguchi and Sugiura (Noguchi and Sugiura, 2000; 2002) has identified O-H vibrational modes of an active water molecule bound to the catalytic site. Analysis of the S_2/S_1 difference spectra revealed a positive and negative band at 3618 cm^{-1} and 3583 cm^{-1}, respectively, both of which were down-shifted following substitution with H_2^{18}O and D_2O. This result clearly indicated that the infrared absorption peaks observed at these frequencies arise from the O-H stretching vibrations of an active water molecule bound to the OEC in the S_2 and S_1 states. The vibrational mode of the other O-H bond could

not be identified due to absorption saturation by bulk water in the 3500-3100 cm^{-1} range.

The O-H vibrational frequency is also sensitive to various molecular properties including H-bonding interactions, metal binding, molecular symmetry and de/protonation reactions of water (see Noguchi and Sugiura, 2000 and references therein). Hydrogen-bonding induces a down-shift in the O-H vibrational mode to the lower frequency range and as such, the difference in frequency *relative* to the free vibration of water in vapour becomes a useful indication of the H-bond strength (i.e., $\Delta\upsilon = \upsilon_{free} - \upsilon_{H-bond}$ where $\upsilon_{free} = 3704$ cm^{-1}). A larger $\Delta\upsilon$ value reflects a stronger H-bond interaction. In the case of the S_2/S_1 difference spectra, the $\Delta\upsilon$ values of 86/119 cm^{-1} revealed that the active water molecule is weakly H-bonded and that the strength of this interaction becomes less on the $S_1 \rightarrow S_2$ transition. Furthermore, in a (1:1) H_2O/D_2O mixture used to induce intramolecular decoupling, the two bands were differentially down-shifted (4/12 cm^{-1} for the 3618/3585 cm^{-1} bands, respectively) but to a lesser extent to that observed for water in vapour (52 cm^{-1}). The authors interpreted this result to indicate that the active water molecule has an asymmetric structure in which one O-H group exhibits stronger H-bonding character between the S-states measured. Indeed, *ab initio* calculations based on the reported frequency shifts observed by Noguchi and Sugiura are in agreement with this conclusion (Fischer and Wydrzynski, 2001).

The results from these FTIR studies clearly indicate that *at least* one active water molecule is bound to the active site of PSII in both the S_1 and S_2 states.

1.5.4 ^{18}O Isotope Exchange

The most definitive information regarding substrate-water interactions has come from rapid oxygen isotope exchange measurements between $H_2^{18}O$ enriched solvent-water and the photogenerated O_2 using mass spectrometric techniques. This approach is sensitive to substrate isotope interactions and yields important information on the binding affinities; *however,* it is less precise in determining the chemical identity of the binding site, which is possible, for example, with FTIR spectroscopy.

Briefly, the experimental procedure involves the rapid transfer of PSII samples into labeled water of known oxygen isotopic composition (i.e., ^{16}O enriched water or ^{18}O enriched water) and then determination of the isotope incorporation into the

photogenerated O_2. In the original mass spectrometric measurements by Radmer and Ollinger, dark-adapted samples showed no isotopic enrichment of the photogenerated O_2 following incubation in $H_2^{18}O$ (Radmer and Ollinger, 1980). Furthermore, in a following study on the flash-induced higher S_2 and S_3 states, similar results were obtained (Radmer and Ollinger, 1986; Bader et al., 1987). Clearly, the data indicated that there was no 'non-exchangeable' water present at the catalytic site prior to O-O bond formation and as such the results supported the hypothesis that the substrate-water only enters the reaction sequence during the last transitional step. There were, however, experimental limitations in these measurements where the isotope equilibration times were restricted to ≥ 30 s. Thus there remained the possibility that bound forms of the substrate-water could undergo more rapid rates of ^{18}O exchange than what could be detected (Rutherford, 1989; Debus, 1992). More recently, our group has developed a stirred, 'closed' chamber system that has enabled rapid mixing and isotope equilibration times ($t_{1/2}$ ~4 ms) and thereby facilitated a ~5000-fold improvement in the kinetic resolution over the earlier mass spectrometric measurements (Messinger et al., 1995; Hillier et al., 1998). The results have provided the first direct evidence of substrate-bound intermediates of the OEC during the catalytic S-state cycle.

The data obtained at $m/e = 34$ (mass = 34; which measures the mixed labelled $^{16}O^{18}O$ or $^{18}O^{16}O$ product) clearly shows strong biphasic behavior in all of the S-states (Hillier and Wydrzynski, 2000). Detailed analysis of the S_3 state data revealed a slow and fast phase kinetic component with rate constants of 2.2 ± 0.1 s^{-1} and 38 ± 4 s^{-1}, respectively (Hillier et al., 1998). The two kinetic components were interpreted to represent the independent exchange by the two substrate-water molecules at separate sites within the OEC. The data also revealed that the 'slowly' exchanging water is bound to the OEC throughout the entire S-state cycle (Hillier and Wydrzynski, 2000). However, the kinetics of the 'fast' exchanging water in the S_2, S_1 or S_0 states were equal to or faster than the injection response (i.e., $k_{inj} = 175$ s^{-1}) for the S_2 state measurements or to the total *turnover* sequence time (i.e., $k_t = 100$ s^{-1}) for the S_1 state measurements and cannot be resolved by the existing experimental set-up. Thus there remained the possibility that the second substrate-water molecule only enters the reaction sequence after the formation of the S_3 state.

In contrast, the plots at $m/e = 36$ (which measures the double labeled $^{18}O^{18}O$ product) exhibit only a single exponential phase where the observed rate-constant is virtually

identical to that of the slow phase kinetic in the m/e = 34 data (Hillier and Wydrzynski, 2000). This result shows that the overall incorporation of ^{18}O into the O_2 produced is limited throughout the S-state cycle by the substrate-water undergoing the slower isotopic exchange process and that the biphasic behavior in the m/e = 34 data does not arise from PSII heterogeneity. These data provide further evidence in support of independent substrate binding sites within the OEC.

1.6 RESEARCH OBJECTIVES

The intended aims of my research were to examine the dependence of substrate-water binding on the extrinsic protein and inorganic cofactors associated with photosynthetic water oxidation by photosystem II. The first experimental chapter (Chapter 3) addresses a proposed role for the 17- and 23-kDa extrinsic proteins in regulating substrate-water accessibility to the catalytic site. The role of Ca^{2+} and the effect of substitution with Sr^{2+} are next examined in Chapter 4, in an attempt to provide direct information for the involvement of Ca^{2+} as a substrate binding site. The results presented in both of these experimental chapters detail extensive measurements of PSII enriched membrane samples in terms of the S-state dependent ^{18}O exchange behavior (S_1, S_2 and S_3 states) and sample characterization through analysis of the SDS-PAGE, O_2 flash oscillations and steady activities for the different extraction/reconstitution procedures used. Finally, the proposed role for bicarbonate as a transitional electron donor between solvent-water and the OEC is investigated in Chapter 5. Although similar experiments had been previously reported by Radmer and Ollinger (1980), the earlier kinetic limitations left open the possibility that the bound bicarbonate could undergo more rapid rates of ^{18}O exchange than what could be detected.

The theory behind the ^{18}O exchange measurements is described in Chapter 2 and is designed to give the reader a fundamental understanding of the experimental procedures used and methods of data analysis. Inherent problems associated with the flash-turnover sequence(s) required for S-state cycling, corrections for background O_2, and finally determination of the ^{18}O enrichment and injection limitations are also presented.

Chapter 2   Oxygen Isotope Exchange Measurements by Mass Spectrometry

2.1 MASS SPECTROMETRY

Mass spectrometry is an analytical tool that provides selectivity in mass. The principle of this technique is based on ion optics in which a beam of charged molecules exhibiting a range of kinetic energies are separated by mass when placed in magnetic field. This relationship can be defined mathematically by Equation 2-1:

$$\frac{M}{Z} = \frac{B^2 r^2}{2V_{acc}}$$

Equation 2-1

where a molecule with molecular mass, M, and charge, Z, when accelerated by a potential, V_{acc}, will move in a circular path of radius, r, when placed in a magnetic field, B. Since the mass of the charged ion is directly proportional to the deflection radius within the applied magnetic field (i.e., $M \propto r^2$), the detection of different masses then becomes a property of spatial dependence. Thus, through the application of this technique, the incorporation of ^{18}O into the photogenerated O_2 produced by photosystem II can be detected at either $m/e = 34$ ($^{16}O^{18}O$) or at $m/e = 36$ ($^{18}O^{18}O$).

2.2 DETERMINATION OF THE ^{18}O EXCHANGE

2.2.1 ^{18}O Isotope Exchange Measurements

Isotopic determinations of the flash-induced O_2 produced by PSII-enriched samples were recorded at $m/e = 34$ and $m/e = 36$ using an in-line mass spectrometer (Vacuum Generation MM6, Winsford UK). A stirred, closed chamber system with 160 μL internal volume (Figure 2-1) was used for the rapid equilibration of 25 μL of $H_2^{18}O$ (98.5% enrichment, ISOTECH, Miamisburg, OH) with the sample. Injection of the labeled water was achieved using a Hamilton CR700-200 spring-loaded syringe triggered by a computer-actuated solenoid. A silicon membrane (Mempro MEM 213, 1 MIL thickness) layered on top of a teflon frit support disc was used to separate the liquid phase from the mass spectrometer inlet line that allowed only for the passage of gases. Samples were activated using saturating light flashes (fwhh ~ 8 μs) provided by a battery of xenon flash lamps (FX-1163 lamp with internal reflector, 4 μF at 1 kV capacitor, EG & G, Salem, MA) through a fibre optic situated directly in front of the sample chamber window. The flash and injection sequences used to measure the ^{18}O exchange (Figure 2-2) were controlled *via* a visual basic computer program and

accurate timing intervals were established from digital oscilloscope (Tektronix, model 350).
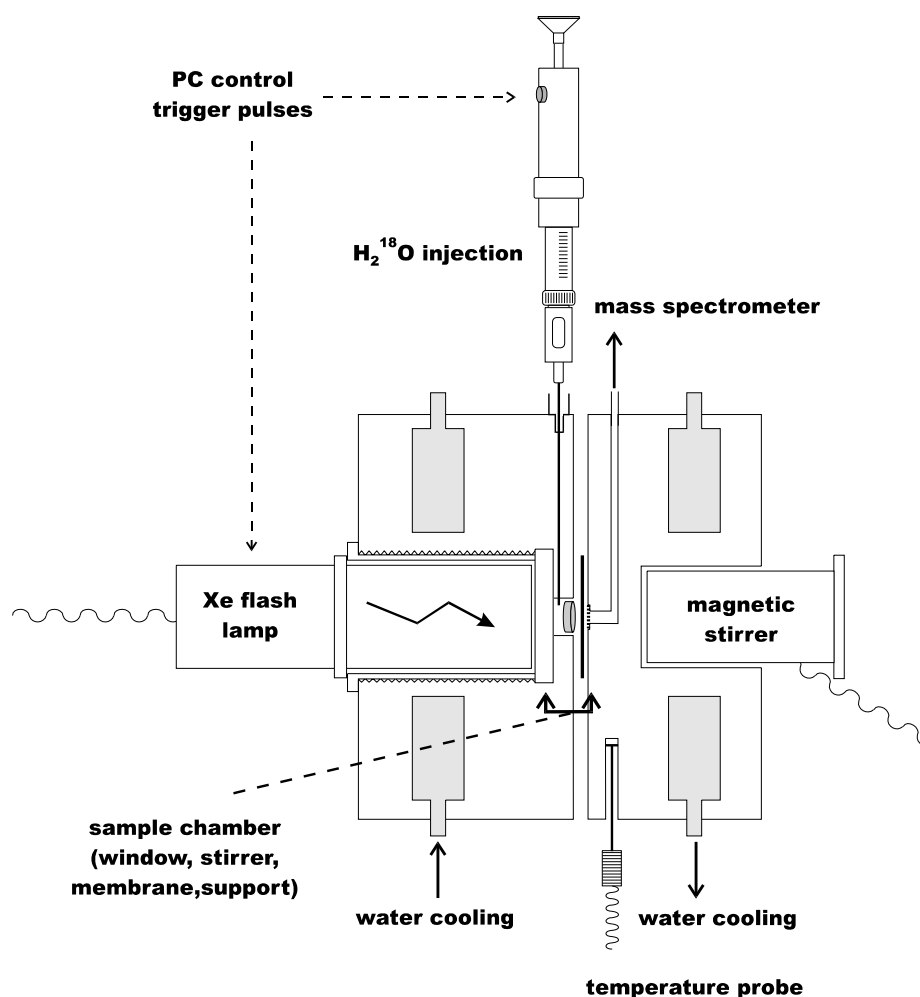
Figure 2-1 **Diagram of the sample chamber used to make the ^{18}O exchange measurements. The different components are indicated.**

The ^{18}O exchange measurements were made in the presence of 1 mM $K_3Fe(CN)_6$ and 400 μM phenyl-para-benzoquinone (PPBQ) as electron acceptors. Samples were first preset in the S_1 state by a single preflash followed by a 10 min dark adaptation at room temperature. For each exchange measurement, the electron acceptors were added to an aliquot and the aliquot was loaded into the sample chamber in the dark and degassed for 10 min at $10^{\circ}C$ prior to the particular flash/injection sequence used (Figure 2-2). For optimal S/N, the final sample concentration was adjusted to 0.5 mg of Chl mL^{-1} for the S_3 state measurement and 0.25 mg of Chl mL^{-1} for the S_2 and S_1 state measurements. In the latter measurements, the short delay times (~5 ms) between turnover flashes necessitated the use of a battery of three flash lamps in which each flash lamp was

optically coupled to the sample chamber window *via* a 3-to-1 fibre optic. To compensate for a reduction in the overall flash intensity through this arrangement, the chlorophyll concentration was lowered to ensure light saturation.

Figure 2-2 illustrates the flash and injection protocols used to probe the various S-states during the ^{18}O exchange measurements. The desired S-state was generated from the enriched S_1 state population through the application of a discrete number of activating preflash(es). Rapid injection of the labeled water ($H_2{}^{18}O$) was then made and a variable exchange time (Δt) allowed for the ^{18}O enriched solvent-water to exchange with the substrate-water bound at the catalytic site. The rapid turnover flash(es) advance the enzyme through to the $S_3 \rightarrow [S_4] \rightarrow S_0$ transition where the rate of incorporation of the ^{18}O isotope into the photogenerated O_2 was determined at either *m/e* = 34 or *m/e* = 36 as a function of the exchange time (Δt). Finally, a series of normalization flashes were applied at 0.05 Hz and these data used in the final analysis to compensate for small variations in sample concentration and membrane permeability between measurements. In order to minimize S-state deactivation between the normalization flashes, measurements were made at 10^oC.
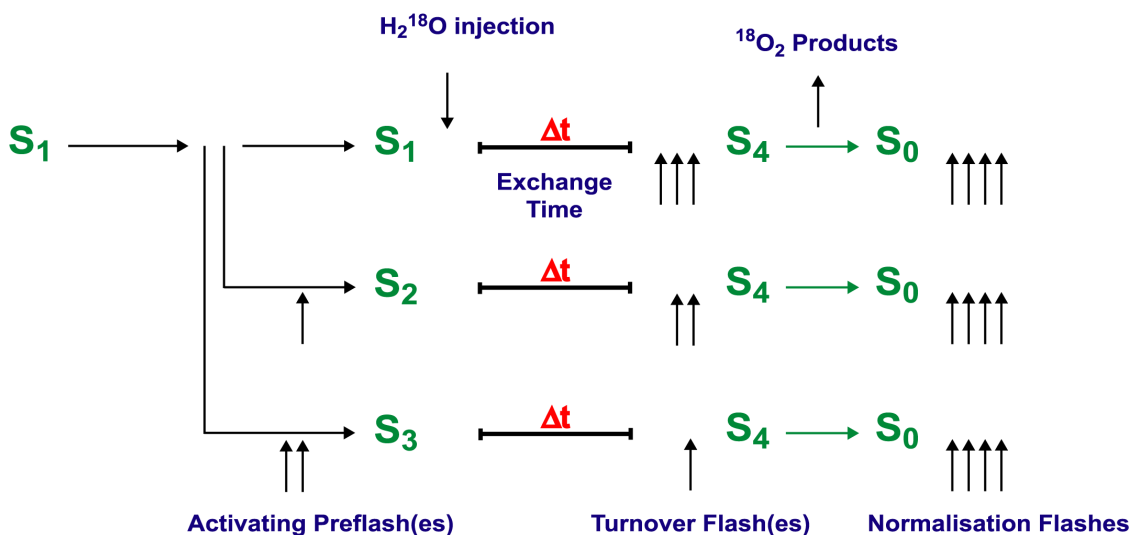
Figure 2-2   **Flash and injection protocol used to probe the various S-states during the ^{18}O exchange measurements.**

2.2.1.1 Optimizing the Turnover Flash Spacing

In probing the ^{18}O exchange behavior, special consideration had to be given to the flash spacing used in the double and triple turnover flash experiments (i.e., the S_2 and S_1 state measurements, respectively). Information on the S-state dependent substrate-water binding affinities is determined from the rate of incorporation of the oxygen isotope into the photogenerated O_2. Thus following $H_2^{18}O$ enrichment, the rapid turnover of the S-state population from either the S_2 or S_1 states is fundamental to the resolution of the rate of fast exchange. However, the use of closely spaced flashes (i.e., ms separation) results in only partial turnover of the S-states which is effectively manifested as a decrease in the yield of O_2 produced on the $S_3 \rightarrow [S_4] \rightarrow S_0$ transition. The oscillation patterns depicted in Figure 2-3 illustrate the effect of turnover flash spacing for PSII enriched membrane samples at $m/e = 34$. In probing the ^{18}O exchange behavior in the S_2 state, a normal period of four oscillation pattern is observed when the spacing between the second and third flash is set to 1000 ms (i.e., 2 Δt 3 = 1000 ms). In contrast, when the double flash spacing is set to 5 ms (i.e., 2 Δt 3 = 5 ms), only partial turnover of the centers is observed (Figure 2-3B) while the effect is even more pronounced in the S_1 state measurement where a triple flash turnover is required (i.e., 1 Δt 2 Δt 3 = 5 ms; Figure 2-3C). Despite the increased damping in the oscillation patterns, the 5 ms flash spacing used in the S_2 and S_1 state measurements is critical to the resolution of the fast kinetic component and provides sufficient S/N for the evaluation of the ^{18}O exchange behavior.
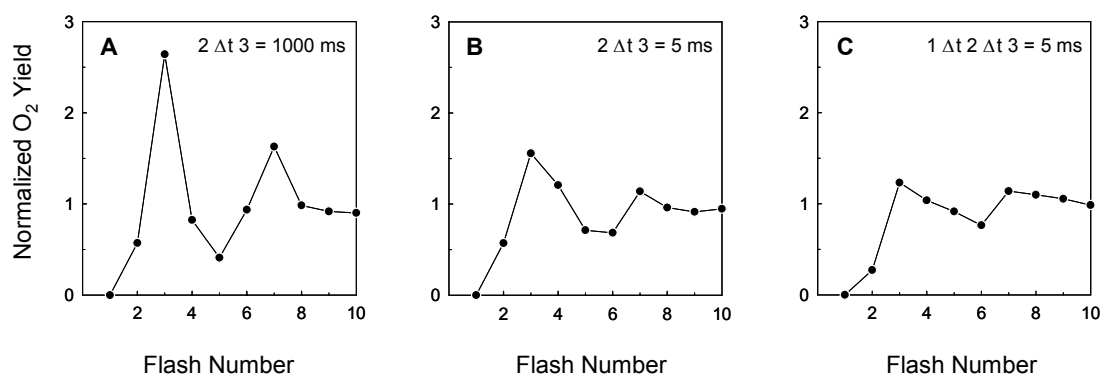
Figure 2-3 The S-state turnover dependence as a function of flash spacing at $m/e = 34$ following $H_2^{18}O$ enrichment at 10°C: (A) S_2 state double flash spacing 2 Δt 3 of 1000 ms, (B) S_2 state double flash spacing 2 Δt 3 of 5 ms and (C) S_1 state triple flash spacing 1 Δt 2 Δt 3 of 5 ms.

2.2.1.2 Double Hit Dependence

An inherent problem of S-state cycling is that on any given flash there is a finite probability that some centers will undergo a double excitation event (double hit parameter, β) due to the band width of the xenon pulse (i.e., 10 μs). During multiple turnover flash experiments (i.e., measurement of the S_2 and S_1 states), consideration must be given to the double hit contribution (Y_{2x}) arising from the first turnover flash in the S_2 state measurement and from the first and second turnover flashes in the S_1 state measurement. However, due to the slow diffusion time of the gas from the sample chamber to the mass spectrometer, the underlying double hit contribution cannot be readily distinguished from the true yield of O_2 on the final turnover flash. The double hit contribution can, however, be determined by performing a separate series of ^{18}O exchange measurements between turnover flashes as a function of the exchange time for those centers that undergo a double hit. The results are shown in Figure 2-4 for the S_2 and S_1 states.

The biphasicity in the Y_{2x} data is a consequence of the biphasic ^{18}O exchange behavior of the substrate water (see below). The solid lines derive the theoretical applied double hit concentration used to correct the data as a function of the exchange time (Δt). It should be noted that in the S_2 and S_1 state experiments, the Y_{2x} contribution to the $m/e = 36$ data was below the S/N as to be effectively ignored (Hillier, 1999).
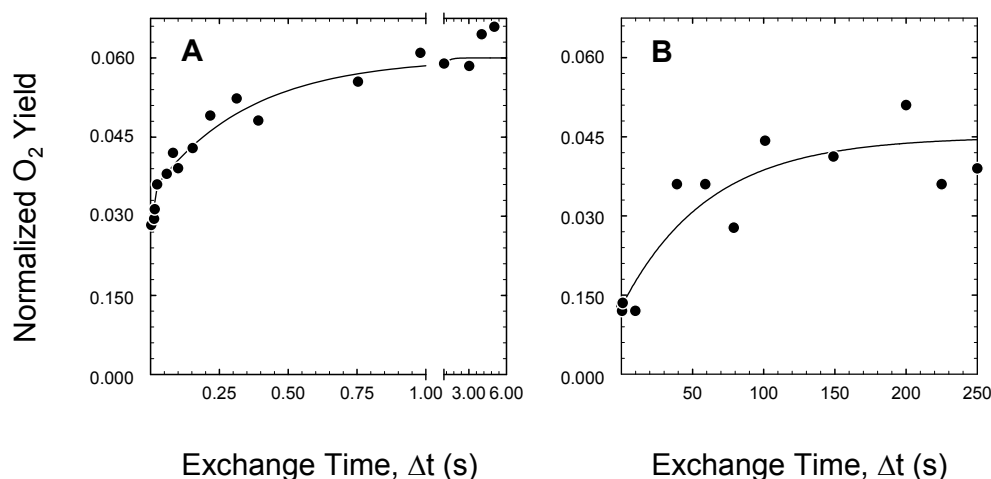
Figure 2-4   **The extent of the double hit dependence (Y_{2X}) on the normalized O_2 yield as a function of the exchange time at m/e= 34 for (A) the S_2 state and (B) the S_1 state. Note the differing time axes are set according to the kinetic parameters. See text for details.**

2.2.2 Data Correction and Analysis

The O_2 background introduced into the sample during the injection of $H_2^{18}O$ (Y_{inj}) was subtracted from the photogenerated O_2 by performing a pre-injection under the same conditions but without illumination. To reduce the size of the O_2 background, small quantities of glucose (0.5 M), glucose oxidase (1.7 U μL^{-1}) and catalase (3 U μL^{-1}) were added to the labeled water prior to injection without interference to the photogenerated O_2. The signal amplitude for the third flash (Y_3) in the turnover sequence less the contribution from the injection (Y_{inj}) and double hits (Y_{2x}; as described above) were normalized to the sum of flashes four to seven to correct for small variations in sample concentration and membrane permeability between measurements, i.e.,

$$Y_{3N} = \frac{[Y_3 - Y_{inj} - Y_{2x}]}{\displaystyle\sum_{n=4}^{7} Y_n}$$

Equation 2-2

For any given $^{34}Y_3$ measurement, a reproducible value for the injection contribution of $Y_{inj} \leq 1.5\%$ was achieved, while for the $^{36}Y_3$ measurements, the Y_{inj} was ~25-40% due to a contribution by background argon (^{36}Ar).

The Y_{3N} value at each exchange time (Δt) was then further normalized to the value obtained after complete isotopic exchange (i.e. 10 s). Finally, the data at fast exchange times ($\leq$ 10 ms) was corrected to compensate for the increasing levels of ^{18}O enrichment and decreasing levels of sample concentration during the injection response (k_{inj} = 175 s^{-1}; see section 2.2.3 below). Thus, for the Y_{3N} values at $\leq$ 10 ms, the following correction was made:

$$Y_{3C(t)} = \frac{Y_{3N(t)}}{[1 - \exp(-175t)][1 + (\Delta Chl(\exp(-175t)))]}$$

Equation 2-3

where
$$\Delta Chl = \frac{[Chl]_{t=0} - [Chl]_{t=\infty}}{[Chl]_{t=\infty}}$$

Equation 2-4

For the two substrate-waters exchanging at separate sites , the oxygen isotope configurations at the catalytic site following $H_2^{18}O$ enrichment can be illustrated in Figure 2-3:
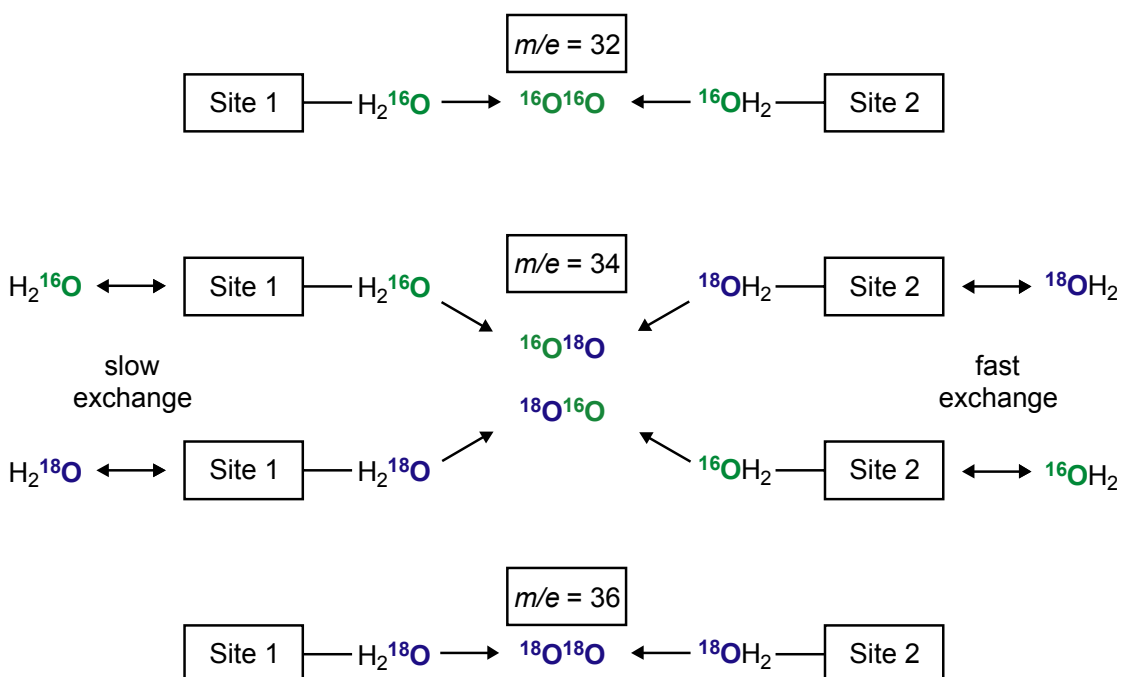
Figure 2-5   **Oxygen isotope configurations following $H_2^{18}O$ enrichment.   Site 1 ('slow' exchange) and site 2 ('fast' exchange) represent the separate substrate-water binding sites within the OEC.   The oxygen isotope distributions of the substrate-water and photogenerated O_2 are indicated: $m/e = 32$ ($^{16}O^{16}O$), $m/e = 34$ ($^{16}O^{18}O$ or $^{18}O^{16}O$) and $m/e = 36$ ($^{18}O^{18}O$).**

It is noted that the measurements of the ^{18}O discrimination for O_2-evolution derive a negligible isotopic discrimination (i.e. $\Delta = 0.06$ ‰; Guy et al., 1993).

Photogeneration of the $^{18}O^{18}O$ product will be rate-limited by the substrate-water undergoing the slowest exchange process. Thus, the corrected plots of $^{36}Y_{3C}$ *versus* Δt at $m/e = 36$ exhibit only one kinetic phase and were analyzed in terms of a single exponential function i.e.

$$^{36}Y_{3C} = [1 - \exp(^{-36}kt)]$$

Equation 2-5

In contrast, the plots of $^{34}Y_{3C}$ *versus* Δt at $m/e = 34$, are clearly biphasic and were analysed as the sum of two exponential functions, i.e.

$$^{34}\text{Y}_{3C} = 0.57[1 - \exp(-^{34}k_2t)] + 0.43[1 - \exp(-^{34}k_1t)]$$

Equation 2-6

The two phases are unequal in amplitude with the fast phase constituting slightly more than half of the total signal. The basis for this difference in amplitude is explained by the enrichment condition for two, independent exchanging sites. As the apparent kinetics differ by at least a factor of 10, the fast phase of exchange is virtually complete before the slow phase begins. Thus, at short Δt only one substrate-water is exchanging at the catalytic site. This means at an ^{18}O enrichment of $\varepsilon = 12\%$ (see 2.2.4 below), the mass distribution at 32:34:36 for the two oxygen isotopes (following the binomial expansion described by Equation 2-7 below) will be 88:12:0. On the other hand, at longer Δt when the second substrate-water is also exchanging, the mass distribution will be 77.44:21.12:1.44. Therefore, the relative contributions of the fast and slow phases will be unequal, with the fast exchanging water representing ~57% (i.e. 21/21.12) of the total amplitude and the slow phase ~43%. This empirical approach yields an accurate fit to the $m/e = 34$ data for a variety of temperatures and S-states (Hiller et al., 1998; Hiller and Wydrzynski, 2000; Hendry and Wydrzynski, 2002).

Sigma Plot (SPSS, Chicago, IL) was used to fit the data according to Equations 2-5 and 2-6.

2.2.3   Determination of the Injection and Mixing Profile

To determine the kinetic limitation of the injection and mixing response, fluorescein dye was injected into the sample chamber under normal experimental conditions, and the fluorescence yield determined as a function of the mixing time. A 25 μL injection of 1% (*w/v*) fluorescein was made into 160 μL of sample buffer at 10°C and the rise in fluorescence (F_0) was profiled using a PAM 101 (Waltz Inc., Germany) modulated fluorometer at 100 kHz frequency. The fluorescence was excited by a LL-450 LED source and detected by an ED-101US/D photodiode using LS-450 and LL-500 (Corion) cut-off filters. The results are presented in Figure 2-6:
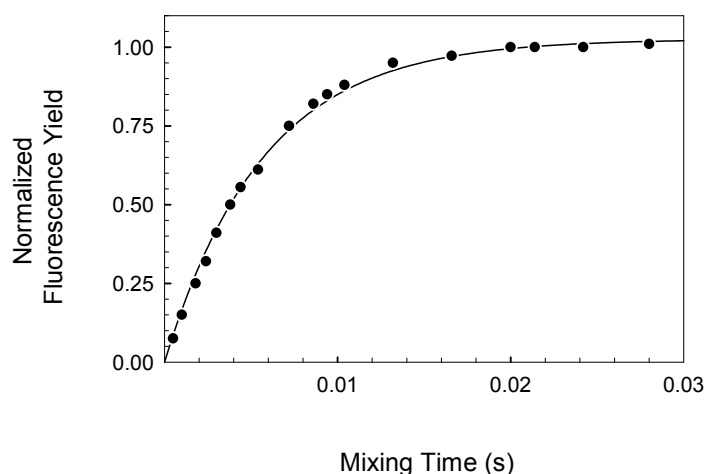
Figure 2-6 **The injection and mixing response of the sample chamber profiled by fluorescence yield measurements as a function of the mixing time. The solid line is a kinetic fit to the data.**

The data was fitted using a single exponential function and yielded a rate constant of k_{inj} = 175 ± 9 s^{-1}, where k_{inj} represents the overall kinetic limitation to the ^{18}O exchange measurements. An inherent delay of 9.75 ms was measured between the time of electronic triggering (assumed to be instantaneous) and the rise in fluorescence levels detected in the sample chamber. This value was taken into consideration in the analysis of the ^{18}O exchange data.

2.2.4   Determination of the ^{18}O Enrichment

Rapid H$_2$^{18}O isotopic equilibration with CO$_2$ is a consequence of the normal de/hydration reactions of CO$_2$ and is catalyzed by the inherent carbonic anhydrase activity retained by the thylakoid membrane preparation used in these particular measurements. The level of ^{18}O enrichment in the sample chamber can thus be determined from the ratio of isotopically labelled CO$_2$ peaks at *m/e* = 44, 46 and 48 according to the binomial expansion:

$$44:46:48 = (1-\varepsilon)^2 : 2\varepsilon(1-\varepsilon) : \varepsilon^2 = 1$$

Equation 2-7

where ε represents the ^{18}O enrichment. Typically $\varepsilon = 12.0 \pm 0.4\%$ for a 25 μL injection of ~98.5% enriched H$_2$^{18}O into 160 μL of sample (or buffer). The contribution of

natural abundance $H_2{}^{18}O$ to the overall signals at $m/e = 34$ and 36 is minimal and effectively ignored.

Chapter 3   Substrate-Water Binding in Extrinsic Protein Depleted Photosystem II

3.1 INTRODUCTION

3.1.1 Substrate Accessibility: A Generic Hypothesis

In many enzymatic mechanisms, an important parameter in defining the reaction path is one of substrate and/or solvent accessibility to the active site. Examples include carbonic anhydrase (which catalyzes the pH dependent reversible hydration reaction of CO_2; reviewed in Tripp et al., 2001) and cytochrome P450. The catalytic site of carbonic anhydrase II (CAII) contains a zinc bound water molecule that is hydrogen-bonded to polar residues on the hydrophilic face of the active site 'cleft'. It is proposed that this H-bond network functions to stabilize and orient the water group for nucleophilic attack on CO_2, thereby producing bicarbonate. The selective modification of conserved residues contained within the active site of CAII and which are believed to coordinate CO_2 binding, lead to a significant reduction in the enzymatic activity (Fierke et al., 1991). The decrease in activity most likely reflects the inability of the zinc bound water to approach CO_2 with optimal orientation. It was concluded that the three-dimensional structure of the CAII cleft is important in optimizing the substrate trajectory and thereby maximizing the rate of catalysis (Fierke et al., 1991; Alexander et al., 1991).

Cytochrome P450 catalyzes the incorporation of an oxygen atom into endogenous (e.g., steroids) and xenobiotic substrates. The exclusion of solvent-water from the active site of this enzyme is essential for efficient enzymatic function. To prevent electron uncoupling during substrate binding, a water ligand covalently bound to the central heme iron must be displaced from the active site (Oprea et al., 1995). A two-state model was proposed in which the side-chain of a conserved arginine residue is thought to flip between a closed (stable) and open (metastable) state. In the open conformation a functional water channel (or aqueduct) is formed allowing the internal water to exit to the protein surface, thereby excluding it from the active site.

These examples clearly illustrate the importance of regulating substrate and/or solvent accessibility during enzyme catalysis. A unique aspect of the photosystem II enzyme is that the solvent-water is ultimately the source for the substrate-water. This has made probing substrate-water interactions within PSII difficult. However, with the application of improved time-resolved mass spectrometry this problem has been largely overcome (reviewed in Hillier and Wydrzynski, 2001). In photosystem II, the

regulation of solvent-water access to the OEC may be important, by preventing unwanted side reactions of water and its oxidation intermediates (e.g., the production of H_2O_2) and thereby maximizing the formation of O_2 (Wydrzynski et al., 1996). Such regulation of the solvent-water accessibility could be achieved through S-state dependent protein conformational changes (Messinger et al., 1991) or through protein specific water channels, which may involve the extrinsic proteins (Wydrzynski et al., 1996).

3.1.2 Functional Significance of the Extrinsic Proteins

In higher plants, three extrinsic proteins of approximately 17-, 23- and 33-kDa molecular mass are involved in regulating the O_2-evolving activity (reviewed in Seidler, 1996). It is generally accepted that the stoichiometry of these proteins follows a 1:1:1 ratio per PSII reaction center, although there is conflicting evidence to suggest two bound forms of the 33-kDa protein per PSII reaction center (Leuschner and Bricker, 1996; Betts et al., 1997). In this case, it has been suggested that one copy of the protein may bind to a structural site and the other to a regulatory site (Betts et al., 1997). The 33-kDa protein or manganese stabilizing protein (MSP), as the name suggests is required to stabilize the ligation of the Mn cluster in the dark, and to promote efficient redox cycling in the light (Vander Meulen et al., 2002). The MSP was initially implicated in Mn ligation (Abramovicz and Dismukes, 1984; Yamamoto et al., 1984) although evidence later emerged to show that the 33-kDa protein could be removed from PSII in the dark without the concomitant release of the Mn cluster (Miyao and Murata, 1984; Ono and Inoue, 1984). Indeed, the function of the extrinsic proteins has been widely studied by dissociation and reconstitution experiments (reviewed in Seidler, 1996). Removal of the MSP through genetic manipulation in cyanobacteria (e.g., Burnap and Sherman, 1991) or by biochemical treatment in higher plant PSII (Ono and Inoue, 1983) leads to a significant reduction in the O_2-evolving activity and an increased sensitivity to photoinhibition (Burnap et al., 1996).

Dissociation and reconstitution experiments using Ex-depleted PSII (PSII membranes depleted of the 17- and 23-kDa extrinsic subunits) revealed that the 23-kDa extrinsic protein is involved in Ca^{2+} retention (Murata and Miyao, 1985; Ädelroth et al., 1995), while the 17- and 23-kDa proteins constitute a diffusion barrier which prevents fast equilibration of the Cl^- binding site with the external medium (Wincencjusz et al., 1998). Removal of the 17- and 23-kDa extrinsic proteins by incubation in 1-2 M NaCl

largely inhibits O_2-evolution (Åkerlund et al., 1982; Kuwabara and Murata, 1983). The activity can be restored by adding non-physiological concentrations of Ca^{2+} (e.g., 10-20 mM) to the assay buffer or by rebinding of the 23-kDa extrinsic protein in the presence of millimolar concentrations of Ca^{2+} for extended periods of time (Murata and Miyao, 1985). Interestingly, the rebinding of the 23-kDa protein in the absence of Ca^{2+} did not lead to any restoration of the activity (Ghanotakis et al., 1984). Recently Vrettos et al. (2001a) showed that the free energy of binding for Ca^{2+} to the OEC decreases by 2.5 kcal/mol in Ex-depleted PSII. The authors discussed this result in terms of a change in the local dielectric around the Ca^{2+}-binding site following the removal of these proteins. Indeed, it would appear that the 23-kDa extrinsic subunit plays an important role in modulating Ca^{2+} binding to the donor side of PSII.

Ex-depleted PSII also exhibit an increased sensitivity to reduction by NH_2OH and hydroquinone, implying that in the absence of these proteins, the catalytic site is more exposed to the bulk medium than in the intact system (Ghanotakis et al., 1984; Vander Meulen et al., 2002). Furthermore, the 17- and 23-kDa extrinsic proteins are known to affect the integer spin EPR signals of the Mn cluster providing firm evidence to show that these subunits have a regulatory effect on the magnetic properties of the Mn_4 cluster (Campbell et al., 1998; Britt et al., 2000). Clearly, these data suggest that the 17- and 23-kDa extrinsic proteins modulate both the structural and functional properties around the OEC reaction sphere.

3.1.3   Experimental Aims

In an effort to address the relation of the extrinsic proteins to the accessibility hypothesis, the experiments described within this chapter investigate the role of the 17- and 23-kDa extrinsic subunits on the substrate-water binding properties. The ^{18}O-isotope exchange measurements were made on Ex-depleted PSII membranes at $m/e = 34$ and 36 as a function of S-state. Interestingly, the data provides the first direct evidence to show that both substrate-water molecules are bound to the catalytic site in the S_2 state. The results are discussed in terms of the dielectric environment around the substrate-binding sites and the available models concerning O-O bond formation.

3.2 MATERIALS AND METHODS

3.2.1 Sample Preparation

3.2.1.1 Isolation of PSII enriched membrane fragments

Thylakoid membranes were prepared from fresh market spinach (*Spinacea oleracea*) by grinding de-veined leaves in 30 mM MES/NaOH (pH 6.3), 350 mM sorbitol, and 10 mM NaCl for 15 s in a Waring blender at 4^oC. All procedures were carried out under dim green light at 4^oC unless otherwise stated. The homogenate was filtered through two layers of cotton gauze and two layers of nylon mesh (20 μm pore size) and centrifuged for 10 min at $10000 \times g$. The sample was washed once in a buffer containing 30 mM MES/NaOH (pH 6.3), 15 mM NaCl, 5 mM $MgCl_2$, resuspended at 2.5 mg of Chl mL^{-1} and allowed to stand on ice in the dark for 1 h. Thylakoid membranes were solubilized in 5% Triton X-100 buffered in 30 mM MES/NaOH (pH 6.3), 15 mM NaCl and 5 mM $MgCl_2$, by gentle stirring for 20 min in the dark (Berthold et al., 1981). The PSII samples were collected by centrifugation at $36000 \times g$ and were washed and resuspended in a final buffered medium containing 30 mM MES/NaOH (pH 6.3), 15 mM NaCl, 5 mM $MgCl_2$ and 400 mM sucrose. The samples were snap frozen in liquid N_2 and stored at -80^oC until measurement.

3.2.1.2 Depletion of the 17- and 23-kDa Extrinsic Proteins

Depletion of the 17- and 23-kDa extrinsic proteins from the PSII samples was essentially performed according to the method of Kuwabara and Murata (1983) by incubation in 1 M NaCl. At 10 min intervals during the incubation, the sample was gently passed twice through a teflon homogenizer. Following a second 30 min treatment, the samples were washed twice in the final buffered medium, snap frozen in liquid N_2, and stored at -80^oC until measurement.

3.2.2 Chlorophyll *a/b* Determination

Chlorophyll concentrations were determined according to the method of Porra et al., (1989). Chlorophyll was extracted in buffered (2.5 mM sodium phosphate buffer [pH 7.8]) 80% aqueous acetone, and the residual protein fraction removed by centrifugation at 12000 rpm (Sorvall MC 12V). The chlorophyll absorption peaks at 646.6 and 663.6 nm were measured using a Carey 300 UV-VIS spectrophotometer. The amounts of Chl

a, Chl *b* and total Chl (Chl *a* + *b*), expressed as µg Chl mL^{-1}, was calculated according to the following equations:

$$\text{Chl } a = 12.25 \ [A_{663.6}] - 2.55 \ [A_{646.6}]$$

<div align="right">Equation 3-1</div>

$$\text{Chl } b = 20.31 \ [A_{646.6}] - 4.91 \ [A_{663.6}]$$

<div align="right">Equation 3-2</div>

$$\text{Chl } a + b = 17.76 \ [A_{646.6}] + 7.34 \ [A_{663.6}]$$

<div align="right">Equation 3-3</div>

where $[A_{663.6}]$ and $[A_{646.6}]$ indicates the absorption value at the specified wavelength. Unless otherwise stated, Chl refers to the total chlorophyll (i.e., Chl *a* + *b*).

3.2.3   SDS PAGE

Polyacrylamide gel electrophoresis (PAGE) was performed according to the method of Laemmli (1970). The resolving gel matrix contained a linear gradient of 10-17.5% (*w/v*) acrylamide/bis solution (37.5:1, Bio-Rad) and an adjusted concentration of Tris/HCl (pH 8.8) to 0.6 M. Both the stacking and resolving gel components contained 6.0 M urea. Prior to loading, the protein samples were heat-treated for 5 min at 90°C in a denaturing buffer consisting of 0.0625 M Tris/HCl (pH 6.8), 2% (*w/v*) SDS, 0.1% bromophenol blue, 10% glycerol, and 5% β-mercaptoethanol. Electrophoresis was initially conducted at 15 mA for 30 min or until the protein had properly stacked and entered the resolving gel matrix. The current was then increased to 50 mA and the sample(s) run for 1-2 h. The gel was stained using Coomassie Brilliant Blue R-250 stain and the protein bands were visualized after de-staining the gel in a solution consisting of 43% MeOH and 7% GlAc. Typically, 10 µg of Chl was loaded per lane. Densitometry scans were obtained using a 1650 Bio-Rad Scanning Densitometer and the individual bands in each lane were normalized relative to one another using CP47 as a standard to account for small variations in protein loading.

3.2.4 Oxygen Evolution

3.2.4.1 Steady State O_2-Evolution: Clark Electrode

Initial steady-state rates of O_2-evolution were measured at 25°C with a Clark-type electrode (Hansatech, model CBD1) using continuous saturating illumination (custom built 150 W tungsten light source, $viz > 5000$ µmol m^{-2} s^{-1}). A typical assay contained 10 µg Chl mL^{-1} in the presence of 1 mM $K_3Fe(CN)_6$ and 400 µM phenyl-p-benzoquinone (PPBQ) buffered in 30 mM MES/NaOH (pH 6.3), 15 mM NaCl, 5 mM $MgCl_2$ and 400 mM sucrose.

3.2.4.2 Kok Analysis

Deconvolution into the relative S-state distributions and determination of the miss (α) and double hit (β) parameters were obtained from O_2 yield flash patterns measured by the mass spectrometer using the matrix vector analysis described in Messinger et al., (1991). The program used to fit the data was based on the following formulae:

$$Y_n = (1-\alpha)[S_3]_{n-1} + \beta[S_2]_{n-1}$$

<div align="right">Equation 3-4</div>

where Y_n is the oxygen yield after the nth flash and $[S_3]_{n-1}$ and $[S_2]_{n-1}$ are the population of the S_2 and S_3 states before the nth flash. The transition vector ($\mathbf{K}$) then describes the univalent forward reactions of the S-state cycle that gives rise to the S-state population distribution before ($\mathbf{S_{n-1}}$) and after ($\mathbf{S_n}$) the nth flash according to Equation 3-5:

$$\mathbf{S_n = KS_{n-1}}$$

<div align="right">Equation 3-5</div>

where

$$\mathbf{S_n} = \begin{bmatrix} S_0 \\ S_1 \\ S_2 \\ S_3 \end{bmatrix} \quad \text{and} \quad \mathbf{K} = \begin{bmatrix} \alpha & 0 & \beta & 1-\alpha-\beta \\ 1-\alpha-\beta & \alpha & 0 & \beta \\ \beta & 1-\alpha-\beta & \alpha & 0 \\ 0 & \beta & 1-\alpha-\beta & \alpha \end{bmatrix}$$

MatLab (version 5.3) was used to execute the matrix vector analyses (see Appendix 1) to derive the miss and double hit parameters, beginning from the dark adapted S_1 state $[S_1] = 100\%$.

3.3 RESULTS

Figure 3-1 shows the SDS-PAGE analysis of Ex-depleted PSII samples following treatment with 1 M NaCl. Densitometry analysis of the gel pattern indicated that Ex-depleted PSII samples retain less than 8% of the 17- and 23-kDa extrinsic proteins and greater than 90% of the 33-kDa extrinsic protein. The Coomassie Blue staining intensities of individual protein bands were normalized to the staining intensity of the CP47 band to account for variation in protein loading between lanes. As shown in Table 3-1 (page 48), the removal of these proteins lowers the overall O_2-evolving activity to ~20% of the control, which could then be restored to ~80% of the control by the addition of 15 mM $CaCl_2$.
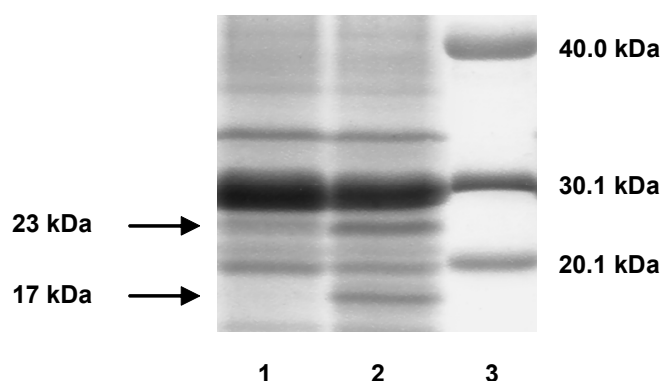
Figure 3-1   **SDS-PAGE analysis of Ex-depleted PSII membranes following treatment with 1 M NaCl: lane (1) Ex-depleted PSII membranes; lane (2) native PSII membranes; lane (3) molecular weight markers as indicated.**

Figure 3-2 shows the normalized O_2-flash yield patterns observed for the various PSII membrane samples at $m/e = 34$ following complete isotopic equilibration after the addition of $H_2^{18}O$ (i.e., at an exchange time > 10 s). The control samples reveal normal period four oscillations, clearly indicating that under these measuring conditions, normal S-state turnovers occur. Based on the Kok analysis of these data, the effective miss parameter for the control sample is 10.5%. In contrast, for the Ex-depleted PSII sample the O_2 flash oscillations exhibit much heavier damping, with an effective miss parameter of 25.5%. The increased miss parameter correlates with the reduced steady-state O_2-evolving activity for these samples (Table 3-1). As is commonly observed, the

addition of 15 mM $CaCl_2$ to Ex-depleted PSII restores back not only a large part of the steady-state O_2-evolving activity (Table 3-1), but also the normal oscillation pattern (Figure 3-2), where the estimated miss parameter approaches the control value (i.e. 10.5%). In contrast, the addition of $MgCl_2$ to Ex-depleted PSII has little effect on the steady-state O_2-evolving activity or the derived Kok parameters (Table 3-1). This last observation indicates a Ca^{2+} specific effect on O_2-evolution.
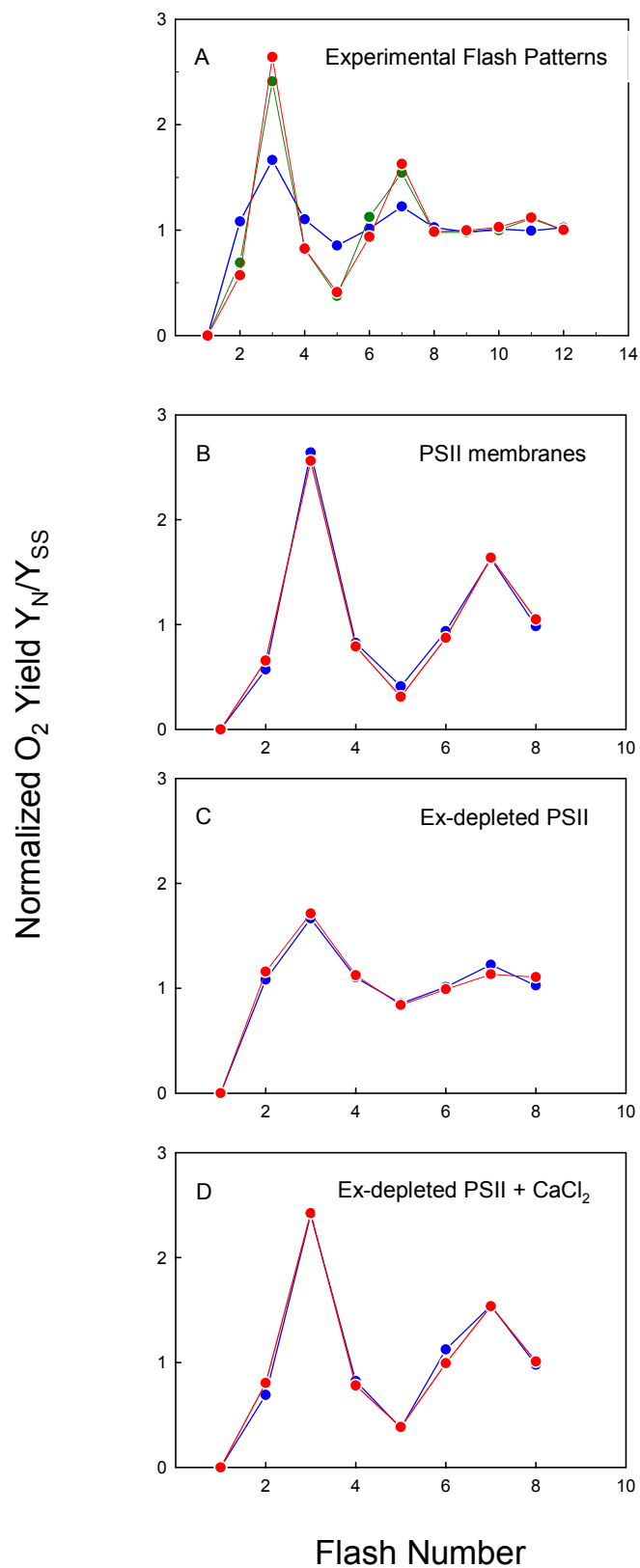
Figure 3-2 **(A) Normalized O_2 flash yield oscillations at *m/e* = 34 for PSII membranes (red circles), Ex-depleted PSII membranes (blue circles), Ex-depleted PSII membranes reconstituted with CaCl$_2$ (green circles). Measurements were performed at 10°C following complete isotopic equilibration after the addition of $H_2^{18}O$. (B), (C), and (D) show the theoretical fits based on the Kok analysis of these data (blue circles). The derived miss (α) and double hit (β) parameters are listed in Table 3-1.**

To determine the influence of the 17- and 23-kDa extrinsic proteins on the substrate-water binding to the catalytic site, the ^{18}O-exchange was measured at $m/e = 34$ (which measures the $^{16}O^{18}O$ product) for the variously treated PSII membrane samples in the S_3, S_2 and S_1 states. The results are shown in Figure 3-3 where the corrected O_2 yield after the third flash in the turnover sequence ($^{34}Y_{3C}$) is plotted as a function of the $H_2{}^{18}O$ exchange time (Δt) in the various S-states. For the control PSII samples the ^{18}O-exchange measurements in the S_3 state exhibit strong biphasic behavior. According to Equation 2-5, the rate constants for the slow and fast exchanging waters are $^{34}k_1 = 2.5 \pm 0.2$ s^{-1} and $^{34}k_2 = 30 \pm 2$ s^{-1}, respectively (Table 3-1). These values compare very closely with those previously reported for thylakoids (Hillier et al., 1998) and for other PSII membrane samples in the S_3 state (Hillier et al., 2001).

Figures 3-3 also shows the first ^{18}O-exchange measurements for PSII membrane samples in the S_2 and S_1 states. The biphasic exchange behavior is maintained in both of these states as well, in which the rate constants for the slow exchanging water are $^{34}k_1 = 1.9 \pm 0.3$ s^{-1} for the S_2 state and $^{34}k_1 = 0.022 \pm 0.002$ s^{-1} for the S_1 state. These rate constants are almost identical to those reported for the slow component in the S_2 and S_1 states in thylakoids (Hillier and Wydrzynski, 2000). However, as in the measurements of thylakoids, rate constants for the fast component in PSII-enriched samples remain unresolvable, where $^{34}k_2 \geq 175$ s^{-1} for the S_2 state is limited by the injection response time and $^{34}k_2 > 100$ s^{-1} for the S_1 state is limited by the total time of the turnover flash sequence. This data provides evidence to show that treatment with 5% Triton X-100 has little effect on the overall substrate-water binding through the S-state cycle and that the biphasic exchange behavior is inherent to PSII.
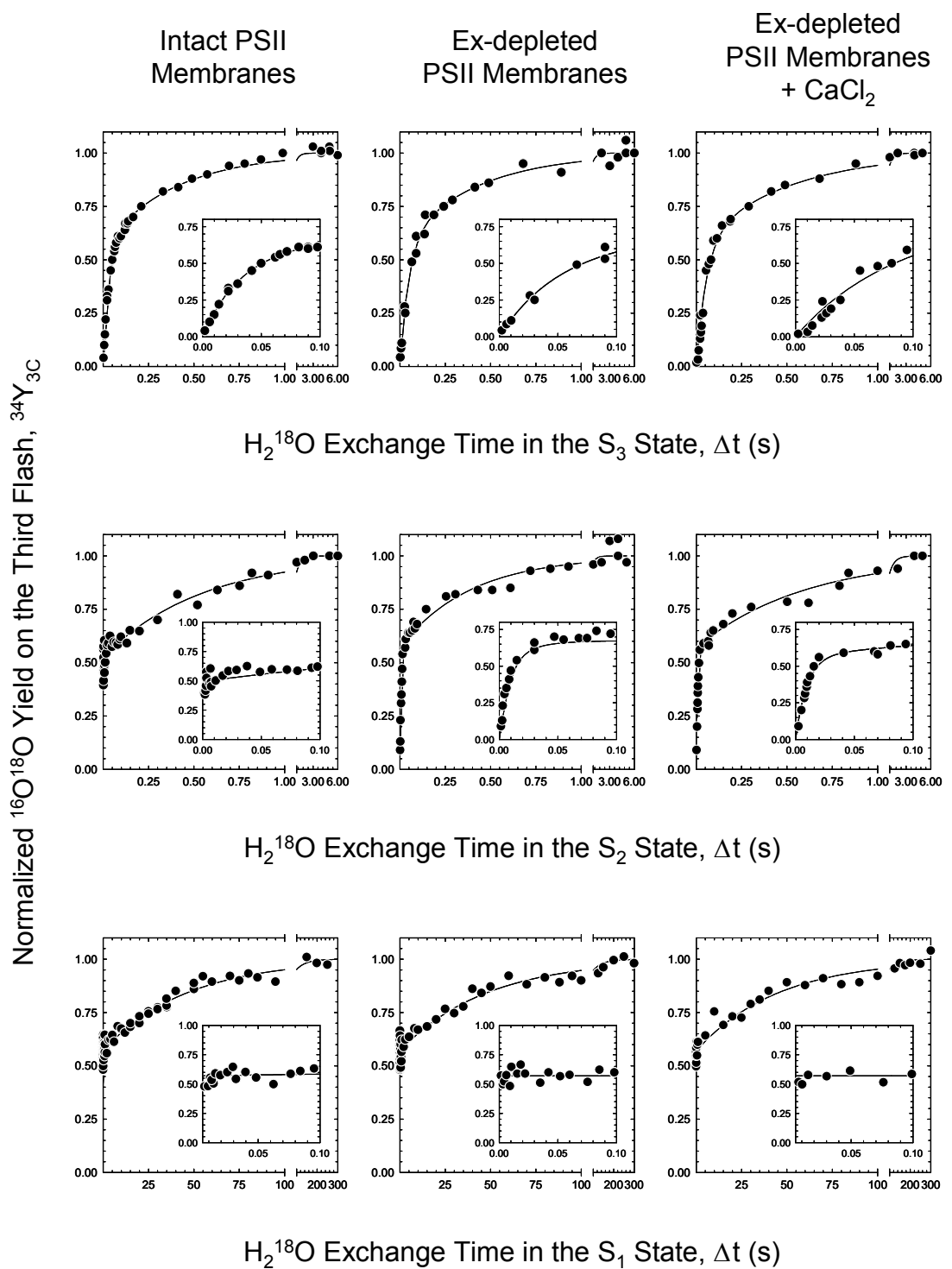
Figure 3-3 ^{18}O exchange measurements in the S_3, S_2 and S_1 states for intact PSII membranes, Ex-depleted PSII membranes and Ex-depleted PSII membranes incubated for 2 h in 15 mM $CaCl_2$. Measurements were made at $m/e = 34$ as a function of the exchange time (Δt) at 10^oC. Solid lines are a kinetic fit to the corrected O_2 yield on the third flash ($^{34}Y_{3C}$) according to Equation 2-6. The graph inset reveals an expanded time ordinate for the first 100 ms. Note that the differing time axes are set according to the kinetic parameters. Each data point represents a 30 min measurement.

Table 3-1 O_2-evolving activities at 25⁰C, Kok parameters and ^{18}O exchange rate constants determined at $m/e = 34$ at 10⁰C for the variously treated PSII-enriched membrane samples

| | O_2-evolving activity | | Kok parameters | | ^{18}O exchange rate constants[*] | | | | | |
| | | | | | S₃ state | | S₂ state | | S₁ state | |
	[1]rate	% cont.	[2]α (%)	[3]β (%)	$^{34}k_1\ (s^{-1})$	$^{34}k_2\ (s^{-1})$	$^{34}k_1\ (s^{-1})$	$^{34}k_2\ (s^{-1})$	$^{34}k_1\ (s^{-1})$	$^{34}k_2\ (s^{-1})$
PSII Membranes	862 ± 63	100	10.5	9.2	2.5 ± 0.2	30 ± 2	1.9 ± 0.3	≥ 175	0.022 ± 0.003	> 100
[4]Ex-depleted PSII Membranes	200 ± 6	23	25.2	18.5	2.4 ± 0.5	20 ± 3	2.6 ± 0.3	120 ± 14	0.021 ± 0.003	> 100
[5]Ex-depleted PSII Membranes + $CaCl_2$	696 ± 18	81	11.0	11.5	2.0 ± 0.7	18 ± 4	1.6 ± 0.2	102 ± 8	0.022 ± 0.003	> 100
[6]Ex-depleted PSII Membranes + $MgCl_2$	208 ± 21	24	26.3	19.3	2.3 ± 0.7	26 ± 6	1.6 ± 0.3	98 ± 10	[7]n.d.	n.d.

[1]rate of O_2-evolution expressed as μmol O_2 (mg Chl)$^{-1}$ h^{-1}; [2]miss parameter; [3]double hit parameter; [4]PSII membranes depleted of the 17 and 23 kDa extrinsic proteins; [5,6]Ex-depleted PSII membranes incubated for 2 h in 15 mM $CaCl_2$ or $MgCl_2$; [7]not determined; [*]see text for details.

Although the resolution of the fast phase kinetics in the S_2 state is limited by the injection response (i.e., $k_{inj} = 175$ s^{-1}), closer examination of the data in Figure 3-3 reveals a *hint* of a resolvable fast phase component, with a number of $^{34}Y_{3C}$ values of $\leq$ 0.50 measured at short exchange times ≤ 15 ms. This behavior is also apparent in the exchange data for the S_2 state in thylakoids (Hillier and Wydrzynski, 2000; Hillier, 1999). In exploring the role of the 17- and 23-kDa extrinsic proteins in the mechanism of O_2 evolution, we initially found for Ex-depleted PSII samples in the S_3 state there is a slowing down in the fast phase component by ~30% compared with the control (Hillier et al., 2001). The same effect is clearly demonstrated in the S_3 state data shown in Figure 3-3, where $^{34}k_2$ decreases from 30 ± 2 s^{-1} to 20 ± 3 s^{-1} (Table 3-1). More importantly, however, a similar trend is also observed for the S_2 data, to the point where the fast component now becomes completely resolvable and yields $^{34}k_2 = 120 \pm 14$ s^{-1} (Table 3-1). Interestingly, the slow exchange component remains unaffected under these conditions. To confirm this last observation, measurements were also made at *m/e* $= 36$ (which measures the $^{18}O^{18}O$ product) for Ex-depleted PSII in the S_2 state. The data is shown in Figure 3-4 and reveals only a single exchange component with a corresponding rate constant of 2.5 ± 0.2 s^{-1} (Table 3-2). This value is virtually identical to $^{34}k_1$ in the S_2 state (Table 3-1) and confirms that the rate of $^{18}O^{18}O$ formation is limited by the substrate-water undergoing the slowest exchange process. These results conclusively show that under these conditions, the second substrate-water molecule is bound to the catalytic site in the S_2 state.
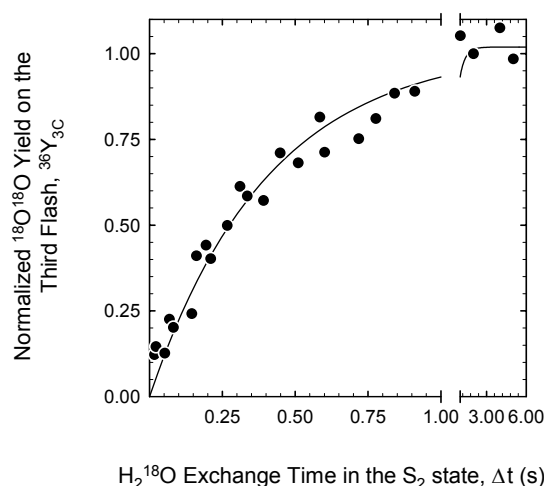
Figure 3-4 **^{18}O exchange measurements made at *m/e* = 36 for Ex-depleted PSII membranes in the S_2 state at 10°C. The solid line is a kinetic fit to the corrected O_2 yield after the third flash in the turnover sequence ($^{36}Y_{3C}$) according to Equation 2-5.**

Table 3-2   Comparison of the ^{18}O exchange rates determined at *m/e* = 34 and *m/e* = 36 (^{36}k) for PSII-enriched membranes and Ex-depleted PSII-enriched membranes in the S_3 and S_2 states at 10°C

	S$_3$ State			S$_2$ State		
	^{36}k (s^{-1})	$^{34}k_1$ (s^{-1})	$^{34}k_2$ (s^{-1})	^{36}k (s^{-1})	$^{34}k_1$ (s^{-1})	$^{34}k_2$ (s^{-1})
PSII membranes	2.4 ± 0.2	2.5 ± 0.2	30 ± 2	[1]n.d.	1.9 ± 0.3	≥ 175
[2]Ex-depleted PSII	2.4 ± 0.4	2.4 ± 0.5	20 ± 3	2.5 ± 0.2	2.6 ± 0.3	120 ± 14

[1]not determined; [2]PSII membranes depleted of the 17- and 23-kDa extrinsic proteins.

A similar trend could not be observed for the S_1 state of Ex-depleted PSII, where the fast exchange component remains unresolvable (i.e. $^{34}k_2$ > 100 s^{-1}). There are no $^{34}Y_{3C}$ points ≤ 0.50 measured at short ^{18}O-exchange times. However, like in the S_2 and S_3 states, the slow rate of exchange in the S_1 state is virtually unaffected by the removal of the 17- and 23-kDa proteins. The $^{34}k_1$ value in the S_1 state is 0.021 ± 0.003 s^{-1} (Table 3-1) and is nearly identical to the corresponding rate constant obtained for the control PSII-enriched sample (Table 3-1) as well for intact thylakoids (Hillier and Wydrzynski, 2000).

The 17- and 23-kDa extrinsic proteins are known to modulate the binding affinity of the functional Ca2+ (Ghanotakis et al., 1984), in which the removal of these proteins leads to a slow release of Ca2+. After long incubation times (1-2 h), the resulting low O2 evolution activity in Ex-depleted PSII samples can be restored to ~80% of the control level by the addition of millimolar concentrations of CaCl2 (Table 3-1). The addition of CaCl2 also restores back the normal O2 flash oscillations (Figure 3-2). In view of these observations, we measured the 18O-exchange behavior of Ex-depleted PSII samples in the presence of 15 mM CaCl2. The results are shown in Figure 3-3 and the corresponding rate constants are listed in Table 3-1. In the S_3 state $^{34}k_1$ = 2.0 ± 0.7 s^{-1} and $^{34}k_2$ = 18 ± 4 s^{-1}, in the S_2 state $^{34}k_1$ = 1.6 ± 0.2 s^{-1} and $^{34}k_2$ = 102 ± 8 s^{-1}, and in the S_1 state $^{34}k_1$ = 0.022 ± 0.003 s^{-1} and $^{34}k_2$ > 100 s^{-1}. Comparison of these data with the ^{18}O-exchange measurements made on Ex-depleted PSII alone shows that there is no further effect of Ca^{2+} under these conditions. The addition of Mg^{2+} instead of Ca^{2+} has little effect on the ^{18}O-exchange rates, with values of $^{34}k_1$ = 2.3 ± 0.7 s^{-1} and $^{34}k_2$ = 26 ±

6 s^{-1} for the S$_3$ state and $^{34}k_1 = 1.6 \pm 0.3$ s^{-1} and $^{34}k_2 = 98 \pm 10$ s^{-1}, respectively for the S$_2$ state. Thus, the specific slowing down in the rate of fast exchange in the S$_3$ and S$_2$ states of Ex-depleted PSII samples is due only to the loss of the 17- and 23-kDa extrinsic proteins.

3.4 DISCUSSION

Based on the time resolution of the current experimental set-up (~6 ms), a measurable kinetic isotope effect will conclusively show the existence of bound substrate-water in PSII. This is justified by the observations that O_2 release upon the $S_3 \rightarrow [S_4] \rightarrow S_0$ transition occurs in ~2 ms (Razeghifard and Pace, 1999) while the rest of the S-state cycle from S_0 to S_3 takes at most another 1 ms (Babcock et al., 1976; Razeghifard et al., 1997). Thus, any ^{18}O-exchange that is slower than ~3 ms will be indicative of bound water. Hence, the exact determination of the slow phase ^{18}O-exchange kinetics in the S_0, S_1, S_2, and S_3 states (Hillier and Wydrzynski, 2000) conclusively showed that one substrate water molecule is bound to the OEC throughout the S-state cycle. However, since the fast phase ^{18}O-exchange kinetics in the earlier measurements could only be resolved in the S_3 state, the possibility remained opened that the second substrate water molecule binds to the OEC only after the formation of the S_3 state.

In an effort to address the possible influence of the 17- and 23-kDa extrinsic proteins on substrate-water binding, measurements of the S-state dependent ^{18}O-exchange were extended to PSII-enriched membrane samples depleted of these proteins (Ex-depleted PSII). Interestingly, following the removal of the proteins the rate constant for the fast exchange component in the S_3 state decreases by ~30%, from 30 ± 2 s^{-1} to 20 ± 3 s^{-1} (Table 3-1), while the rate constant for the slow exchange component remains virtually unchanged. However, most importantly, in the S_2 state there is also a slowing down of the fast exchange component, to the point where it is kinetically resolved for the first time using the current experimental set-up. As in the S_3 state, there is virtually no effect in the Ex-depleted PSII sample on the slow exchange component in the S_2 state (Figure 3-3, Table 3-1).

The fact that two distinct ^{18}O-exchange rates can be measured in the S_2 state of Ex-depleted PSII indicates that *both* substrate water molecules must be bound to the OEC under these conditions. Although we cannot unambiguously determine the fast phase exchange kinetics in the S_2 state for native PSII samples, closer examination of the ^{18}O-exchange data reveals a *hint* of a resolvable fast exchange component. For both PSII-enriched membrane preparations (Figure 3-3) and thylakoids (Hillier and Wydrzynski, 2000), a number of $^{34}Y_{3C}$ values ≤ 0.50 at exchange times ≤ 15 ms can be measured outside of the expected error. For Ex-depleted PSII in the S_3 state, there is a slowing down of the fast exchanging water by ~30%. Assuming a similar trend in the S_2 state,

where the fast component is at the detectable kinetic limit of 175 s^{-1} (due to the injection response), then it is likely that *both* substrate-water molecules are bound to the OEC in the S_2 state of the intact system as well.

In support of the above arguments, it is noted that the removal of the 17- and 23-kDa extrinsic proteins from PSII results in a much lower overall O_2-evolving activity, which can be largely restored by the addition of 15 mM $CaCl_2$ (Table 3-1). Upon measuring the ^{18}O-exchange of Ex-depleted PSII in the presence of $CaCl_2$, the fast exchange component in the S_2 state still remains resolvable with $^{34}k_2 = 102 \pm 8$ s^{-1}. Thus, even in this highly active sample, both substrate-water molecules must be bound to the OEC in the S_2 state and it is the loss of the 17- and 23-kDa extrinsic proteins that slows down the rate of fast exchange.

In contrast, no effect of the protein removal was observed in the ^{18}O-exchange behavior in the S_1 state, in which the fast phase component remains completely unresolved. This last observation leaves open the possibility that the second substrate-water molecule binds to the OEC only after the formation of the S_2 state.

It is important to note that the slow phase ^{18}O-exchange kinetics in the S_3, S_2 and S_1 states remain virtually unaffected by the removal of the 17- and 23-kDa extrinsic proteins and that only the fast phase kinetics in the S_3 and S_2 states are slowed down. We have argued that the local dielectric around the substrate binding sites can influence the ^{18}O-exchange kinetics (Hillier et al., 2001). Thus, it could be that the removal of the 17- and 23-kDa proteins increases the exposure of the fast exchanging site to the solvent water. A consequent increase in the regional hydration around this site could then give rise to a change in the local dielectric (Dwyer et al., 2000; Pitera et al., 2001) and an altered ^{18}O-exchange rate. Interestingly, there would have to be an asymmetry in the dielectric distribution within the OEC, since the slow exchanging site is unaffected by the removal of the proteins. Such a situation would strongly imply that the two substrate binding sites are located in different chemical environments. This is illustrated in Scheme 3-1.

CaMn$_4$

Intact OEC

H$_2$O—⌐—OH$_2$

~ 60 Å to lumen

OH$_2$

OH$_2$

OH$_2$

OH$_2$

CaMn$_4$

Ex-depleted OEC

H$_2$O—⌐—OH$_2$

~ 10 Å to lumen

OH$_2$

OH$_2$

OH$_2$
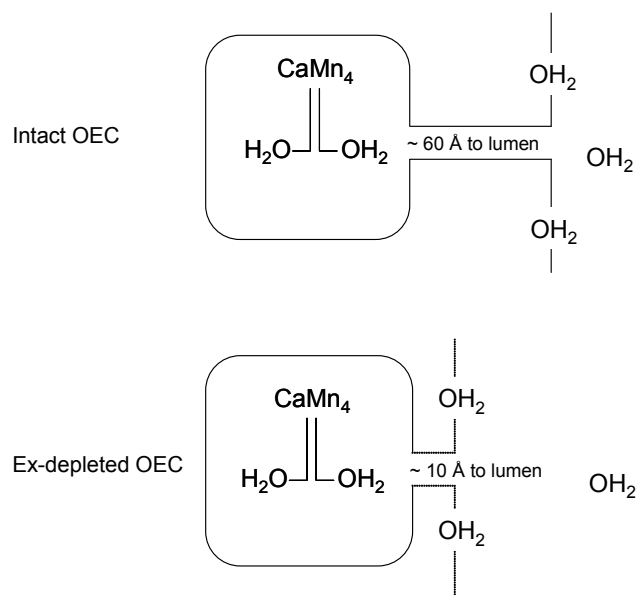
Scheme 3-1   Increased solvent-water penetration at the catalytic site following the removal of the 17- and 23-kDa extrinsic proteins.

Indeed, recent experimental evidence has shown that there can be an increase in the regional polarizability of a protein when the water permeability increases (Dwyer et al., 2000). The energetic cost of water permeation can be estimated from the energy of a charge-dipole interaction according to Equation 3-6:

$$\Delta G \text{ (kJ/mol)} = \frac{-289.11 Z \mu \cos\theta}{D r^2}$$

<div align="right">Equation 3-6</div>

where Z is the charge interacting with μ, the dipole moment of water (1.84 Debye), θ is the orientation of the of the dipole (assumed to be aligned with the magnetic field of the charge, i.e., $\theta = 180^\circ$), D is the dielectric and r the distance in Å. Assuming the effective dielectric constant of the OEC is similar to that determined for P$_{680}$ ($\varepsilon_{eff} = 8$; Mulkidjanian et al., 1996; Haumann et al., 1997), then a water molecule 5 Å from the Mn cluster will incur an energetic cost of 2-3 kJ/mol per unit of charge. Based on the activation energy calculations for the ^{18}O-exchange rates (Hillier et al., 1998), the observed decrease in the fast rate of exchange ($^{34}k_2$) for Ex-depleted PSII in S$_3$ and S$_2$ states reflects an energy difference of similar proportion.

In view of these findings, it is unlikely that the 17- and 23-kDa extrinsic proteins form a substrate accessibility barrier between the aqueous solvent environment and the hydrophobic pocket of the OEC, although a proposed role for the 33-kDa protein in this process should not be excluded at this point. Unfortunately, removal of the 33-kDa subunit in higher plants ($\geq$ 1 M CaCl$_2$ treatment; Ono and Inoue, 1983) also involves removal of the 17- and 23-kDa subunits as well, and yields a preparation that is of insufficient activity for determining the substrate-water binding properties unless elevated concentrations of CaCl$_2$ are present. However, given the Ca^{2+}-independent effect on the ^{18}O exchange behavior in Ex-depleted PSII, it would be interesting to determine the rates of ^{18}O exchange for the aforementioned preparation measured in the presence of ~mM concentrations of CaCl$_2$. These measurements will be the focus of future work.

Chapter 4   Calcium/Strontium Effects on

Substrate-Water Binding

4.1 INTRODUCTION

4.1.1 The Role of Ca^{2+} in O_2-Evolution

Calcium is an essential constituent of the oxygen evolving complex although its exact mechanistic role has not been properly established. Calcium is absolutely required for optimal O_2-evolving activity by photosystem II; its depletion abolishes the activity which can be partially restored by the addition of non-physiological concentrations of Ca^{2+}, or to a lesser extent, Sr^{2+} (Ghanotakis et al., 1984; Ono and Inoue, 1988; Boussac and Rutherford, 1988b; Yocum, 1991). The addition of Sr^{2+} to Ca^{2+}-depleted preparations was shown to reactivate the same number of centers as Ca^{2+}, but with slower turnover of the S-state cycle producing a lower overall rate of O_2-evolution at saturating light intensities (Boussac and Rutherford, 1988b; Boussac et al., 1992; Westphal et al., 2000). Removal of the 17- and 23-kDa extrinsic proteins facilitates Ca^{2+} release, while preparations depleted of these proteins require elevated concentrations of Ca^{2+} (and Cl^-) for optimal O_2-evolving activity (Ghanotakis et al., 1985; Miyao and Murata, 1985). These observations have led to the suggestion that the extrinsic proteins modulate the binding affinity of the Ca^{2+}-site by providing a low dielectric environment in the vicinity of the OEC (Vrettos et al., 2001a; Vander Meulen et al., 2002).

A number of different roles have been proposed for Ca^{2+} in the mechanism of O_2-evolution. Early suggestions implicated a structural role in maintaining the stability of the Mn_4 cluster (Ghanotakis and Yocum, 1990) and/or in optimizing the structure of the local ligand environment (Yocum, 1991). However, many have argued that if the role of Ca^{2+} within the OEC were purely structural, then other metal cations with similar properties to Ca^{2+} would at least restore back partial activity to Ca^{2+}-depleted preparations (e.g. Vrettos et al., 2001a). Interestingly, Sr^{2+} is the only other metal cation that yields a functionally active site. Moreover, a recent study by Bouckaert et al. (2001) showed that divalent metal ions in general can bind to the Ca^{2+}-site in concanavalin A with limited perturbation to the overall protein structure. Interestingly, Cd^{2+}, which has an ionic radius very similar to that of Ca^{2+} (0.97 *versus* 0.99 Å, respectively), restored back the concanavalin A activity (Pandolfino et al., 1980), yet if anything is inhibitory to PSII (Vrettos et al., 2001a). The significance of this finding is discussed later.

Indeed, the many functional roles proposed for Ca^{2+} in O_2-evolution are classified according to either (1) direct involvement in the formation of the O-O bond or (2) a more general role in optimizing the catalytic efficiency of the OEC. The former role is consistent with the many mechanistic models that promote Ca^{2+} as a substrate binding site within the OEC reaction sphere (Pecoraro et al., 1998; Vrettos et al., 2001b; Kuzek and Pace, 2001) while more general roles for Ca^{2+} include regulating electrostatic constraints of the OEC manifested by pK_a shifts of carboxylate groups throughout the S-state cycle (Boussac et al., 1992), providing a docking site for the Cl⁻ cofactor (Tommos and Babcock, 1998) and in a gate-keeper type role (Sivaraja et al., 1989; Vander Meulen et al., 2002).

4.1.2   Structural Properties of the Ca^{2+}-Binding Site

Although the recent 3.8 Å X-ray crystal structure of *Synechococcus elongatus* (Zouni et al., 2001) has identified the position, size and shape of the associated Mn_4 electron density map, it failed to provide any detailed information for the location of Ca^{2+}, despite the mounting experimental evidence for the structural proximity of Ca^{2+} to the Mn_4 complex (Noguchi et al., 1995; Booth et al., 1996; Latimer et al., 1998; Cinco et al., 1998). The Ca^{2+}-site has been extensively probed using a number of different techniques. EXAFS measurements indicate a significant Mn-Ca^{2+}(Sr^{2+}) interaction at ~3.3 Å (Latimer et al., 1995; Cinco et al., 1998) while further measurement of the Mn fine edge spectra for Ca^{2+}-depleted preparations revealed that the ~3.3 Å Fourier peak is strongly diminished in three modified S-states (S_1', S_2' and S_3'; Latimer et al., 1998). The latter result is consistent with the assignment of Mn-Mn *and* Mn-Ca interactions at this distance (reviewed in Robblee et al., 2001). Other measurements suggest that Ca^{2+} is connected with the manganese cluster *via* a carboxylate bridge (Yachandra et al., 1993). This was later confirmed by Noguchi et al. (1995) who identified COO⁻ stretching modes of an aspartate or glutamate residue interacting with Ca^{2+}. Comparison of the S_2/S_1 FTIR difference spectra from native and Ca^{2+}-depleted preparations revealed that certain positive (S_2) and negative (S_1) spectral features were lost following the specific removal of Ca^{2+} from these preparations.

Experiments involving metal ion replacement of the Ca^{2+}-site have also been used in an attempt to elucidate the role of Ca^{2+} in O_2-evolution. Two main factors will determine the selectivity of the Ca^{2+}-site: (1) the size of the binding cavity and (2) the negative charge density of the ligand array (Vrettos et al., 2001a). Using steady state enzyme

kinetics, Vrettos et al. (2001a) examined the reversible inhibition of O_2-evolution by a series of mono-, di- and tri-valent metal cations that compete with Ca^{2+} for its binding site within the OEC. The results indicated that the Ca^{2+}-site is highly size selective; only di-valent and tri-valent metal cations of similar ionic radii to Ca^{2+} were found to compete with Ca^{2+} for its binding site. The inhibition of O_2-evolution by tri-valent cations has been effectively excluded from nature owing to the limited concentration of these cations *in vivo* while the authors proposed that mono-valent cations are unable to bind to the Ca^{2+}-site due to the high negative charge density of the carboxylate oxygens that typically comprise the coordinating array of Ca^{2+}-sites. In support of these arguments is the observation that Na^+, with an ionic radius very close to that of Ca^{2+}, showed no inhibitory effect on O_2-evolution even at high (molar) concentrations. However, this conclusion is in contradiction with results obtained by Ono et al. (2001) who measured competitive inhibition of O_2-evolution by K^+, Rb^+ and Cs^+ and interestingly all of which have larger ionic radii than Ca^{2+}. In conjunction with intermediate measurements of the thermoluminescence (TL) and S_2 state EPR, the authors provided conclusive evidence to show that the Ca^{2+}-site is indeed occupied by K^+, Rb^+ and Cs^+. Moreover, the effects of Ca^{2+}-site substitution with mono- and di-valent metal cations on the structure of the protein matrices of the OEC were examined using FTIR spectroscopy (Kimura et al., 2002). Substitution with K^+, Rb^+ and Cs^+ perturbed the protein matrices in the vicinity of the Mn_4 cluster that interrupted the structural and/or conformational rearrangements during the $S_1 \rightarrow S_2$ transition. Cation substitution also induced new vibrational modes in the S_1/S_2 difference spectra that disappeared following reconstitution with Ca^{2+}. The data illustrate that the role of Ca^{2+} within the OEC extends beyond its physical properties (i.e., valence and ionic radius).

4.1.3 The Redox and Magnetic Properties of Ca^{2+}-depleted OEC

Magnetic resonance measurements have also been extensively applied to the study of the Ca^{2+}- site. For Ca^{2+}-depleted preparations, redox transitions beyond the S_3 state are interrupted while the formation of novel EPR signals (denoted here as S_n') suggests that the magnetic environment of the Mn_4 cluster is perturbed. The S_2' state multiline signal is stable for long periods of time (hours) at room temperature, while narrower hyperfine ^{55}Mn splittings (55 G *versus* 88 G for the native sample) and more lines (at least 25) indicate that the ligand character to the Mn is disrupted (Boussac et al., 1989; Sivaraja et al., 1989; Ono and Inoue, 1990). Interestingly, formation of the S_2' state EPR signal was shown to be dependent on the presence of chelators used during the Ca^{2+}-depletion

procedure (e.g., citrate, EGTA, EDTA) although the line shape and stability of the signal does not exhibit variations depending on chelator (Boussac et al., 1990a; Ono and Inoue, 1990). Further illumination at 277 K resulted in the formation of a broad spectral feature centered at $g = 2$ which was ascribed to a formal S_3' state. The identity of the organic radical responsible for the S_3' signal was initially assigned to oxidized histidine (Boussac et al., 1990b; Berthomieu and Boussac, 1995), although alternative models based on ENDOR and ESSEM spectra suggest that the radical is in fact $Y_Z^\bullet$ (Hallahan et al., 1992; Gilchrist et al., 1995; Tang et al., 1996; Force et al., 1997). Additionally, recent EPR data from Ono's laboratory suggests that the redox transitions in Ca^{2+}-depleted OEC are more complex than was previously thought (Astashkin et al., 1997; Mino et al., 1998). Two new EPR signals at $g = 11$ and 15 were detected in Ca^{2+}-depleted PSII preparations following two turnovers of the OEC beyond the modified S_2' state. The S (spin) $= 2$ signals are thought to arise from a Mn(IV)-Mn(IV) or Mn(III)-Mn(III) dimer or a Mn(III) monomer (Mino et al., 1998).

The binding of metal cations to the Ca^{2+}-site also modifies the redox and magnetic properties of the Mn_4 cluster. Membrane preparations reconstituted with Sr^{2+} induced the formation of the $g = 4.1$ S_2 state split signal concomitant with a decrease in the overall intensity of the multiline signal (Boussac and Rutherford, 1988b). The modified character of the MLS (decreased line spacing and redistributed splittings) indicates that the magnetic properties of the Mn_4 cluster are somehow altered when the Ca^{2+}-site is occupied by Sr^{2+}. Further studies involving alkali metal cation substitution also revealed that the physical properties of the OEC are modified. Preparations supplemented with either K^+, Rb^+ or Cs^+ exhibit altered redox properties as indicated by an up-shift in the thermoluminescence (TL) band while neither $g = 4.1$ nor multiline signals were detected in these samples (Ono et al., 2001).

4.1.4 Experimental Aims

The specificity of Ca^{2+} for O_2-evolution highlights its functional importance in optimizing structural, redox and magnetic constraints of the OEC. Indeed, many of the current mechanistic models for O_2-evolution invoke Ca^{2+} as a substrate-binding site within the reaction sphere of the catalytic site (Pecoraro et al., 1998; Siegbahn, 2000; Vrettos et al., 2001b; Kuzek and Pace, 2001). To address this proposal, the rates of ^{18}O exchange were determined for Ca^{2+}-depleted preparations reconstituted with either $SrCl_2$ or $CaCl_2$.

Previous investigations of Ca^{2+}-depleted preparations has identified problems associated with the extent of Ca^{2+}-release from PSII. Accordingly, Ca^{2+}-depleted preparations were obtained using (1) low pH/citrate treatment (Ono and Inoue, 1988) and (2) NaCl/A23187/EGTA washing of native PSII-enriched membranes (Kalosaka et al., 1990; Vrettos et al., 2001a). The results are presented in terms of the S-state dependent effects of Sr^{2+}-reconstitution on the ^{18}O exchange behavior.

4.2 MATERIALS AND METHODS

4.2.1 Ca²⁺-Depletion Procedures

4.2.1.1 Preparation of Ca²⁺-Depleted PSII

Acid induced Ca^{2+}-depletion from PSII membranes was performed according to the low-pH/citrate treatment of Ono and Inoue (1988) using the modifications of Latimer et al. (1995). Samples were washed in 0.25 mM MES/NaOH (pH 6.3), 15 mM NaCl and 400 mM sucrose and resuspended at 4 mg Chl mL^{-1}. The samples were then diluted with an equal volume of citrate buffer (20 mM citrate (pH 3.0), 15 mM NaCl, 400 mM sucrose), and incubated at 0°C for 5 min with gentle stirring. The preparation was then immediately bought to physiological pH by diluting (1:2) in a wash buffer consisting of 50 mM MES/NaOH (pH 6.3), 15 mM NaCl, 400 mM sucrose (Ultragrade, BDH) and 100 μM EGTA. The Ca^{2+}-depleted membranes were collected by centrifugation at 36000 × g for 20 min at 4°C and resuspended in the same wash buffer (25 mM MES/NaOH pH 6.3 instead of 50 mM MES/NaOH pH 6.3) containing either 50 mM SrCl$_2$ or 50 mM CaCl$_2$ (or no addition for Ca^{2+}-depleted samples). The Sr- or CaCl$_2$-containing buffers were allowed to equilibrate with the sample for 2-3 h at 4°C. Finally, the sample was pelleted and resuspended in a small amount of the supernatant and then frozen in liquid N$_2$ and stored at –80°C until measurement. All glassware and centrifuge tubes were washed with 2 M HNO$_3$ and the buffers used were treated with Chelex-100 (Bio-Rad) to ensure minimal Ca^{2+} contamination from the chemicals used.

4.2.1.2 Preparation of Ca²⁺/Ex-depleted PSII

An alternative method for depleting Ca^{2+} from photosystem II involves a combined NaCl/EGTA/A23187 treatment to remove both the functional Ca^{2+} ion and the 17- and 23-kDa extrinsic proteins (Kalosaka et al., 1990; Vrettos et al., 2001a). Photosystem II membrane fragments were resuspended at 0.5 mg Chl mL^{-1} in 40 mM MES/NaOH (pH 5.0), 1.5 M NaCl, 1 mM EGTA and 20 μM A23187 and gently stirred for 2.5 h in the dark at 4°C. The sample was then pelleted by centrifugation at 36000 × g and washed using the same low pH buffer but lacking Ca^{2+} ionophore (A23187). This second low pH treatment was found to remove Ca^{2+} more completely from PSII (Brudvig, personal communication). The sample was then resuspended in a wash buffer consisting of 40 mM MES/NaOH (pH 6.3), 400 mM sucrose (Ultragrade, BDH), 15 mM NaCl and 1

mM EGTA and washed (twice) in the same buffer minus the EGTA. Following centrifugation at $36000 \times g$, the membranes were resuspended in the wash buffer (minus EGTA) containing either 50 mM $CaCl_2$ or 50 mM $SrCl_2$ and allowed to equilibrate for 2-3 h at $4^{\circ}C$. As with the low pH/citrate treatment described above, all glassware and centrifuge tubes used in this procedure were acid-washed and the buffers treated with Chelex-100 (Bio-Rad) to ensure minimal Ca^{2+} contamination from the chemicals used.

Details regarding the measurement of chlorophyll concentrations, steady state O_2-evolution, SDS-PAGE analysis, ^{18}O exchange, O_2 flash yield oscillations (and derivation of Kok parameters) has been outlined in Chapters 2 and 3.

4.3 RESULTS

Typical extraction procedures for the removal of Ca^{2+} from photosystem II employ a combination of NaCl, chelator(s) (citrate, EGTA, EDTA and/or chelex), illumination, low pH and the Ca^{2+} ionophore A23187. In this study, Ca^{2+}-depleted samples were prepared using (1) low pH/citrate (Ono and Inoue, 1988) (2) NaCl/A23187/EGTA treatment (Kalosaka et al., 1990; Vrettos et al., 2001a) of native PSII membranes. The high ionic strength exposure (i.e., > 1 M NaCl) of the NaCl/A23187/EGTA treatment targets the specific removal of the 17- and 23-kDa extrinsic subunits which are known to enhance the binding affinity of Ca^{2+} (and Cl^-) to the OEC. In contrast, the low pH/citrate treatment induces the temporary dislocation of the extrinsic proteins, which rebind to the holoenzyme under physiological conditions (i.e., at pH ~6.3-6.5). Hereafter, preparations depleted of Ca^{2+} using low pH/citrate treatment of PSII are referred to as 'Ca^{2+}-depleted PSII' and using the NaCl/A23187/EGTA treatment are referred to as 'Ca^{2+}/Ex-depleted PSII'.

To estimate the protein composition of Ca^{2+}-depleted samples prepared under low pH/citrate and NaCl/A23187/EGTA conditions, the Coomassie blue staining intensities of the extrinsic protein bands were determined using densitometry analysis of polyacrylamide gels run under denaturing/reducing conditions. The data presented in Table 4-1 shows that the low pH/citrate treatment of intact PSII leads to a ~20% loss of each of the three extrinsic subunits, while the combined NaCl/A23187/EGTA treatment results in > 97% of PSII centers that lack the 17- and 23-kDa extrinsic subunits (Table 4-1).

Table 4-1 **Extrinsic protein composition of Ca^{2+}-depleted and Ca^{2+}/Ex-depleted PSII preparations**

	[1]Normalized extrinsic protein composition		
	33-kDa	23-kDa	17-kDa
PSII membranes	1.00	1.00	1.00
[2]Ca^{2+}-depleted PSII	0.83	0.79	0.81
[3]Ca^{2+}/Ex-depleted PSII	0.91	0.03	0.02

[1]protein content was estimated from densitometry scans of the Coomassie blue staining intensities of extrinsic protein bands; [2]low pH/citrate induced Ca^{2+}-depletion of PSII membranes; [3]NaCl/A23187/EGTA induced Ca^{2+}-depletion of PSII membranes. Bands were normalized relative to CP47 to account for variation in protein loading between lanes.

As expected, removal of the OEC-bound Ca^{2+} from PSII largely inhibits O$_2$-evolution. The residual activities of Ca^{2+}-depleted and Ca^{2+}/Ex-depleted PSII are 5% and 2%, respectively, of the rate determined for native PSII membranes (Table 4-2). Partial reconstitution of the activity is achieved by incubating these preparations in 25 mM CaCl$_2$ or SrCl$_2$ for extended periods of time (*viz* 2-3 h). Rates of O$_2$-evolution for Ca^{2+}-depleted preparations reconstituted with CaCl$_2$ are 63% of the control activity, and 32% for preparations reconstituted with SrCl$_2$, while a similar trend is also observed for Ca^{2+}/Ex-depleted PSII with rates of 47% and 19% of the control activity, respectively (Table 4-2). The extent of irreversible damage caused to a given population of PSII centers using the different Ca^{2+}-extraction conditions might explain the different degree of reconstitution observed between preparations. In theory, maximum rates of recovery will be limited to ~80% in Ca^{2+}-depleted PSII and ~90% in Ca^{2+}/Ex-depleted PSII according to the population of centers that retain the 33-kDa protein (Table 4-1).

Table 4-2   O₂-evolving activities and Kok parameters for Ca^{2+}-depleted PSII membranes

	O₂-evolution		Kok parameters	
	[1]rate	% of cont.	[2]α (%)	[3]β (%)
PSII membranes	681 ± 9	100	11.9	4.6
[4]Ca^{2+}-depleted PSII membranes	34 ± 7	5	[5]n.d.	n.d.
[6]Ca^{2+}-depleted PSII membranes + $CaCl_2$	429 ± 19	63	17.5	6.5
[7]Ca^{2+}-depleted PSII membranes + $SrCl_2$	219 ± 32	32	19.2	8.1
PSII membranes	767 ± 11	100	10.1	4.2
[8]Ca^{2+}/Ex-depleted PSII membranes	15 ± 8	2	n.d.	n.d.
[9]Ca^{2+}/Ex-depleted PSII membranes + $CaCl_2$	360 ± 15	47	18.1	7.3
[10]Ca^{2+}/Ex-depleted PSII membranes + $SrCl_2$	146 ± 22	19	21.7	9.2

[1]rates of O₂-evolution expressed as $\mu mol\ O_2\ (mg\ Chl)^{-1}\ h^{-1}$; [2]miss parameter; [3]double hit parameter; [4]low pH/citrate induced Ca^{2+}-depletion of native PSII membranes; [5]not determined; [6,7]low pH/citrate-treated PSII incubated for 2-3 h in 25 mM $CaCl_2$ and $SrCl_2$, respectively; [8]NaCl/A23187/EGTA induced Ca^{2+}-depletion of native PSII membranes; [9,10]NaCl/A23187/EGTA-treated PSII incubated for 2-3 h in 25 mM $CaCl_2$ and $SrCl_2$, respectively. See text for details.

Figure 4-1 shows the normalized O₂-flash yield oscillations at $m/e = 34$ for (A) Ca^{2+}-depleted PSII and (B) Ca^{2+}/Ex-depleted PSII reconstituted with $CaCl_2$ and $SrCl_2$. The measurements were made at $10^{o}C$ following complete isotopic equilibration after the addition of $H_2{}^{18}O$ (i.e., at an exchange time > 10 s). The Ca^{2+}-depleted samples reveal normal period four oscillations in the presence of $CaCl_2$ and $SrCl_2$ (Figure 4-1). According to the Kok analysis of these data (see Appendix 1), the effective miss parameter of Sr^{2+}-reconstituted preparations is 19.2% for Ca^{2+}-depleted PSII and 21.7% for Ca^{2+}/Ex-depleted PSII while for Ca^{2+}-reconstituted preparations, the effective miss parameters are 17.5% and 18.1%, respectively (Table 4-2). The heavier damping in the reconstituted membrane preparations correlates with the reduced steady-state O₂-

evolving activities in these samples, however, the period four oscillations indicate normal turnover of the S-states.
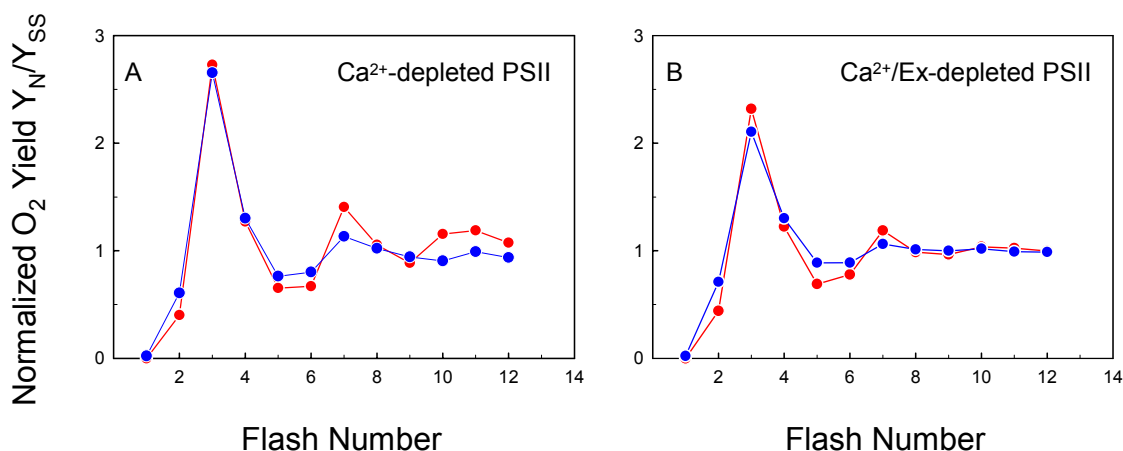
Figure 4-1 The O_2 flash yields are normalized to the steady state value of 1 at *m/e* = 34 for Ca^{2+}-depleted PSII membrane preparations reconstituted with 25 mM CaCl₂ (red circles) and SrCl₂ (blue circles). Measurements were made at 10°C following complete isotopic equilibration with $H_2^{18}O$. (A) Ca^{2+}-depleted PSII and (B) Ca^{2+}/Ex-depleted PSII. The derived miss and double hit parameters are listed in Table 4-2.

To determine the effect(s) of Sr^{2+} replacement of the Ca^{2+}-site on the substrate-water binding behavior, the rates of ^{18}O exchange were determined for Ca^{2+}- and Ca^{2+}/Ex-depleted PSII preparations reconstituted with 25 mM SrCl₂. Preparations depleted of Ca^{2+} and subsequently reconstituted with 25 mM CaCl₂ were used as a control in these measurements. The isotopic determinations of the flash-induced O_2 produced by the Ca^{2+}- and Sr^{2+}-reconstituted preparations were recorded at *m/e* = 34 in the S_3, S_2 and S_1 states at 10°C. The results are shown in Figure 4-2 where the corrected O_2 yields after the third flash in the turnover sequence ($^{34}Y_{3C}$) are plotted as a function of the $H_2^{18}O$ exchange time (Δt) in the various S-states. The data exhibit strong biphasic exchange behavior in all of the S-states measured. According to Equation 2-5, the rate constants for the slow and fast exchanging components are listed in Table 4-3. Comparison of these data indicate that the overall rates of ^{18}O exchange for Ca^{2+}-reconstituted preparations are nearly identical to that of intact PSII (Table 4-3). The only apparent exception is observed in the S_3 state data where the slow exchanging component yields $^{34}k_1 = 1.4 \pm 0.1$ s^{-1} compared to $^{34}k_1 = 2.5 \pm 0.2$ s^{-1} for intact PSII (Table 4-3). Similarly, analysis of the S_3 state data for Sr^{2+}-reconstituted preparations indicates that the fast phase component remains relatively unchanged, in which the rate constant of $^{34}k_2 = 23 \pm 5$ s^{-1} compares closely with the control value of $^{34}k_2 = 27 \pm 3$ s^{-1} for Ca^{2+}-reconstituted

and $^{34}k_2 = 30 \pm 2$ s^{-1} for intact PSII preparations. Like in the control samples, the rate of fast exchange remains unresolved in the S$_2$ and S$_1$ states of Sr^{2+}-reconstituted PSII where $^{34}k_2$ yields >175 s^{-1} and >100 s^{-1}, respectively.
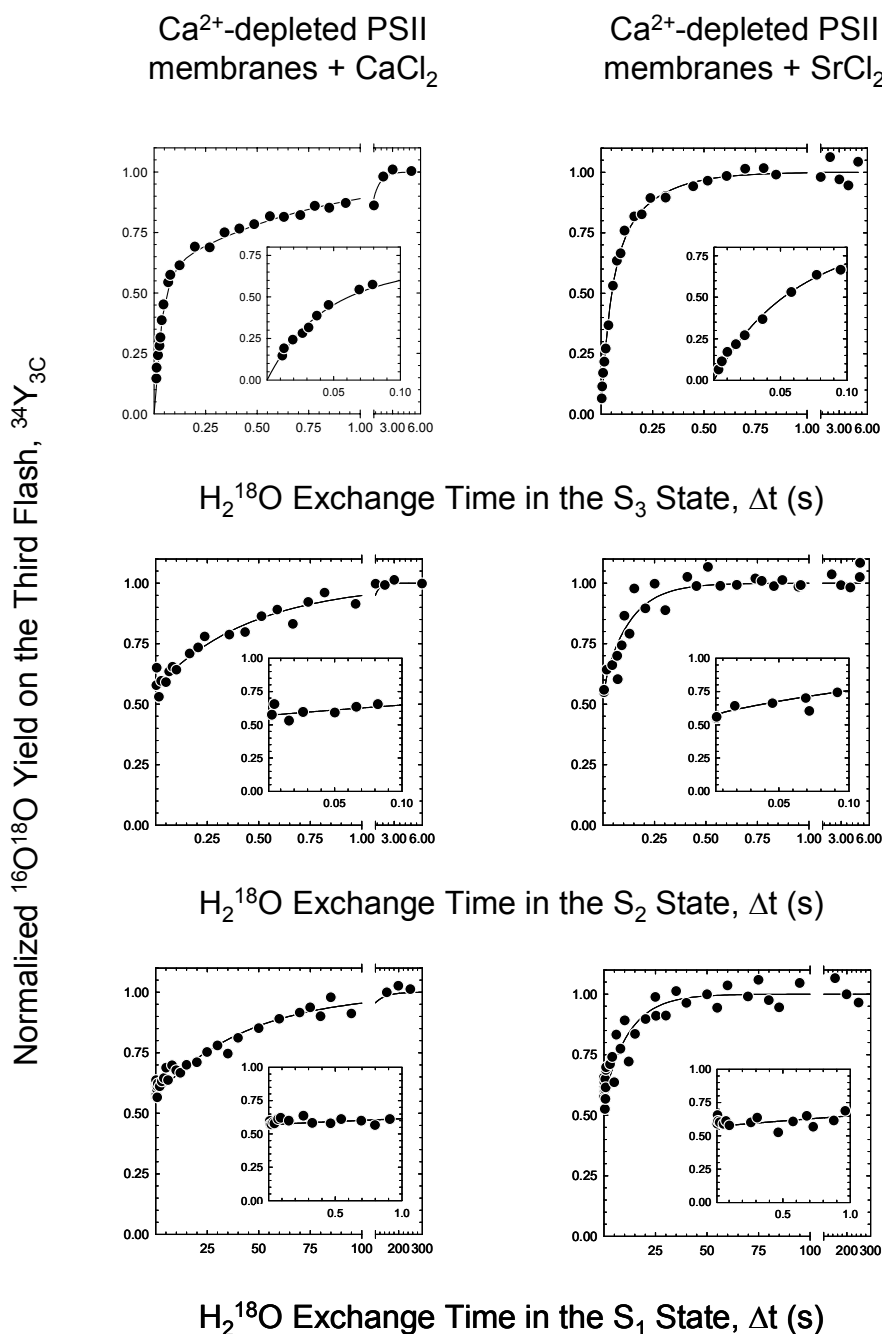
Figure 4-2 ^{18}O exchange measurements in the S$_3$, S$_2$ and S$_1$ states for Ca^{2+}-depleted PSII reconstituted with 25 mM CaCl$_2$ and SrCl$_2$. Measurements were made at m/e = 34 as a function of the exchange time (Δt) at 10°C. Solid lines are kinetic fits to the data according to Equation 2-6. The graph inserts reveal expanded time ordinates for the first 100 ms in the S$_3$ and S$_2$ state data and 1000 ms for the S$_1$ state data. Note the differing time axes are set according to the kinetic parameters. Each data point represents a 30 min measurement.

Table 4-3 ^{18}O exchange rate constants determined at m/e = 34 and m/e = 36 for Ca^{2+}- and Sr^{2+}-reconstituted PSII membranes at 10°C

	^{18}O exchange rate constants*								
	S$_3$ state			S$_2$ state			S$_1$ state		
	$^{34}k_1$ (s^{-1})	$^{34}k_2$ (s^{-1})	^{36}k (s^{-1})	$^{34}k_1$ (s^{-1})	$^{34}k_2$ (s^{-1})	^{36}k (s^{-1})	$^{34}k_1$ (s^{-1})	$^{34}k_2$ (s^{-1})	^{36}k (s^{-1})
[1]PSII Membranes	2.5±0.2	30±2	2.4±0.2	1.9±0.3	≥175	2.1±0.3	0.022±0.003	>100	n.d.
[2]Ca^{2+}-depleted PSII membranes+ CaCl$_2$	1.4±0.1	27±2	n.d.	2.1±0.3	>175	n.d.	0.023±0.002	>100	n.d.
[3]Ca^{2+}-depleted PSII membranes + SrCl$_2$	5.2±1.6	23±5	5.8±0.3	7.7±2.4	>175	9.4±0.6	0.082±0.012	>100	n.d.

[1]exchange rates obtained from Table 3-1; [2,3]low pH/citrate induced Ca^{2+}-depleteion of PSII membranes and reconstituted for 2-3 h in 25 mM CaCl$_2$ or SrCl$_2$. See text for

details.

The most significant finding is revealed by the data for the slow exchanging water in Sr^{2+}-reconstituted PSII (Figure 4-2, Table 4-3). In the S_3 state, there is a ~3-4-fold increase in exchange rate from $^{34}k_1 = 1.4 \pm 0.1$ s^{-1} in the Ca^{2+}-reconstituted control to $^{34}k_1 = 5.2 \pm 1.6$ s^{-1} in the Sr^{2+}-reconstituted PSII (Table 4-3). Interestingly, a similar trend is also observed in the earlier S-states where the exchange rates increase from $^{34}k_1 = 2.1 \pm 0.3$ s^{-1} to $^{34}k_1 = 7.7 \pm 2.4$ s^{-1} in the S_2 state and from $^{34}k_1 = 0.023 \pm 0.002$ s^{-1} to $^{34}k_1 = 0.082 \pm 0.012$ s^{-1} in the S_1 state, respectively, upon Sr^{2+}-reconstitution. To confirm this observation, measurements were also made at $m/e = 36$ for Sr^{2+}-reconstituted preparations in the S_3 and S_2 states which provides an independent determination of $^{34}k_1$. The data are presented in Figure 4-4 and as expected, reveal mono-exponential kinetics with corresponding rate constants of $^{36}k = 5.8 \pm 0.3$ s^{-1} for the S_3 state, and $^{36}k = 9.4 \pm 0.6$ s^{-1} for the S_2 state (Table 4-3). These values compare closely with the exchange rates obtained for the slow phase component in the $m/e = 34$ data where $^{34}k_1 = 5.2 \pm 1.6$ s^{-1} and 7.7 ± 2.4 s^{-1}, for the S_3 and S_2 states, respectively (Table 4-3). These data clearly indicate a Sr^{2+}-specific effect on the rate of the slow exchanging water across each of the S-states measured.
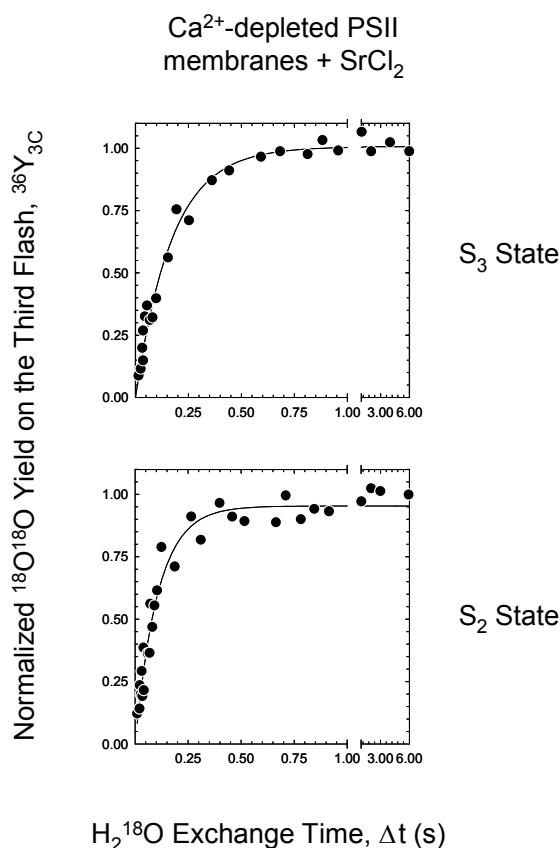
Figure 4-3 **^{18}O exchange measurements made at $m/e = 36$ for Ca^{2+}-depleted PSII reconstituted with 25 mM $SrCl_2$ in the S_3 and S_2 states at 10°C. Solid lines are kinetic fits to the corrected O_2 yield after the third flash in the turnover sequence ($^{36}Y_{3C}$) according to Equation 2-4.**

The ^{18}O exchange measurements were also extended to Ca^{2+}/Ex-depleted PSII reconstituted with CaCl$_2$ and SrCl$_2$ in the S$_3$ and S$_2$ states. The data presented in Chapter 3 clearly reveals a slowing down of the fast exchanging water by ~30% in the S$_3$ and S$_2$ states of Ex-depleted PSII, to the point where the fast kinetic component is resolved for the first time in the S$_2$ state (Figure 3-3, Table 3-1). For obvious reasons, it is expected a similar trend would extend to Ca^{2+}/Ex-depleted PSII. Moreover, the measurements provide an independent evaluation of the Sr^{2+}-induced effects on the ^{18}O exchange behavior (Figure 4-2, Table 4-3). The results are presented in Figure 4-4 and the corresponding rate constants determined according to the biphasic analysis of these data (Equation 2-6) are listed in Table 4-4.
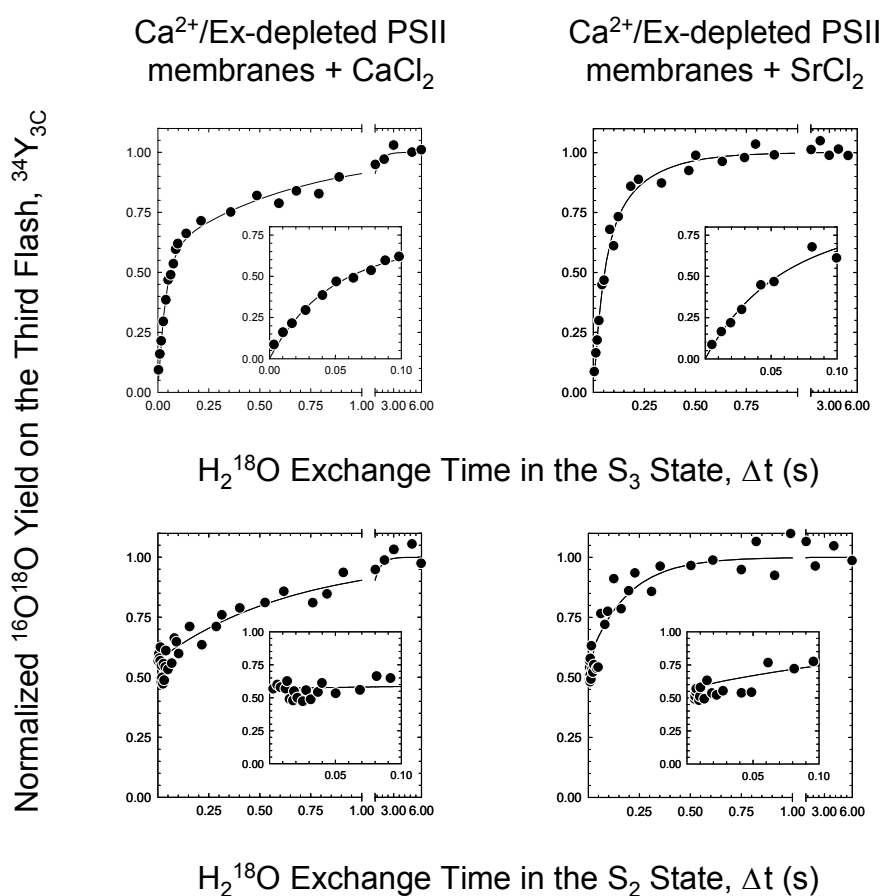
Figure 4-4 ^{18}**O exchange measurements in the S$_3$ and S$_2$ states for Ca^{2+}/Ex-depleted PSII reconstituted with 25 mM CaCl$_2$ and SrCl$_2$. Measurements were made at** *m/e* **= 34 as a function of the exchange time (Δt) at 10°C. Solid lines are kinetic fits to the data according to Equation 2-6. The graph insert reveals expanded time ordinates for the first 100 ms. Note the differing time axes are set according to the kinetic parameters. Each data point represents a 30 min measurement.**

Table 4-4 ^{18}O exchange rate constants for Ca^{2+}/Ex-depleted PSII reconstituted with $CaCl_2$ and $SrCl_2$ at 10^oC

	S_3 State		S_2 State	
	$^{34}k_1$ (s^{-1})	$^{34}k_2$ (s^{-1})	$^{34}k_1$ (s^{-1})	$^{34}k_2$ (s^{-1})
[1]Ca^{2+}/Ex-depleted PSII membranes + $CaCl_2$	1.5 ± 0.2	27 ± 3	1.5 ± 0.5	> 175
[2]Ca^{2+}/Ex-depleted PSII membranes + $SrCl_2$	5.1 ± 2.1	22 ± 6	5.3 ± 1.4	> 175

[1,2]NaCl/A23187/EGTA induced Ca^{2+}-depletion of PSII membranes and incubated for 2-3 h in 25 mM $CaCl_2$ and $SrCl_2$, respectively. See text for details.

In terms of the ^{18}O exchange behavior, the data presented in Table 4-4 reveals similar findings to Ca^{2+}-depleted PSII reconstituted with $CaCl_2$ and $SrCl_2$ (Table 4-3). Rate constants for the slow phase of exchange increase from $^{34}k_1 = 1.5 \pm 0.2$ s^{-1} in the Ca^{2+}-reconstituted control to $^{34}k_1 = 5.1 \pm 2.1$ s^{-1} in Sr^{2+}-reconstituted preparations in the S_3 state and from $^{34}k_1 = 1.5 \pm 0.5$ s^{-1} to $^{34}k_1 = 5.3 \pm 1.4$ s^{-1} in the S_2 state, respectively (Table 4-4). Interestingly, the data presented in Figure 4-4 and Table 4-4 also shows that the rate of fast exchange in Ca^{2+}- and Sr^{2+}-reconstituted preparations remains relatively unchanged in either the S_3 or S_2 states, despite the fact that > 97% of centers in Ca^{2+}/Ex-depleted PSII lack the 17- and 23-kDa extrinsic proteins (Table 4-1). The exchange rates for Ca^{2+}-reconstituted PSII are $^{34}k_2 = 27 \pm 3$ s^{-1} in the S_3 state and $^{34}k_2 > 175$ s^{-1} in the S_2 state while for Sr^{2+}-reconstituted PSII, the exchange rates yield $^{34}k_2 = 22 \pm 6$ s^{-1} and $^{34}k_2 > 100$ s^{-1}, respectively. Surprisingly, these result contrast to the data presented in Chapter 3 in which the removal of the 17- and 23-kDa extrinsic subunits was shown to slow the fast phase of exchange by ~30% in both the S_3 and S_2 states. However, it is important to emphasize that the biochemical treatments used to prepare Ex-depleted and Ca^{2+}/Ex-depleted PSII involve slightly different conditions (i.e., the presence of chelators in the Ca^{2+}/Ex-depleted procedure). Further discussion of this point is given in the following section.

4.4 DISCUSSION

Although the exact role of Ca^{2+} in O_2-evolution remains unresolved, the numerous experimental data that demonstrates its structural and functional intimacy with the OEC has fueled intense interest within the photosynthesis community. Recent proposals for Ca^{2+} assign a direct role in the water oxidation chemistry as a substrate-water binding site, orienting the water for nucleophilic attack on a Mn=O group during the $S_3 \rightarrow [S_4] \rightarrow S_0$ transition (Vrettos et al., 2001b; Pecoraro et al., 1998; but also see Siegbahn, 2000; Kuzek and Pace, 2001). In an effort to address these proposals, the rates of ^{18}O exchange were determined for PSII preparations depleted of Ca^{2+} and subsequently reconstituted with either $SrCl_2$ or $CaCl_2$ (Figures 4-3, 4-5 and Tables 4-3, 4-4).

Owing to the sensitivity of the mass spectrometric technique (i.e., detection of centers that are only active in O_2-evolution), measurement of the ^{18}O exchange in Ca^{2+}- and Sr^{2+}-reconstituted PSII provides a highly selective tool for probing the involvement of Ca^{2+} in the water oxidation chemistry. Since Sr^{2+} is the only other metal ion that replaces Ca^{2+} and still maintains O_2-evolving activity, the application of this technique does not extend to biochemical preparations in which the Ca^{2+}-site is occupied by other metal ions of similar (and dissimilar) physical properties to Ca^{2+} (e.g. Cd^{2+}, La^{3+}, Dy^{3+}).

The fact that the ^{18}O exchange in Ca^{2+}-reconstituted preparations behaves like the ^{18}O exchange determined for native PSII, indicates that the structural (and therefore functional) integrity of the OEC has been restored to those centers that are active in O_2-evolution. This observation alone has important implications for the interpretation of the Sr^{2+}-reconstituted ^{18}O exchange data: any modification of the S-state dependent exchange behavior will be a direct consequence of Sr^{2+} occupation of the Ca^{2+}-site. Comparison of the Ca^{2+}- and Sr^{2+}-reconstituted exchange rates reveals a ~3-4-fold increase in the rate of the 'slow' (i.e. $^{34}k_1$) exchanging water for Sr^{2+}-reconstituted PSII across each of the S-states measured (Tables 4-3, 4-4). Moreover, the rate constants derived from the kinetic fits to the $m/e = 36$ data for Ca^{2+}-depleted preparations in the S_3 and S_2 states provides an independent determination of $^{34}k_1$ (Figure 4-3, Table 4-3) and confirms a Sr^{2+}-specific effect on the slow rate of substrate-water exchange.

In contrast, the rate for the 'fast' exchanging remains comparatively unchanged in Sr^{2+}-reconstituted PSII in the S_3 state in which the exchange rates fall within the detectable

kinetic limit of ≤ 175 s^{-1}. A preliminary determination of the ^{18}O exchange behavior for Sr^{2+}-reconstituted PSII in the S$_3$ state revealed a more significant decrease in the rate constant for the fast exchanging water from $^{34}k_2 = 28 \pm 1.8$ s^{-1} in Ca^{2+}-reconstituted PSII to $^{34}k_2 = 15 \pm 7.2$ s^{-1} in Sr^{2+}-reconstituted PSII (Hillier, 1999). However, the results presented here indicate that the fast kinetic component is little affected by Sr^{2+} occupation of the Ca^{2+}-site in the S$_3$ state, at least within the experimental error of the measurements (Tables 4-3, 4-4). Moreover, there is no detectable change in the rate of fast exchange for Sr^{2+}-reconstituted PSII in the S$_2$ and S$_1$ states in which $^{34}k_2$ remains unresolved (i.e. > 175 s^{-1} and > 100 s^{-1}, respectively).

In view of these findings, it is likely that the Ca^{2+} cofactor is directly involved in binding the slowly exchanging water. Among other things, chemical factors that can influence the rate of water exchange at a metal site include the charge, ionic radius and electronic occupancy of d-orbitals (Hillier and Wydrzynski, 2001; Richens, 1997). As a general rule, water exchange will increase as the ionic radii of the metal center increases. Since Sr^{2+} has a larger ionic radius than that of Ca^{2+} (1.12 Å *versus* 0.99 Å), the difference in the exchange rates between Sr^{2+}- and Ca^{2+}-reconstituted PSII is readily explained by Sr^{2+} occupation of the Ca^{2+}-site.

The rates of water exchange (k_{ex}) for hydrated metal ion complexes [M(H$_2$O)$_n$]$^{m+}$ have been extensively characterized (reviewed in Lincoln and Merbach, 1995; Richens, 1997). The rate constants for [Ca(OH$_2$)$_{6-10}$]$^{2+}$ and [Sr(OH$_2$)$_6$]$^{2+}$ approach $\sim 10^8$-10^9 s^{-1} which compared to rates for the slowly exchanging water for Ca^{2+}- and Sr^{2+}-reconstituted PSII preparations reported here (where $^{34}k_1 \sim 10^0$-10^1 s^{-1}) is $\sim$7-8 orders of magnitude quicker. However, it is important to appreciate that the ^{18}O exchange kinetics reflect an exchange reaction between water in the aqueous solvent environment and water bound within the hydrophobic interior of the OEC. If the substrate-water undergoing to the slower exchange process is indeed bound Ca^{2+}, then it is important to consider that other parameters can influence the exchange kinetics such as the positive charge density of the Mn$_4$ cluster and/or steric hindrance by the immediate (and distal) ligand environment.
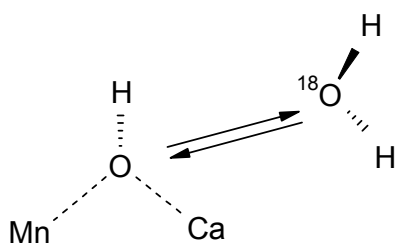
Scheme 4-1   Water forms a bridging ligand between Mn and Ca^{2+}.

Based on the XANES assignment of Mn oxidation state transitions, it is generally accepted that the Mn$_4$ cluster is predominantly composed of Mn(III) and Mn(IV) ions. Although the water exchange rates for hexa-hydrated Mn(III) and Mn(IV) ions are not known (the strong oxidizing potential of these ions dictates that they do not readily exist as aqueous ions in solution), comparison with Fe or Ru ions in different oxidation states reveals that the water exchange rate decreases by ~10^4 for a formal oxidation state increase from +2 to +3 (Hillier and Wydrzynski, 2001). Similarly, comparison with Cr(III) provides an estimate for the water exchange rate at Mn(IV) since the two ions are isoelectronic with a stable d^3 configuration. It is therefore expected that the water exchange rates for hydrated Mn(IV) should be ~10^{-6}-10^{-4} s^{-1} while for hydrated Mn(III) in the range of 10^{-2}-10^0 s^{-1} (Hillier and Wydrzynski, 2001). These predictions are in close agreement with computational studies by Kuzek and Pace (2001) for water ligand exchange in the primary coordination sphere of aquo Mn(III)(H$_2$O)$_6$ and Mn(IV)(H$_2$O)$_6$ which is estimated to be in the region of 10^0-10^1 s^{-1} and 10^{-7}-10^{-8} s^{-1}, respectively. Additional factors other than the oxidation state of the metal ion make the prediction of the exchange rates within the metalloprotein domain of the OEC more complicated (such as the protonation state of the substrate-water [and neighbouring ligands], the pK of the reaction sphere, *Jahn-Teller* distortions and the character of the ligand environment). If the substrate-water in question does indeed form a bridging ligand between Ca^{2+} and a higher oxidation state Mn ion (as depicted in Scheme 4-1), then it is possible to reconcile water exchange rates in the measured range (i.e. $^{34}k_1 = 10^0$-10^1 s^{-1}). Although it is impossible to discern the precise chemical nature of the binding site based on the observed rates of ^{18}O exchange and comparison with the known rates of water exchange for aquo ions, the results nevertheless reveal a distinct correlation between Sr^{2+} replacement at the Ca^{2+}-site and an increase in the rate of slow exchanging water across the three S-states measured (Tables 4-3, 4-4). The results provide the most

definitive evidence to date for the involvement of Ca^{2+} as a substrate binding site in PSII.

Perhaps the most intriguing question surrounding the nature of the Ca^{2+}-site relates to its specificity: Ca^{2+} aside, why is Sr^{2+} the only other metal cation that restores back partial O_2-evolving activity to Ca^{2+}-depleted preparations? This question has been recently addressed by Brudvig's laboratory in which they hypothesize that the electronegativity of the ion (and therefore its Lewis acidity) tunes the Brønsted acid-base properties of a coordinated water molecule involved in a proton-coupled electron-transfer pathway and/or is a substrate in O_2 formation (Vrettos et al., 2001a). Comparison of the pK_a values for aquo ions reveals that Sr^{2+} [13.18] and Ca^{2+} [12.7; Perrin, 1969] are similar Lewis acids while the authors propose that other metal cations fail to support O_2-evolution because the pK_a of these ions lies outside of the optimal range required for activity by PSII. As a result, substitution with metal cations other than Ca^{2+} or Sr^{2+} at the Ca^{2+}-site could either disrupt the hydrogen-bonding network or lead to protonation of basic sites within the OEC thereby altering the overall redox potential of the Mn_4 cluster. A similar proposal was presented by Penner-Hahn and co-workers to explain changes in the 2.7 Å Mn-Mn vector following substitution with Sr^{2+} (-0.026 Å) and Dy^{3+} (+0.030 Å), (Riggs-Gelasco et al., 1996). A model was presented in which a Ca^{2+}-bound water molecule forms a hydrogen bond with the μ-oxo bridge between two Mn ions. Based on the Lewis acidity of the substituted metal ion, the strength of the H-bond would then be differentially altered leading to changes in the protonation state of the $Mn_2(\mu\text{-O})_2$ unit and hence the EXAFS detectable Mn-Mn distance. Indeed, this proposal is consistent with EXAFS detectable changes in the model compound $[Mn^{IV}(sapln)(\mu\text{-O})_2]$ following protonation of the bridging oxygen (Baldwin et al., 1994).

Finally, analysis of the ^{18}O exchange behavior for Ca^{2+}/Ex-depleted PSII reveals a surprising result in terms of the effect (or lack thereof) on the rate of the fast exchanging water in the S_3 and S_2 states, given that ~97% of centers lack the 17- and 23-kDa extrinsic proteins (Table 4-4, Table 4-1, respectively). The results from Chapter 3 clearly show a slowing down for the fast exchanging water by ~30% in the S_3 and *vide infra* the S_2 state of Ex-depleted PSII (Table 3-1). To explain why a similar phenomenon is not observed for Ca^{2+}/Ex-depleted PSII, it is noted that the presence of chelators used during (and subsequently present in residual concentration after) the

preparation of these samples could affect the overall rates of water exchange at the catalytic site. A similar phenomenon is also observed in the detection of novel EPR signals associated with Ca^{2+}-depleted PSII which are only observed in the presence of chelators (e.g., citrate, EGTA, EDTA; [Boussac et al., 1990a; Ono and Inoue, 1990]). In Chapter 3, I made arguments based on the observed rates of ^{18}O exchange for an asymmetric distribution of the regional dielectric manifested through increased water permeation in the vicinity of the fast exchanging substrate binding site following removal of the 17- and 23-kDa extrinsic proteins. Given a similar situation for Ca^{2+}/Ex-depleted PSII, it could be argued that the presence of chelator(s) restructures the hydration properties (therefore lowers the regional dielectric) around the (fast exchanging) substrate binding site which results in an increase in the rates of ^{18}O exchange across the S-states measured.

Chapter 5   Is Bicarbonate a Transient Electron Donor to Photosystem II?

5.1 INTRODUCTION

5.1.1 Overview

Bicarbonate is also an essential cofactor required for optimal activity of photosystem II. The 'bicarbonate effect' was first demonstrated by Warburg and Krippahl (1958) who showed that CO_2 accelerated the light-driven production of O_2 by PSII in the presence of ferricyanide, although experimentally this result was difficult to reproduce. Later, Stemler and Govindjee (1973) described a condition in which a significant increase in the rate of the Hill reaction (or electron transport) was observed upon the addition of bicarbonate to CO_2-depleted chloroplasts. Since then, many groups have investigated the bicarbonate phenomenon within PSII (most recently reviewed in van Rensen et al., 1999). Of notable interest is the observation that the bicarbonate requirement is only apparent for the water oxidase (PSII); no influence of bicarbonate has ever been demonstrated for PSI or anoxygenic photosynthetic reaction centers (Shopes et al., 1989; Wang et al., 1992).

The bicarbonate requirement was initially ascribed to the OEC on the donor side of photosystem II (Stemler and Govindjee, 1973; Stemler, 1980) and a model including bicarbonate as a mediator for the photosynthetic water oxidation was proposed (Stemler, 1980). However, isotope exchange measurements by Radmer and Ollinger (1980) using $HC^{18}O_3^-$ were unable to detect any direct involvement of bicarbonate in the O_2-evolving mechanism. Furthermore, numerous experimental data began to accumulate to show that bicarbonate strongly influenced the acceptor side reactions (see below). As a result, arguments that invoked the site of bicarbonate action on the electron acceptor side of photosystem II began to dominate. Recently, Klimov and co-workers re-visited the role of bicarbonate within PSII and have provided additional evidence in support of a bicarbonate requirement for the OEC (reviewed in Klimov and Baranov, 2001). Indeed, it is now apparent that bicarbonate exerts different effects on both the donor and acceptor sides of PSII.

5.1.2 Action of Bicarbonate at the Electron Acceptor Side of Photosystem II

Wydrzynski and Govindjee (1975) provided the first experimental evidence for an acceptor side bicarbonate requirement using Chl a fluorescence induction kinetics on CO_2 (or bicarbonate) depleted thylakoids. The results showed that CO_2-depleted thylakoids exhibited a fluorescence signature characteristic of PSII preparations in

which electron flow between the primary (Q_A) and secondary (Q_B) quinone acceptor molecules was blocked due to herbicide binding. The addition of bicarbonate to the sample restored back normal fluorescence. Subsequent studies of the electron transfer rates between Q_A^- and Q_B using chlorophyll *a* fluorescence yield decay measurements confirmed that the bicarbonate requirement was indeed located between Q_A and Q_B (Eaton-Rye and Govindjee, 1988, Xu et al., 1991). Moreover, the addition of formate (a known inhibitor of the bicarbonate-site at ~mM concentration) to thylakoids increased the amplitude of the $g = 1.82$ $Q_A^- Fe^{2+}$ EPR signal 10-fold (Vermaas and Rutherford, 1984; Nugent et al., 1988) while a formate/bicarbonate effect was also demonstrated by EPR measurements of the $Q_A^- Fe\text{-}Q_B$ complex (Bowden et al., 1991). Based on changes in the Mössbauer spectrum of Fe (Diner and Petrouleas, 1987) and FTIR difference spectroscopy using ^{13}C-labeled bicarbonate (Hienerwadel and Berthomieu, 1995), it was established that bicarbonate forms a (dissociable) bidentate ligand to the non-heme Fe on the acceptor side PSII. Indeed, formate and other carboxylate anions can replace bicarbonate at this site, resulting in inhibition, but it takes prolonged incubation periods and millimolar concentrations (Wincencjusz et al., 1996; Petrouleas et al., 1994). Further modeling studies have implicated a second bicarbonate site at the acceptor side of PSII near the Q_B binding niche, which is believed to be involved in the protonation of Q_B^{2-} (Xiong et al., 1996).

5.1.3 Action of Bicarbonate at the Electron Donor Side of Photosystem II

Until recently, proposals for a bicarbonate requirement at the electron donor side of photosystem II (e.g., Stemler and Govindjee, 1973, Stemler, 1980) were mostly over-looked owing to the large bicarbonate-effect exerted on the $Q_A^- \rightarrow Q_B(^-)$ electron transfer kinetics at the acceptor side of PSII. Recently, experimental evidence has emerged to show that bicarbonate stimulates electron transfer reactions at the donor side of PSII in so-called DT-20 membrane fragments (Klimov et al., 1995a; Wincencjusz et al., 1996) and 'BBY' (PSII-enriched) membrane fragments (Allakhverdiev, 1997) under bicarbonate-depleted conditions or when low concentrations of formate (i.e., ~μM) are present. By monitoring the flash induced absorbance changes at 295 nm, Wincencjusz et al. (1996) showed that the four-step redox cycle of the OEC is blocked by ~μM concentrations of formate while the addition of bicarbonate reversed this effect. Moreover, the donor side bicarbonate requirement was also demonstrated under conditions when the known bicarbonate-dependent step of electron transfer between Q_A

and Q_B was blocked (Klimov et al., 1995a,b). Despite this, the binding site for bicarbonate within the OEC remains to be identified.

5.1.3.1 EPR and FTIR Measurements of Bicarbonate-Depleted PSII

EPR spectroscopy has also been applied to the study of structural and functional aspects of the bicarbonate requirement at the electron donor side of PSII. Formation of the light-induced EPR signal II in formate-treated PSII indicates that electron donation from the OEC to Y_Z^+ is inhibited while the addition of bicarbonate reverses this effect (Klimov et al., 1997a,b). This result suggests that electron donation to Y_Z^+ is bicarbonate-dependent. This proposal is further supported by kinetic measurements in which the rate of re-reduction of Y_Z^+ by the OEC is significantly slowed in the presence of 0.1 mM formate while bicarbonate again reverses the effect (Klimov and Baranov, 2001).

Formate inhibition of PSII activity is also accompanied by structural rearrangement of the Mn cluster: release of one or two free Mn^{2+} atoms per reaction center is revealed by the appearance of the 6-line EPR signal associated with free Mn^{2+} (Klimov and Baranov, 2001; Feyziev et al., 2000). Based on these observations, it was proposed that bicarbonate forms an essential ligand to the Mn-containing OEC. The significance of this proposal was addressed using FTIR difference spectroscopy of bicarbonate-depleted PSII (Yreula et al., 1998). The results indicated considerable modification of the light-induced difference spectrum in which the positive bands at 1589 and 1365 cm^{-1} and the negative bands at 1560, 1541, 1522 and 1507 cm^{-1} disappeared upon bicarbonate-depletion and were partially recovered following the addition of exogenous bicarbonate to the suspension medium. Further investigation of COO^- stretching modes using ^{13}C-FTIR identified that the negative band at 1560 cm^{-1} and positive bands at 1589 and 1365 cm^{-1} could be assigned to bicarbonate. However, detailed analysis of the flash-induced difference spectra is required to identify on which S-state transition(s) these vibrational modes are present in order to reveal more definitive evidence for the possible ligation of bicarbonate to the Mn cluster (Klimov and Baranov, 2001).

5.1.3.2 Involvement of Bicarbonate in Photoactivation

Photoactivation is a multi-step process that requires light-induced Mn^{2+} oxidation and dark binding of Ca^{2+} for reactivation of O_2-evolution in Mn- and Ca^{2+}-depleted

preparations (e.g. Tamura and Cheniae, 1987; Miller and Brudvig, 1990; Ananyev and Dismukes, 1996). Bicarbonate was shown to stimulate assembly of the Mn cluster during photoactivation using catalytic concentrations of Mn^{2+} ($\leq$ 4 Mn per reaction center; Klimov et al., 1995a,b; Allakhverdiev et al., 1997; Klimov et al., 1997a,b; Hulsebosch et al., 1998; Baranov et al., 2000). Interestingly, the stimulatory effects of bicarbonate were not apparent for alternative (exogenous) electron donors to PSII (e.g. NH_2OH and diphenylcarbazide). Using improved illumination procedures for studying photoactivation, Baranov et al. (2000) showed that bicarbonate stimulates this process by accelerating the formation and suppressing the decay, respectively, of the first light-induced assembly intermediate IM_1 [apo-WOC-Mn(OH)$_2^+$]. The authors identified two binding sites for bicarbonate: a high affinity site ($K_D \leq 10$ μM) which stimulates the rate of recovery of O_2-evolving centers through enhanced Mn^{2+} binding, and, a second lower affinity bicarbonate site ($K_D \sim$mM) which also appears to increase the rate of IM_1 formation by lowering the concentration of Ca^{2+} (by free complexation) thereby reducing any direct competition between Ca^{2+} and Mn^{2+} for the Mn^{2+} binding site(s) in the apo-WOC core. The data strongly support the involvement of bicarbonate in assembly of the Mn cluster through either (1) possible ligand to the first Mn, (2) as a Bronsted base to accelerate proton release during the formation of [apo-WOC-Mn(OH)$^+$] or [apo-WOC-Mn(OH)$_2^+$], (3) in donating hydroxide group(s) to the aforementioned precursors of the Mn complex during photoactivation (releasing CO_2) or (4) by participating in electrostatic constraints involved with increasing the local Mn^{2+} concentration (Baranov et al., 2000; Klimov and Baranov, 2001).

Moreover, the formation of bicarbonate-metal complexes with Mn^{2+} is known to lower the redox potential of Mn^{2+} oxidation: the oxidation potential shifts from +1.2 V (aqua Mn^{2+}) to +0.92 V for $Mn^{2+}(HCO_3^-)^+$ and to +0.63 V for $Mn^{2+}(HCO_3^-)_2$, (Kozlov et al., 1997). Collectively, these data have important implications for the redox interaction(s) of Mn^{2+} with the apo-WOC during photoactivation of the Mn cluster.

5.1.3.3 *Bicarbonate: An Oxidizable Electron Donor to PSII?*

The most compelling evidence implicating bicarbonate as a directly oxidizable electron donor to PSII was presented by Metzner et al. (1981) who showed that if ^{18}O bicarbonate was added to suspensions of algal cells or thylakoids, the photosynthetically evolved O_2 was transiently enriched in the heavy isotope. This observation led to the

hypothesis that a bicarbonate-modified species [X(HCO$_3^-$)] could compete with water as an electron donor to PSII. Although the authors never identified the X cofactor, their model hypothesized that oxidation of X(HCO$_3^-$) might form the bicarbonate radical (HCO$_3^\bullet$) or peroxidicarbonic acid (HOOC-O-O-COOH) *via* dimerization.

5.1.4 Experimental Aims

The intended aims of this research were to address the proposal that bicarbonate serves as an oxidizable electron donor to photosystem II (alternative to water or by way of involvement with water through oxidative reactions) and is the immediate source of photosynthetically evolved O$_2$. This hypothesis was originally proposed by Metzner (1978) and Stemler (1980) although a lack of evidence based on the isotopic composition of photosynthetically evolved O$_2$ using ^{18}O-labeled bicarbonate (Radmer and Ollinger, 1980) was not consistent with this proposal. Given the recent evidence to show that bicarbonate stimulates the rate of O$_2$-evolution in the intact holoenzyme, Klimov and Baranov (2001) have argued that the isotopic equilibration of ^{18}O between HC^{18}O$_3^-$ and H$_2$O (catalyzed by the inherent carbonic anhydrase activity in PSII membrane preparations) could mask the detection of ^{18}O$_2$ evolution from HC^{18}O$_3^-$. Accordingly, measurements of the ^{18}O exchange behavior between HC^{18}O$_3^-$ and photosystem II were performed using a membrane preparation devoid of intrinsic carbonic anhydrase activity.

The work described within this chapter was done in part with Professor Slava Klimov (Russian Academy of Sciences, Pushchino, Moscow) with assistance from Dr Tatiana Schutova (Umea Plant Science Center, Department of Plant Physiology, University of Umea, Sweden).

5.2 MATERIALS AND METHODS

5.2.1 CAI3 Culture Maintenance

The CAI3 strain of *Chlamydomonas reinhardtii* has been genetically engineered to have minimal residual carbonic anhydrase activity. The CAI3 strain was imported to Australia by Professor Klimov and subsequently re-cultured for the purpose of this study using the growth facilities provided for by the Research School of Biological Sciences.

5.2.1.1 Growth Medium

The TAPS growth medium contained: 6.71 mM Tris, 2.5% (*v/v*) TAPS salts, 0.0375% (*v/v*) concentrated phosphate, 0.1% (*v/v*) trace elements, 0.1 % (*v/v*) glacial acetic acid and 1.5% (*w/v*) agar (solid medium only).

The TAPS salts contained: 0.30 M NH_4Cl, 16.23 mM $MgSO_4.7H_2O$ and 13.61 mM $CaCl_2.2H_2O$.

The trace elements contained: 18.43 mM H_3BO_3, 25.56 mM $MnCl_2.4H_2O$, 6.29 mM $CuSO_4.5H_2O$, and 6.77 mM $CoCl_2.6H_2O$, 132.46 mM Na_2EDTA, 76.52 mM $ZnSO_4.7H_2O$, 17.95 mM $FeSO_4.7H_2O$, and 0.89 mM $(NH_4)_6Mo_7.4H_2O$.

The concentrated phosphate solution contained: 1.63 M K_2HPO_4 and 1.06 M KH_2PO_4.

Both the TAPS liquid media and solid agar media were autoclaved at 120 psi for 20 min to ensure proper sterilization.

5.2.1.2 Culture Maintenance

The CAI3 strain of *Chlamydomonas reinhardtii* was maintained at 30^oC on TAPS solid medium supplemented with acetate. Liquid cultures were cultivated using mixotrophic growth conditions. Initially, the TAPS/acetate liquid medium was inoculated with cells and placed at 30^oC in a Thermoline Gro-Cabinet. The cultures were left to sit for 4 h, then shaken to ensure cell dispersion and ventilated (air stream, Stella W-40 aquarium air pump) under constant illumination of 80-120 μmol m^{-2} s^{-1} until the OD_{730} reached 0.9-1.2. Millex-FG$_{50}$ air filters (0.2 μm, Millipore) were used for sterile air ventilation.

5.2.2 Sample Preparation

5.2.2.1 Preparation of CAI3 Thylakoid Membranes

Thylakoid membranes were prepared from intact *Chlamydomonas reinhardtii* CAI3 cells according to the isolation procedure used for the purification of thylakoid membranes from *Synechocystis* sp. PCC 6803 (Tang and Diner, 1994; Bricker et al., 1998). All procedures were performed at 4°C under dim green light unless otherwise stated. Cells (typically 20 L) were grown photoheterotrophically to an OD_{730} of 0.9-1.2, harvested at 10000 × g for 10 min and washed once in a buffer consisting of 30 mM MES/NaOH (pH 6.5), 15 mM NaCl, 5 mM $MgCl_2$, and 0.4 M sucrose (hereafter referred to as the 'wash buffer'). The cells were then pelleted and resuspended at 1 mg of Chl mL^{-1} in wash buffer containing 1 mM benzamidine, 1 mM ε-amino caproic acid, 1 mM phenylmethylsulfonylfluoride (PMSF), 50 μg mL^{-1} DNase I (bovine pancreas type IV) and 2 g. L^{-1} bovine serum albumin and allowed to soak for 1 h. The cell suspension was loaded into a pre-chilled bead beater chamber (Bio-Spec) with 1.0 mm diameter glass beads (pre-equilibrated with buffer A) in a ratio of 0.6:0.4, respectively. Cell breakage was achieved in 8 break cycles of 15 s homogenization followed by 5 min cooling. The homogenized cell suspension was decanted from the glass beads and the beads were washed in a total volume of 250 mL of wash buffer to recover additional homogenate. Unbroken cells and residual glass beads were removed by centrifugation at 5000 × g for 5 min. Thylakoid membranes were isolated by centrifugation at 36000 × g for 25 min, and were resuspended at 1-2 mg Chl mL^{-1} in wash buffer, frozen in liquid N_2 and stored at −80°C until required.

5.2.2.2 Preparation of Spinach PSII Membrane Fragments

Isolation of PSII membrane fragments from market fresh spinach was performed according to Berthold et al. (1981) and is described in section 3.2.1.1.

5.2.2.2.1 Depletion of the 33-, 23- and 17-kDa extrinsic proteins from spinach PSII

Depletion the 33-, 23- and 17-kDa extrinsic proteins was achieved by $CaCl_2$ treatment of PSII membrane samples according to the method of Ono and Inoue (1983). Briefly, the PSII membranes were resuspended at 1 mg Chl mL^{-1} in 1 M $CaCl_2$ (~pH 6.3) at 0°C for 30 min and at 10 min intervals, the sample was gently passed twice through a teflon

homogenizer. Following a second 30 min treatment, the sample was then pelleted by centrifugation at 36000 × g and washed and resuspended in a wash buffer consisting of 30 mM MES/NaOH (pH 6.3), 400 mM sucrose, 15 mM NaCl and 5 mM $MgCl_2$. Following a second centrifugation at 36000 × g, the sample was then resuspended in the same wash buffer but containing 25 mM $CaCl_2$ and incubated for 2-3 h at 4°C. Finally, the treated membranes were assayed for O_2-evolution activity before being frozen in liquid N_2 and stored at -80°C until measurement.

5.2.2.3 *Preparation of DT-20 PSII Membrane Fragments*

The DT-20 membrane fragments used in this study were prepared by digitonin/Triton X-100 solubilization of spinach chloroplasts (according to Allakhverdiev et al., 1997) by Dr Tatiana Schutova in Sweden, then shipped to Australia on dry ice and stored at -80°C until measurement.

5.2.3 Chlorophyll *a/b* Determination

Extraction of the chlorophyll pigment from was performed according to the procedure detailed in Chapter 3.2.2 with the following modification: extraction proceeded via incubation for 10-15 mins (on ice) in 0.5 mL of 0.1 M NH_4OH and 4.5 mL of ice cold acetone (Harris, 1988). The remainder of the extraction procedure was performed without modification. The amounts of Chl a, Chl b and total Chl (Chl $a + b$), expressed as μg Chl mL^{-1}, were calculated according to Equations 3-1, 3-2 and 3-3. Unless otherwise stated, Chl refers to the total chlorophyll (i.e., Chl $a + b$).

5.2.4 Bicarbonate-Depletion of Membrane Preparations

Bicarbonate-depletion of CAI3 thylakoids and spinach PSII membranes was achieved by repetitive washing in CO_2-free wash buffer (containing no $MgCl_2$). The latter was prepared by continuous aeration at pH 5.5 for 30 min at room temperature using humidified compressed air that was passed through bicarbamate (soda lime). The wash buffer was then adjusted to physiological pH (6.5) using a freshly made NaOH stock (in Ultrapure Water, Aldrich) and the membranes resuspended in the CO_2/$MgCl_2$-free wash buffer, pelleted by centrifugation at 36,000 × g and this process repeated 2-3 times. The $MgCl_2$ was excluded from the buffer medium as Mg^{2+} forms a complex ion with HCO_3^- in solution and the effect of added bicarbonate on CO_2-depleted samples is reduced.

5.2.5 Determination of the ^{18}O Exchange

5.2.5.1 *Measurement of the ^{18}O Exchange in the Presence of $H_2^{18}O$*

Measurement of the ^{18}O exchange in the presence of $H_2^{18}O$ was determined according to the methods described in Chapter 2.2.1.

5.2.5.2 *Preparation of ^{18}O-Bicarbonate*

^{18}O-bicarbonate was prepared by dissolving unlabeled $NaHCO_3$ in 98.5% atom $H_2^{18}O$ (ISOTECH, Miamisburg, OH) and allowing the solution to equilibrate for ~10 days at room temperature under vacuum seal. Known quantities of solid $NaHC^{18}O_3$ free of $H_2^{18}O$ were obtained by drying aliquots of the solution under a stream of N_2 for 15-20 minutes also under vacuum seal.

5.2.5.3 *Measurement of the ^{18}O Exchange in the Presence of $HC^{18}O_3^-$*

Measurement of the ^{18}O exchange was performed according to the method described in Chapter 2.2.1 with the following modifications:

(1) to reduce the probability of the **chemical** conversion of $HC^{18}O_3^- \rightarrow CO_2 + H_2^{18}O$, the $NaHC^{18}O_3$ was dissolved in $H_2^{16}O$ (pre-equilibrated at 4^oC and containing 1.7 U μL^{-1} glucose oxidase and 3 U μL^{-1} catalase) **immediately** prior to measurement (i.e. < 30 s) and drawn up into the spring-loaded syringe which had also been equilibrated to a temperature of 4^oC.

(2) measurements were made at 4^oC to reduce the **chemical** and (residual) **enzymatic** conversion of $HC^{18}O_3^- \rightarrow CO_2 + H_2^{18}O$.

(3) a slightly modified flash/injection protocol was used to obtain the integrated signal over a 10-flash or 100-flash sequence (1 Hz) in the presence of 1-2 mM $HC^{18}O_3^-$.

(4) measurements were made in the presence of 400 μM 2,6-dichloro-p-benzoquinone (DCBQ) instead of PPBQ as the artificial electron acceptor (thought to promote better activity of HCO_3^--depleted preparations; Klimov, personal communication). A concentration of 1 mM $K_3Fe(CN)_6$ was used (in

addition to DCBQ) as the water soluble electron acceptor in these measurements.

5.3 RESULTS

Characterization of CAI3 thylakoids was undertaken to determine that the O_2-evolution, O_2-flash yield oscillations and substrate-water binding properties exhibited normal behavior. The information presented in Table 5-1 shows that initial rates of O_2-evolution for native thylakoids were typically 400-500 µmol O_2 (mg Chl)$^{-1}$ h^{-1}. Following repetitive washing in CO_2-free wash buffer to remove bound bicarbonate, the rate dropped to ~81% of the control activity and was restored to ~89% following the addition of 10 mM bicarbonate to the sample.

Table 5-1 O_2-evolving activities for the variously treated CAI3 thylakoids at 25°C

	[1]Rate	% of cont.
[2]CAI3 thylakoids	462 ± 32	100
[3]HCO$_3^-$-depleted CAI3 thylakoids	374 ± 22	81
[4]HCO$_3^-$-depleted CAI3 thylakoids + 10 mM HCO$_3^-$	411 ± 25	89

[1]rates of O_2-evolution expressed as µmol O_2 (mg Chl)$^{-1}$ h^{-1}; [2]Chlamydomonas thylakoids that lack intrinsic carbonic anhydrase activity; [3]bicarbonate-depleted CAI3 thylakoids; [4]bicarbonate-depleted CAI3 thylakoids + 10 mM HCO$_3^-$. See text for details.
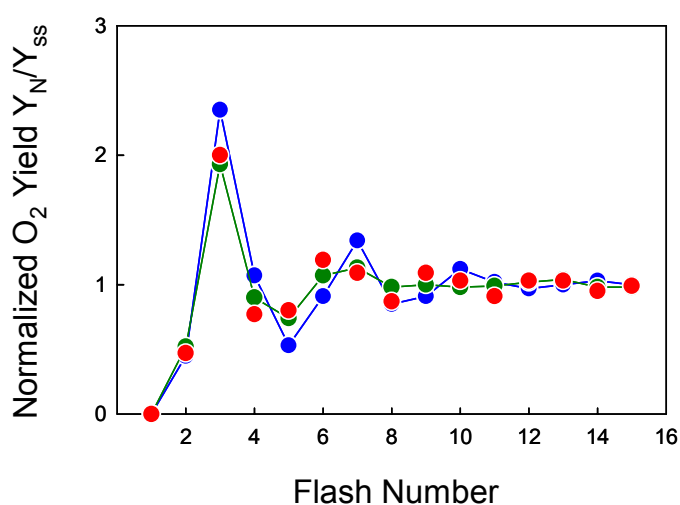

Figure 5-1   Normalized O_2 flash yield oscillations at *m/e* = 34 for CAI3 thylakoids (blue circles), HCO$_3^-$-depleted CAI3 thylakoids (green circles) and HCO$_3^-$-depleted CAI3 thylakoids reconstituted with 10 mM HCO$_3^-$. Measurements were made at 4°C following complete isotopic equilibration after the addition of H$_2^{18}$O.

Figure 5-1 shows the normalized O_2-flash yield oscillation patterns at $m/e = 34$ following complete isotopic equilibration after the addition of $H_2{}^{18}O$. The data clearly indicate that the O_2-evolving mechanism ($\pm$ $HCO_3{}^-$) follows normal period of four oscillations.

Measurement of the $H_2{}^{18}O$ exchange at $m/e = 34$ was also used to determine if there was any effect on the substrate-water binding kinetics in a preparation lacking intrinsic carbonic anhydrase activity. The results are presented in Figure 5-3 at $4^{\circ}C$ and indicate that the normal biphasic exchange behavior inherent to PSII is also present in CAI3 thylakoids. According to the biphasic analysis of these data (Equation 2-5), the exchange rates for $HCO_3{}^-$-depleted CAI3 thylakoids in the S_3 state are $^{34}k_1 = 2.0 \pm 0.3$ s^{-1} for the slow exchanging water and $^{34}k_2 = 23 \pm 3$ s^{-1} for the fast exchanging water and for $HCO_3{}^-$-depleted CAI3 thylakoids reconstituted with 10 mM $HCO_3{}^-$, the rates are $^{34}k_1 = 2.3 \pm 0.5$ s^{-1} and $^{34}k_2 = 17 \pm 2$ s^{-1}, respectively.
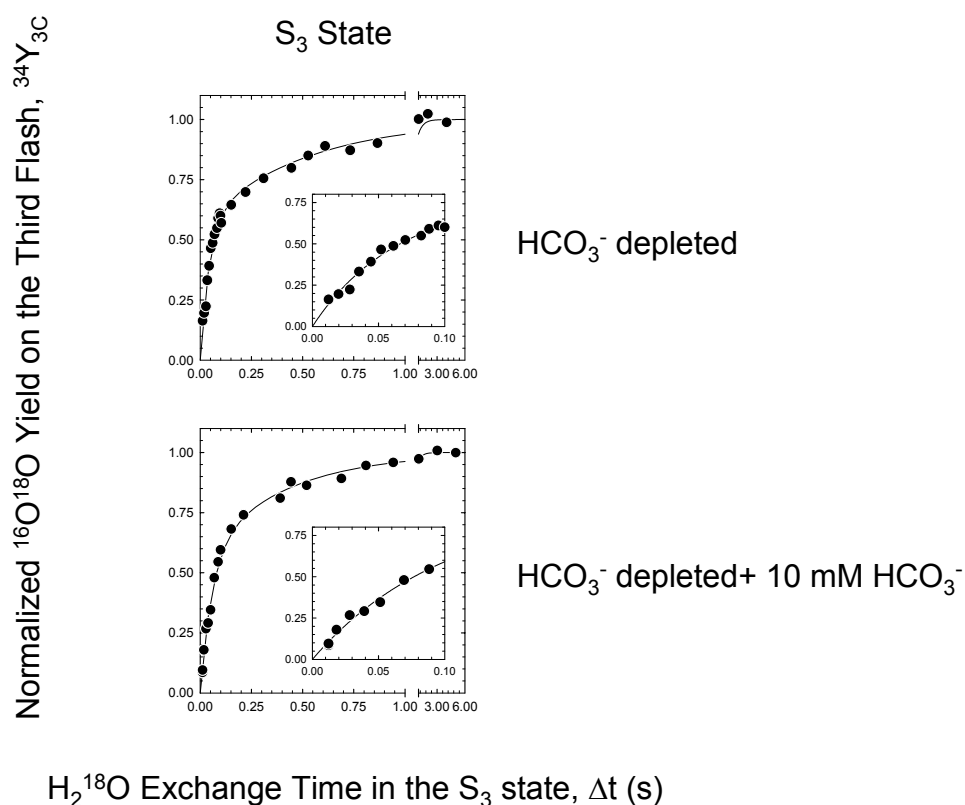
Figure 5-2 ^{18}O **exchange measurements in the S_3 state for $HCO_3{}^-$-depleted CAI3 thylakoids and $HCO_3{}^-$-depleted CAI3 thylakoids reconstituted with 10 mM $HCO_3{}^-$. Measurements were made at $m/e = 34$ as a function of the exchange time (Δt) at $4^{\circ}C$. Solid lines are kinetic fits to the data according to Equation 2-5. The graph inserts reveal expanded time ordinates for the first 100 ms. Each data point represents a 30 min measurement.**

Although the rates of ^{18}O exchange were not determined for native *Chlamydomonas* thylakoids, comparison of the bicarbonate-depleted and bicarbonate-reconstituted ^{18}O exchange rates with data obtained for spinach thylakoids at $5^{\circ}C$ ($^{34}k_1 = 1.3 \pm 0.3$ s^{-1}, $^{34}k_2 = 24 \pm 4$ s^{-1}; Hillier et al., 1998) indicates that the substrate-water binding properties are very similar and that removal of the intrinsic carbonic anhydrase activity through genetic manipulation has little effect on the overall O_2-evolving mechanism.

To determine if bicarbonate is a transitional electron donor to PSII, exchange measurements were made in the S_3 state for bicarbonate-depleted CIA3 thylakoids in the presence of 1-2 mM $HC^{18}O_3^-$. The initial results indicated no obvious flash-induced ^{18}O enrichment of the photosynthetically evolved O_2 at either $m/e = 34$ or $m/e = 36$ under different experimental conditions (i.e. pH 5.5, 6.5 and 7.5 using varying concentrations of $HC^{18}O_3^-$ [1-100 mM] and measured at different exchange times [i.e. 50 ms to 10 s]). However, following injection of the $HC^{18}O_3^-$ into the sample chamber, a pre-flash artifact was observed that remained relatively stable over long periods of time (*viz* > 10 min). The artifact is not attributed to background O_2 introduced into the chamber during the injection event as the signal amplitude at $m/e = 32$ measured in parallel to that at $m/e = 34$ clearly showed a rapid rise and decay profile which is clearly associated with Y_{inj} (Figure 5-3). The artifact is connected with $HC^{18}O_3^-$ as the amplitude of the signal roughly doubles when the concentration of $HC^{18}O_3^-$ is increased from 1 mM to 2 mM.

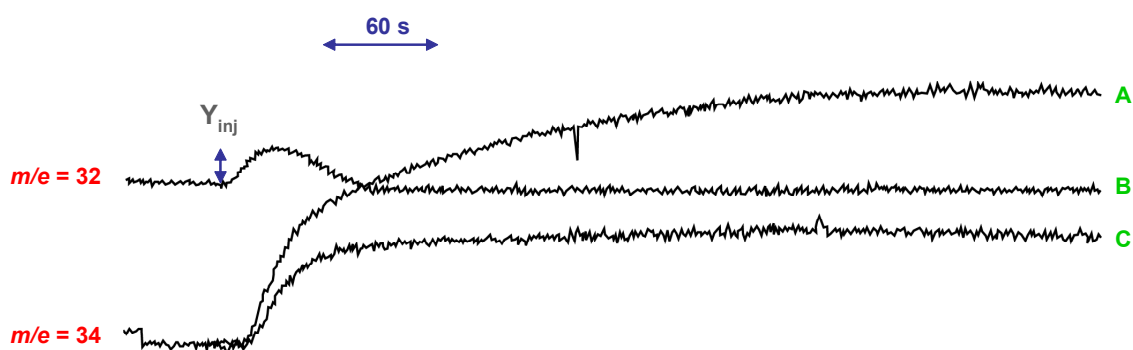**Figure 5-3**   The injection artifact at $m/e = 34$ following the introduction of $HC^{18}O_3^-$ into the sample chamber. (A) 2 mM $HC^{18}O_3^-$ at $m/e = 34$; (B) 1 mM $HC^{18}O_3^-$ at $m/e = 34$; and (C) 1 mM $HC^{18}O_3^-$ at $m/e = 32$.

Interestingly, the injection artifact is not observed for $NaHC^{16}O_3^-$ dissolved in $H_2^{18}O$ at equal concentrations. Moreover, the measurements were repeated in the absence of sample (i.e. buffer only) to establish whether the artifact is a consequence of some form of chemical reaction catalyzed by the sample itself. Interestingly, the artifact was observed in the presence of buffer but absent when only water (instead of buffer/sample) was added to the sample chamber. This last observation raises important question(s) as to the identity of the gas produced (at $m/e = 34$) during the injection of labeled bicarbonate into the sample chamber. The fact that it takes ≥ 60 s to stabilize (concentration dependent) compromises the kinetic resolution of these measurements: the detection of any (minor) contribution to the flash-induced ^{18}O enrichment of the photogenerated O_2 at ≤ 60 s will be masked the effect of the injection artifact.

Accordingly, the measurements were repeated but this time the integrated signal over a 100-flash sequence (spaced at 1 Hz) was recorded at $m/e = 34$ for different concentrations of $HC^{18}O_3^-$ following stabilization of the injection artifact. The results are presented in Figure 5-4 and clearly show that there is no detectable increase in the rate of $^{16}O^{18}O$ production over and above the contribution arising from natural abundance $H_2^{18}O$ (i.e. $\leq 0.02\%$; Figure 5-4A).
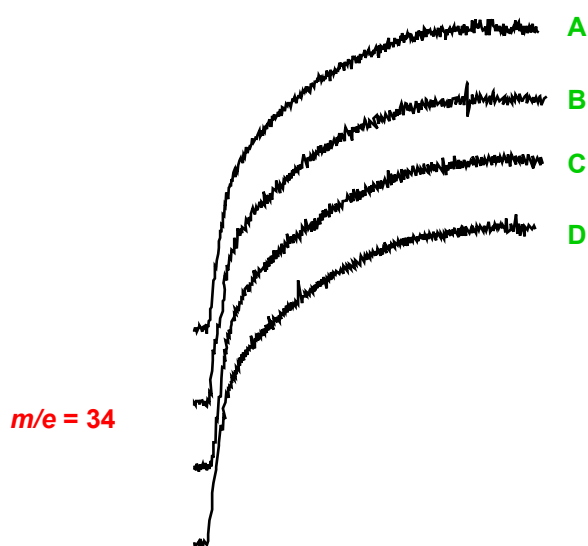
Figure 5-4 **Measurement of the $^{16}O^{18}O$ production at $m/e = 34$ over a 100-flash sequence following injection of $HC^{18}O_3^-$ and stabilization of the injection artefact. (A) no $HC^{18}O_3^-$ (i.e. natural abundance $H_2^{18}O$); (B) 1 mM $HC^{18}O_3^-$; (C) 10 mM $HC^{18}O_3^-$; and (D) 100 mM $HC^{18}O_3^-$.**

Similarly, a pH-dependence assay was also performed to determine if there were any observed effects on the ^{18}O enrichment. The pK_a for the de/hydration reaction $HCO_3^- \leftrightarrow CO_2 + H_2O$ is ~6.2 (Stumm and Morgan, 1970). The measurements conducted at pH 8-9 (where the concentration of bicarbonate ions is at its greatest and without compromising the overall activity of the preparation) however, failed to show any ^{18}O enrichment effect of the photogenerated O_2 at either $m/e = 34$ or $m/e = 36$.

To avoid pre-injection mixing of labeled bicarbonate solutions (i.e. $NaHC^{18}O_3$ and $H_2^{16}O$), the following injection aliquot was prepared for different concentrations of ^{18}O-bicarbonate as depicted in Figure 5-5:
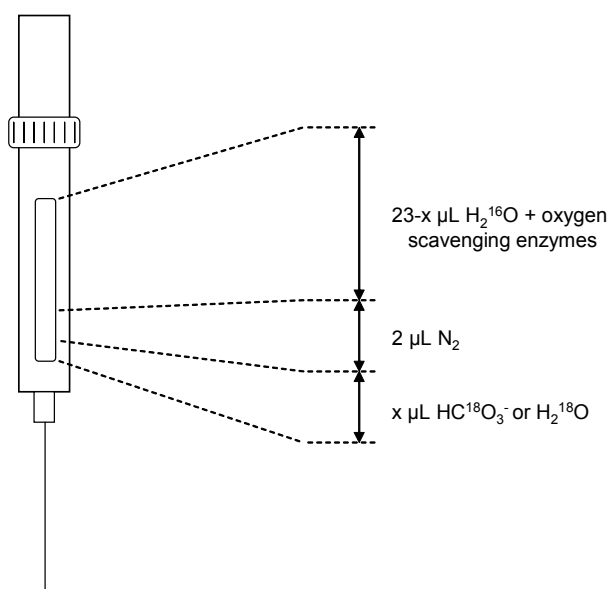
Figure 5-5 **Schematic representation of the injection aliquot used to prevent pre-injection mixing of NaHC^{18}O$_3$ and H$_2$^{16}O.**

The use of N_2 allows the separation between the $HC^{18}O_3^-$ stock (i.e. $NaHCO_3$ dissolved in $H_2^{18}O$) and the diluting $H_2^{16}O$ component (to yield the desired $HC^{18}O_3^-$ concentration) until mixing occurs post-injection within the sample chamber. Using this approach, the probability of ^{18}O "leaking" from $NaHC^{18}O_3$ dissolved in $H_2^{16}O$ prior to the injection is avoided. Injection of $H_2^{18}O$ (instead of $NaHC^{18}O_3$ dissolved in $H_2^{18}O$) was used as a control in these measurements. Like the earlier measurements of the $HC^{18}O_3^-$ exchange, the results indicated that there is also no effect of added $HC^{18}O_3^-$ on the rates of $^{16}O^{18}O$ or $^{18}O^{18}O$ production measured at $m/e = 34$ and $m/e = 36$, respectively.

Similar measurements of the $HC^{18}O_3^-$ exchange were also extended to DT-20 membrane fragments (data not shown). Like bicarbonate-depleted CAI3 thylakoids, there was no obvious detection of an ^{18}O enrichment of the photosynthetically evolved O_2 despite the fact that these measurements (and the measurements for bicarbonate-depleted CAI3 thylakoids) were made at extremely high sensitivity (i.e. ≤ 5 mV compared to the $H_2{}^{18}O$ exchange measurements which are usually measured at between 50-200 mV depending on the activity of the preparation).

Recent evidence presented by Lu and Stemler (2002) showed that the carbonic anhydrase activity associated with PSII membrane preparations in maize (*Zea mays*) is located on the lumenal side of photosystem II and can be extracted in active form by washing preparations in 1 M $CaCl_2$ (this procedure removes the 33-, 23- and 17-kDa extrinsic proteins; Ono and Inoue, 1983). It is proposed that the CA activity is required for hydration of CO_2 (instead of dehydration of HCO_3^-) yielding bicarbonate ions that play an essential catalytic role in O_2-evolution (Stemler and Lu, 2001). In light of this proposal, measurement of the $HC^{18}O_3^-$ exchange was performed at *m/e* = 34 on spinach PSII membranes treated with 1 M $CaCl_2$ to test if there were any stimulatory effects of ^{18}O-bicarbonate in the absence of the proposed lumen-located CA activity. Even at an enrichment level well above natural abundance (i.e. ~100 mM $HC(^{18})O_3^-$), there was no obvious ^{18}O enrichment of the photosynthetically evolved O_2 due to ^{18}O-bicarbonate using flash-induced and 100-flash (1 Hz) illumination conditions.

5.4 DISCUSSION

Characterization of bicarbonate-depleted and bicarbonate-depleted/reconstituted CAI3 thylakoids through analysis of the O_2-evolution properties and substrate-water binding behavior suggests that the inherent O_2-evolving mechanism remains typical of most PSII preparations. Exchange rates for the two substrate-waters in the S_3 state do not show any significant variation outside of the experimental error of these measurements in the presence or absence of bicarbonate (Figure 5-2). Moreover, the magnitudes of the exchange rates are very similar to those values reported for spinach thylakoids at a similar temperature (Hillier et al., 1998).

Kinetic limitations in the earlier mass spectrometric measurements by Radmer and Ollinger (1980) in the presence of $HC^{18}O_3^-$ left open the possibility that ^{18}O-bicarbonate could undergo more rapid rates of exchange in photosystem II than could be detected. In this present study, the improved kinetic resolution associated with the mass spectrometer system developed within the Photobioenergetics Group (enabled by more rapid isotope mixing and equilibration times; Hiller et al., 1998) was applied to preparations exhibiting an enhanced bicarbonate requirement (i.e. bicarbonate-depleted samples) to determine whether or not bicarbonate serves as an oxidizable electron donor to photosystem II (Metzner, 1978; Stemler, 1980; Klimov and Baranov, 2001). By measuring the ^{18}O isotopic enrichment of the photosynthetically evolved O_2 at $m/e = 34$ and $m/e = 36$ in the presence of $HC^{18}O_3^-$, the significance of this hypothesis was addressed.

The measurements are however, made more complicated by the spontaneous (Miller et al., 1997) and enzymatic (i.e. PSII associated carbonic anhydrase activity; Stemler, 1997; Moskvin et al., 1998) de/hydration cycling of $HCO_3^- \leftrightarrow CO_2 + H_2O$. To reduce the probability of the equilibrium, measurements of the $HC^{18}O_3^-$ exchange were performed at low temperatures (4°C) and in a PSII preparation devoid of intrinsic CA activity (CAI3). Unfortunately, the results revealed no isotopic enrichment of the photosynthetically evolved O_2 produced by photosystem II in the presence of ^{18}O-bicarbonate at $m/e = 34$ and 36 (Figures 5-3, 5-4), despite the fact that a range of different experimental conditions (pH, temperature, $HC^{18}O_3^-$ enrichment) were used in an attempt to enhance the donor side bicarbonate requirement.

The fact that there is no isotopic enrichment of the photogenerated $^{16}O^{18}O$ or $^{18}O^{18}O$ (i.e. at $m/e = 34$ or 36) in the presence of $HC^{18}O_3^-$ raises the following possibilities: (1) bicarbonate undergoes faster rates of exchange than can be detected using the current instrumentation sensitivity; (2) the rapid de/hydration cycle of bicarbonate with CO_2 causes ^{18}O "leaking" from $HC^{18}O_3^-$ (Miller et al., 1997) and effectively masks the effect of electron donation to PSII; (3) the water oxidase component of photosystem II has evolved to exclude bicarbonate as a terminal substrate; or (4) bicarbonate was never an oxidizable electron donor to PSII. The first possibility remains open-ended until such time as further advances in the kinetic resolution of these measurements can be made and the identity of the injection artifact is established. Secondly, it is deemed *unlikely* that the spontaneous and enzymatic dehydration of bicarbonate (albeit under conditions in which significant precautions were employed to reduce the rate of conversion) could explain the lack of signal. Even in the presence of specific CA inhibitors (ethoxyzolamide and acetazolamide; data not shown), the rate of spontaneous conversion is estimated to be in the order of seconds and is unlikely to account for the conversion alone, given the pH range over which these measurements were made.

Finally, the third and fourth proposals remain open for discussion. In recent years, the labs of Dismukes (Princeton) and Klimov (Puschino) have presented evidence to suggest that bicarbonate alters the speciation of Mn^{2+} ions in solution and its redox properties (Baranov et al., 2001). Based on geochemical records that show the concentration of CO_2 (at equilibrium with HCO_3^-) 3-4 billion years ago was 10^2-10^4 above current partial pressure, it is argued that $Mn(HCO_3)^+$ and $[Mn(HCO_3)_2]_n$ would have existed as the major aqueous forms of manganese in the archean period. The authors propose that it is likely that these manganese-bicarbonate complexes formed the initial precursor to the inorganic core of water oxidation/oxygen evolution in the cyanobacterial ancestor (reviewed in Ananyev et al., 2001). Of course, in support of these arguments is the observation that low levels of bicarbonate (i.e. < 25 μM) accelerate the binding and photooxidation of Mn^{2+} in the first step of photoactivation (Baranov et al., 2001) and is supported by synthetic modeling studies using the iso-structural bicarbonate surrogate phosphinate anions ($RRPO_2^-$; Ruettinger and Dismukes, 2000). A model involving bicarbonate as the source of hydroxide required for binding of $Mn(OH)^+$ to the apo-WOC is proposed (Scheme 1 of Ananyev et al., 2001). Indeed, the possibility remains open as to the role of bicarbonate as an electron donor to photosystem II but is beyond the sensitivity of the measurements described here.

Chapter 6   General Discussion

Resolving the exact molecular nature of the oxygen evolving complex (OEC) of photosystem II remains one of the greatest challenges facing science today. Our underlying knowledge of the structural and functional properties of the inorganic $Mn_4O_xCa_1Cl_yHCO_{3z}^-$ core at the heart of the OEC has been principally derived from spectroscopic, biophysical and/or biochemical analyses of membranous and sub-membranous preparations which are enriched in PSII activity. In a recent Nature paper by Zouni et al. (2001), details of the 3.8 Å X-ray crystal structure of a photosystem II core complex from *Synechococcus elongatus* were revealed. For the first time, the physical structure (and position) of the $Mn_{(4)}$ cluster was identified based on calculations of the associated electron density map. In conjunction with spectroscopic evidence (EXAFS and EPR), the data place geometric constraints on predictive models allowed for the Mn complex (reviewed in Carrell et al., 2001). However, at this point in time, the crystal structure is of insufficient resolution to provide detailed information for the involvement of the inorganic cofactors of PSII (Ca^{2+}, Cl^-, HCO_3^-), and to answer questions related to the regulatory mechanism(s) concerning substrate-water binding. In part, the research described within this thesis attempts to address these questions.

Evaluation of the ^{18}O exchange kinetics provides a useful tool for probing the substrate-water binding properties at the catalytic site of water oxidation in PSII. Through the application of time-resolved mass spectrometry and a specialized closed chamber rapid injection/mixing system (Hillier et al., 1998), measurement of the rates of ^{18}O incorporation from $H_2^{18}O$-enriched solvent water into the photogenerated O_2 produced by PSII reflects an exchange process between water in the aqueous solvent environment and intermediate water bound to the catalytic site. Based on the analysis of these data, important information regarding the substrate binding affinities is obtained.

The first determination of the ^{18}O exchange behavior for native PSII membrane preparations were made in the S_3, S_2 and S_1 states. Comparison of these data (Table 6-1) with the ^{18}O exchange data from thylakoids (Hillier and Wydrzynski, 2000) reveals exchange rates that are essentially the same indicating that the initial detergent solubilization step used to prepare these samples has no effect on the substrate-water binding properties. It is important to note that the PSII membrane preparation has the same inherent PSII protein composition as thylakoids but unlike thylakoids lacks a vesicular structure. Thus, the results show that diffusion of bulk water across the thylakoid vesicle into the lumen is not rate-limiting for the ^{18}O exchange.

Table 6-1 Summary of the ^{18}O exchange rates at *m/e* = 34 for the spinach thylakoid and PSII membrane preparations in the S$_3$, S$_2$, and S$_1$ and S$_0$ states at 10^{0}C

	S$_3$ state		S$_2$ State		S$_1$ state		S$_0$ state	
	$^{34}k_1$ (s^{-1})	$^{34}k_2$ (s^{-1})	$^{34}k_1$ (s^{-1})	$^{34}k_2$ (s^{-1})	$^{34}k_1$ (s^{-1})	$^{34}k_2$ (s^{-1})	$^{34}k_1$ (s^{-1})	$^{34}k_2$ (s^{-1})
[1]Thylakoids	2.1 ± 0.2	37 ± 2	2.2 ± 0.1	> 175	0.022 ± 0.002	> 100	8 ± 2	> 100
PSII membranes	2.5 ± 0.2	30 ± 2	1.9 ± 0.3	≥ 175	0.022 ± 0.003	> 100	[5]n.d.	n.d.
[2]Ex-depleted PSII membranes	2.4 ± 0.5	20 ± 3	2.6 ± 0.3	120 ± 14	0.021 ± 0.003	> 100	n.d.	n.d.
[3]Ca^{2+}-depleted PSII + CaCl$_2$	1.4 ± 0.1	27 ± 2	2.1 ± 0.3	> 175	0.023 ± 0.002	> 100	n.d.	n.d.
[4]Ca^{2+}-depleted PSII + SrCl$_2$	5.2 ± 1.6	23 ± 5	7.7 ± 2.4	> 175	0.082 ± 0.012	> 100	n.d.	n.d.

[1]Thylakoid ^{18}O exchange data taken from Hillier and Wydrzynski (2000); [2]PSII membranes depleted of the 17- and 23-kDa extrinsic proteins; [3,4]low pH/citrate induced Ca^{2+}-depletion of PSII membranes and reconstituted for 2-3 h in 25 mM CaCl$_2$ and SrCl$_2$, respectively; [5]not determined. See text for details.

The observation that the ^{18}O exchange rates vary independently during S-state turnover begins to place limitations on the types of mechanisms involved in the water oxidation chemistry. Given that the rates for the slow and fast exchanging waters differ by a factor of ~15 in the S_3 state, supports the proposal that O-O bond formation takes place on the $S_3 \rightarrow [S_4] \rightarrow S_0$ transition in a concerted 'all or nothing' reaction. As such, questions regarding how and where the four oxidizing equivalents are stored, the chemical nature of the substrate binding sites, and at what stage in the catalytic cycle are the two waters bound to the OEC, remain central to the understanding of this mechanism.

The following conclusions are drawn based on the results presented in this study:

Fast Exchanging Water

(1) in the S_1 state, the fast exchange rate remains unresolved in all PSII samples measured, with a rate constant of > 100 s^{-1}

(2) in the S_2 state, it is *likely* that the fast exchange rate is at the detectable kinetic limit of ~175 s^{-1}

(3) on the $S_2 \rightarrow S_3$ transition, the fast exchange rate is slowed down by a factor of ~5 yielding a rate constant of ~30 s^{-1}

(4) in the S_3 state, the fast exchange rate is little affected by Sr^{2+} substitution of the Ca^{2+}-site

Slow Exchanging Water

(1) on the $S_1 \rightarrow S_2$ transition, the slow exchange rate increases by a factor of ~100 whereas on the $S_2 \rightarrow S_3$ transition it remains unchanged

(2) in the S_3, S_2 and S_1 states of Sr^{2+}-reconstituted PSII, the slow exchange rate is increased by a factor of ~3-4 compared to native and Ca^{2+}-reconstituted PSII

With this information at hand, we can begin to build a clearer picture with regard to the mechanism of the O_2-evolution in context of the available spectroscopic evidence in the literature. Accordingly, a working model for the water oxidation chemistry is presented in Schemes 6-1 and 6-2. In Scheme 6-1, the $S_0 \rightarrow S_1$, $S_1 \rightarrow S_2$ and $S_2 \rightarrow S_3$ transitions are described in terms of the activation of Mn/Ca bound oxygen ligands while in Scheme 6-2, the $S_3 \rightarrow [S_4] \rightarrow S_0$ transition is described in terms of a nucleophilic attack mechanism to explain O-O bond formation and regeneration of the (water-bound) S_0 state.
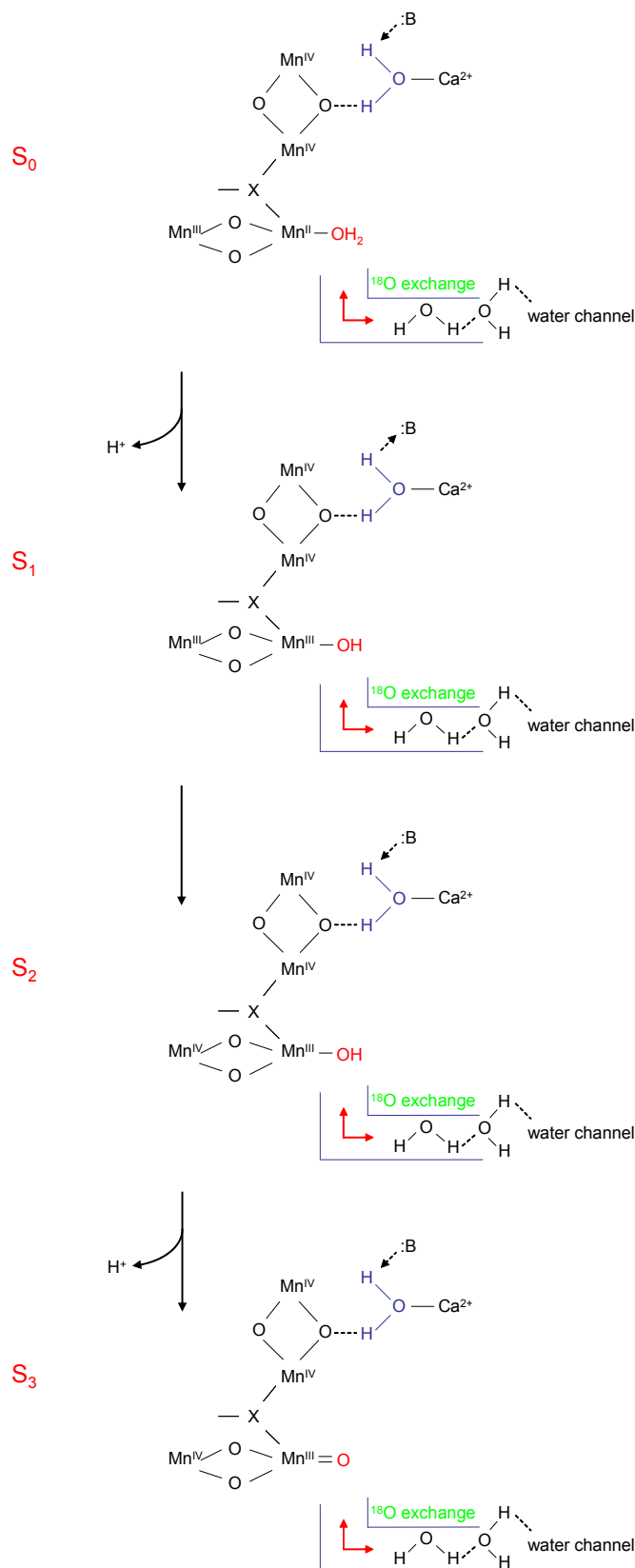
Scheme 6-1 Working model to explain the $S_0{\rightarrow}S_1$, $S_1{\rightarrow}S_2$, and $S_2{\rightarrow}S_3$ transitions during the catalytic cycle of water oxidation. In the S_0, S_1 and S_2 states, two $Mn_2(\mu\text{-}O)_2$ components are linked by a bridging ligand X which can represent either a mono-μ-oxo (-O-O-), carboxylato (-O-C-O-) bridge or HCO_3^- group. The role of a protein residue acting as Lewis base (B) is indicated. The dashed lines represent hydrogen-bonding interactions. The fast and slowly exchanging waters are indicated in red and blue, respectively. See text for details.
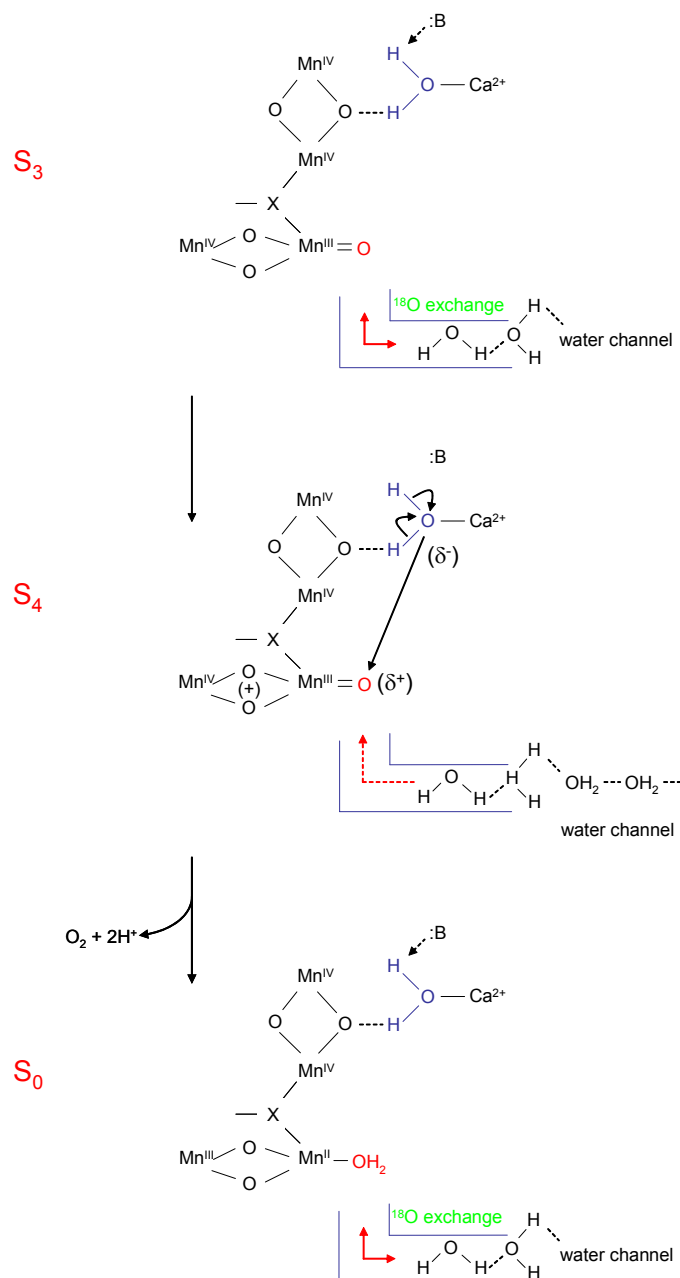
Scheme 6-2 The $S_3 \rightarrow [S_4] \rightarrow S_0$ transition. The bridging ligand (X) between the redox active and non-redox active $Mn_2(\mu\text{-O})_2$ components can be a mono μ-oxo (-O-) bridge, a carboxylato (-O-C-O-) or HCO_3^- group while the role of a protein residue acting as Lewis base (B) is indicated. The dashed lines represent H-bonding interactions. During $S_3 \rightarrow S_4$ the OEC accumulates an additional charge [denoted (+)] across the redox active $Mn_2(\mu\text{-O})_2$ component which in turn activates the depicted oxo ligand for nucleophilic attack generating the O-O bond. Water positioned at the head of the channel then binds to the active site and the S_0 state is regenerated. See text for details.

In this model, the $Mn_4[Ca]$ complex is arranged as a 'dimer of dimers' connected by either a mono-μ-oxo bridge, a carboxylato or HCO_3^- group and invokes that both substrate waters are bound to the catalytic site from the initial reduced S_0 state. The two $Mn_2(\mu\text{-O})_2$ units can be differentiated based on their redox activity (i.e. redox active and

non-redox active; Scheme 6-1). Associated with the catalytic site is a water channel consisting of a network of 'head-to-tail' hydrogen-bonded waters which are free to exchange with water bound at the active site and water in the aqueous solvent environment (i.e. referred to as the ^{18}O exchange; Scheme 6-1). In the S_0 state, the fast exchanging water (-OH$_2$) forms a terminal ligand to a Mn^{II} ion positioned nearest to the entry site of the water channel, while the slowly exchanging water forms a bridging ligand between non-redox active Mn$_2(\mu$-O)$_2$ dimer and Ca^{2+} at a site which is located further into the hydrophobic interior of the OEC. The latter configuration provides the most straight-forward explanation to account for the overall magnitudes of the slow ^{18}O exchange rates throughout the S-state cycle (i.e. $^{34}k_1 \sim 10^{-2}$-10^1 s^{-1}; Table 6-1). Rates of water exchange for Ca(H$_2$O)$_6$ complexes are in the region of $\sim 10^8$-10^9 s^{-1} (Richens, 1997) while computational studies by Kuzek and Pace (2001) predict that water exchange for Mn^{IV}(H$_2$O)$_6$ compounds fall into the range of $\sim 10^{-7}$-10^{-8} s^{-1}. Assuming that there is a mixed influence across the substrate bridge, it is therefore possible to reconcile the measured ^{18}O exchange rates (i.e. Table 6-1).

During the $S_0 \rightarrow S_1$ transition, there is a formal Mn oxidation state increase from Mn$^{II} \rightarrow$ Mn^{III} in the redox active Mn$_2(\mu$-O)$_2$ component (using the Mn XANES assignment of [Mn(II, III, IV, IV)] in the S_0 state; Roelofs et al., 1996; Iuzzolino et al., 1998) which is accompanied by deprotonation (Schlodder and Witt, 1999; Rapapport and Lavergne, 2001) of the terminally ligated, fast exchanging water. During the $S_1 \rightarrow S_2$ transition, the other Mn ion in the redox active Mn$_2(\mu$-O)$_2$ component is shown to undergo a formal oxidation state increase from Mn$^{III} \rightarrow$ Mn^{IV}, yielding a mixed valence [$S = \frac{1}{2}$] Mn$_2(\mu$-O)$_2$ system which gives rise to the S_2 state EPR multiline signal (Dismukes and Siderer, 1981). Although there is no associated deprotonation during this transition (Schlodder and Witt, 1999), the slowing down in the exchange rate of the terminal oxygen ligand to ~ 175 s^{-1} can be explained through a charge delocalization, 'pulling' effect of the accumulated oxidizing equivalent across the redox active Mn$_2(\mu$-O)$_2$ component (Renger, 2001).

In contrast, rates for the slowly exchanging water oscillate with much greater complexity during the in the $S_0 \rightarrow S_1$ and $S_1 \rightarrow S_2$ transitions. During the $S_0 \rightarrow S_1$ transition, the rates of water exchange are decreased by a factor of ~ 400 from ~ 8 s^{-1} to ~ 0.02 s^{-1} while the opposite effect is observed on the $S_1 \rightarrow S_2$ transition where the rates increase from ~ 0.02 s^{-1} to ~ 2 s^{-1} (Hillier and Wydrzynski, 2000; Table 6-1). To account

for this observation, differences in the extent and strength of the hydrogen-bond network in the immediate vicinity of the substrate binding site is invoked (the relative strength of these interactions are illustrated using directional arrows in Scheme 6-1). It is likely that these interactions involve a nearby protein residue which acts as a Lewis base (i.e. ':B'; Scheme 6-1). Thus, during the $S_0 \rightarrow S_1$ transition, the strength of the network is somehow altered and the protonation state of the substrate-water adopts a –OH rather than $-OH_2$ configuration. This in turn leads to a slowing down in the exchange rates (i.e. k_{ex} [$M^{(n)}$-OH_2] > k_{ex} [$M^{(n)}$-OH] > k_{ex} [$M^{(n)}$=O]; Hillier and Wydrzynski, 2001). Similarly, during the $S_1 \rightarrow S_2$ transition, the effect is reversed facilitating an increase in the exchange rates (Table 6-1). In support of this proposal is the identification of an asymmetrically structured 'active' water molecule in the S_2/S_1 FTIR difference spectrum (Noguchi and Sugiura, 2000, 2002). It is noted that the H-bond character of one O-H group weakens during the $S_1 \rightarrow S_2$ transition, a finding which is consistent with the proposal described here (Fischer and Wydrzynski, 2001).

Alternatively, it is noted that the S_0 state ^{18}O exchange measurements are made in a 'light-adapted' state (i.e. from the dark-adapted S_1 state, 4 flashes of light are applied to the sample before the S_0 state is generated). Interestingly, Peterson et al. (2001; 2002) have recently obtained evidence to suggest that PSII undergoes transition from a dark-adapted 'resting state' to a light-adapted 'active-state' during the first two enzymatic cycles following dark-adaptation. This phenomenon could explain the unintuitive kinetic changes of the slowly exchanging water during the $S_0 \rightarrow S_1$ and $S_1 \rightarrow S_2$ transitions.

The chemical nature of the $S_2 \rightarrow S_3$ transition is a matter of considerable debate and many of the available models for O_2-evolution can be divided into metal-centered (Hoganson and Babcock, 1997; Schlodder and Witt, 1999; Dau et al., 2001; Nugent et al., 2001; Vrettos et al., 2001b) and ligand-centered (Haumann and Junge, 1999; Siegbahn, 2000; Messinger et al., 2001; Kuzek and Pace, 2001) oxidation events during this transition. With the application of Mn Kβ X-ray emission spectroscopy (Kβ XES) to monitor oxidation state changes in metal centers (Messinger et al., 2001), there is now increasingly good evidence to support a ligand-centered oxidation on the $S_2 \rightarrow S_3$ transition. There is clearly no change in the exchange rate for the slowly exchanging water during the $S_2 \rightarrow S_3$ transition (Table 6-1). This observation would thus indicate

that the slowly exchanging water is not bound to the redox active $Mn_2(\mu\text{-}O)_2$ component. On the other hand, there is at best a slowing down in the exchange rate of the fast exchanging water by a factor of ~5 during the $S_2 \rightarrow S_3$ transition (Table 6-1). Such a change may reflect a metal centered oxidation event, but this change is much smaller than would be expected (i.e. the rate of oxygen ligand exchange is expected to slow down by ~10^4 s^{-1} for a $Mn^{III} \rightarrow Mn^{IV}$ oxidation state increase; Hillier and Wydrzynski, 2001). Accordingly, the model presented in Scheme 6-1 invokes a ligand centered oxidation event during the $S_2 \rightarrow S_3$ transition which is facilitated by deprotonation of the terminal, fast exchanging –OH group, resulting in the formation of a $Mn^{III}=O$ group. Other proposals have invoked the formation of $Mn^{(n)}=O$ groups in the S_3 state, however, the oxidation character of the metal center is typically Mn^{IV} or Mn^V (e.g. Dau et al., 2001; Vrettos et al., 2001). To account for the relatively fast rate of exchange (i.e. ~30 s^{-1}), Scheme 6-2 shows the oxidation state as Mn^{III} where the overall exchange process of the terminal oxo ligand may be facilitated by a H-bond network that is established with the nearby water channel (Scheme 6-1).

In Scheme 6-2, the $S_3 \rightarrow [S_4] \rightarrow S_0$ transition is illustrated in terms of a nucleophilic attack mechanism to explain the O-O bond formation (Messinger et al., 1995; Vrettos et al., 2001b; Dau et al., 2001). During $S_3 \rightarrow S_4$, an additional charge is accumulated across the redox active $Mn_2(\mu\text{-}O)_2$ component [assigned (+)] which in turn activates the terminal fast exchanging oxygen ligand (depicted as δ^+) for nucleophilic attack by the slowly exchanging bridging oxygen ligand (depicted as δ^-). In a concerted forward reaction, the O-O bond forms and O_2 is released from the active site as are two protons (Schlodder and Witt, 1999). Water positioned at the head of the channel then binds to the active site and the S_0 state is regenerated.

In summary, the model presented above is merely phenomenological, but provides one interpretation of the O-O bond forming mechanism based on the observed rates of ^{18}O exchange and in context of some of the available spectroscopic evidence in literature. The model does not address the involvement of Y_Z in H-abstraction (e.g. Hoganson and Babcock, 1997), however, the involvement of Y_Z in proton release pathways during the earlier S-state transitions remains open for interpretation. Although the work presented here has provided further insight into substrate-water interactions within the OEC, more details regarding the chemical nature of the binding sites are required before the true nature of the S-state transitions can be determined.

Future Research Directions

The immediate extensions of the ^{18}O exchange measurements might explore deuterium isotope effects to probe the nature of the hydrogen-bonding interaction(s) within the immediate vicinity of the substrate binding sites. Measurements of the S-state dependent ^{18}O exchange in the presence of deuterated solvent (D_2O) might help to establish the involvement of hydrogen-bond networks in facilitating substrate-water exchange. In addition, evaluation of the pH dependence would provide more detailed information in relation to the protonation state of the bound substrate water. The work presented here did not address the role of chloride in substrate-water binding. Preliminary measurements of the ^{18}O exchange in the S_3 state of Cl$^-$-depleted and Br$^-$-reconstituted PSII indicates that the rates for the slowly exchanging water are decreased by ~40%.

Measurements of the ^{18}O exchange using site-directed mutants of the cyanobacterium *Synechocystis* sp. PCC 6803 could also provide valuable information regarding the role of protein residue(s) surrounding the catalytic site. However, since the respiratory and photosynthetic reactions are not compartmentalized in cyanobacteria, the associated O_2 up-take reactions complicate the measurement of O_2-evolution. To circumvent this problem, the purification of PSII core complexes would allow for a more accurate determination of the ^{18}O exchange behavior, however, this approach remains labour-intensive.

Measurements of the ^{18}O exchange in the presence of ^{18}O-bicarbonate will need to be repeated to establish the nature of the injection artefact. The fact that the artefact was only observed for $HC^{18}O_3^-/H_2^{16}O$ injection aliquots and not $HC^{16}O_3^-/H_2^{18}O$ suggests the possibility of (solvent) contamination of the ^{18}O-bicarbonate during preparation of the stock.

Appendix 1   Kok Analysis

This program was executed using MatLab, version 5.3.

```
Proc = 8;

i=1;


min_err=[];
outp=zeros(2000,Proc);
outp0=zeros(2000,Proc);
outp1=zeros(2000,Proc);
outp2=zeros(2000,Proc);
outp3=zeros(2000,Proc);

intense=[];

for Intensity=3.5:0.1:4.5,
   for alfa=0.05:0.01:0.40,
      for beta=0.05:0.01:0.40,
         for X=1,

            y[enter data here]./Intensity;
            intense=[intense,Intensity];

            if alfa+beta < 1

S0=zeros(1,Proc);S1=zeros(1,Proc);S2=zeros(1,Proc);S3=zeros
(1,Proc);
               S1(1,1)=X;
               S0(1,1)=1-X;


               for proc=1:1:Proc,

sum1=S0(1,proc)+S1(1,proc)+S2(1,proc)+S3(1,proc);
                  if abs(sum1-1)>10*eps
                     proc
                     error('Summation of the quantities are
not equal to 1')
                  end

                  s1(1)=alfa*S1(1,proc);
                  s1(3)=(1-alfa-beta)*S0(1,proc);

                  s2(1)=alfa*S2(1,proc);
                  s2(2)=beta*S0(1,proc);
                  s2(3)=(1-alfa-beta)*S1(1,proc);
```

```
                        s3(1)=alfa*S3(1,proc);
                        s3(2)=beta*S1(1,proc);
                        s3(3)=(1-alfa-beta)*S2(1,proc);

                        s0(1)=alfa*S0(1,proc);
                        s0(2)=beta*S2(1,proc);
                        s0(3)=(1-alfa)*S3(1,proc);

                        outp(i,proc)=s0(3)+s0(2);
                        outp0(i,proc)=s1(1)+s1(3);
                        outp1(i,proc)=s2(3)+s2(2)+s2(1);
                        outp2(i,proc)=s3(3)+s3(2)+s3(1);
                        outp3(i,proc)=s0(3)+s0(2)+s0(1);

                        S1(1,(proc+1))=sum(s1);
                        S2(1,(proc+1))=sum(s2);
                        S3(1,(proc+1))=sum(s3);
                        S0(1,(proc+1))=sum(s0);

                    end

                    min_err=[min_err,sqrt(sum((y-
outp(i,:)).^2))];

                    axe(i,:)=[alfa beta X];
                    i=i+1;

                end
            end
        end
    end
end


y=[enter data here];
[Y,I] = min(min_err);
S0=outp0(I,:)
S1=outp1(I,:)
S2=outp2(I,:)
S3=outp3(I,:)
oxygen=outp(I,:)
axe(I,:)
figure
set(gcf, 'Position',[5 200 490 360])
plot(y,'r.','markersize',20)
plot(outp(I,:)*intense(I),'b')
plot(outp(I,:)*intense(I),'b.','markersize',20)
axis([1 8 0 3])
set(gca,'xticklabel',[ 1 2 3 4 5 6 7 8])
xlabel('Flash Number')
ylabel('Normalized Oxygen Yield')
```

```
figure
set(gcf,'Position',[500 200 490 360])
plot(S0,'r.','markersize',20)
x2=plot(S1,'b')
plot(S1,'b.','markersize',20)
x3=plot(S2,'g')
plot(S2,'g.','markersize',20)
x4=plot(S3,'k')
plot(S3,'k.','markersize',20)
x6=plot(oxygen,'m')
plot(oxygen,'m.','markersize',20)
ST=S0+S1+S2+S3;
x5=plot(ST,'c')
legend([x1,x2,x3,x4,x5,x6],'S0','S1','S2','S3','total','oxy
gen')
axis([1 8 0 1.2])
set(gca,'xticklabel',[ 1 2 3 4 5 6 7 8])
xlabel('Flash Number')
ylabel('Normalized Oxygen Yield')
```

References

Abramovicz, D. A., and Dismukes, G. C. (1984) Manganese proteins isolated from spinach thylakoid membranes and their role in oxygen evolution II. A binuclear manganese-containing 34 kilodalton protein, a probable component of the water dehydrogenase enzyme. *Biochim. Biophys. Acta* **765,** 318-328.

Ädelroth, P., Lindberg, K., and Andreasson, L-E. (1995) Studies of Ca^{2+} binding in spinach photosystem II using $^{45}Ca^{2+}$. *Biochemistry* **34,** 9201-9207.

Ahlbrink, R., Haumann, M., Cerepanov, D., Borgershausen, O., Mulkidjanian, A., and Junge, W. (1998) Function of tyrosine Y_Z in water oxidation by photosystem II: electrostatic promoter instead of hydrogen abstractor. *Biochemistry* **37,** 1131-1142.

Åhrling, K. A., and Pace, R. J. (1995) Simulation of the S_2 state multiline electron paramagnetic resonance signal of photosystem II: A multifrequency approach. *Biophys. J.* **68,** 2081-2090.

Åkerlund, H.-E., Jansson, C., and Andersson, B. (1982) Reconstitution of photosynthetic water splitting in inside-out thylakoids vesicles and identification of participating polypeptides. *Biochim. Biophys. Acta* **681,** 1-10.

Alexander, R. S., Nair, S. K., and Christianson, D. W. (1991) Engineering the hydrophobic pocket of carbonic anhydrase II. *Biochemistry* **30,** 11063-11072.

Allakhverdiev, S. I., Yruela, I., Picorel, R., and Klimov, V. V. (1997) Bicarbonate is an essential constituent of the water-oxidizing complex of photosystem II. *Proc. Nat. Acad. Sci. USA* **94,** 5050-5054.

Ananyev, G. M., and Dismukes, G. C. (1996) Assembly of the tetra-Mn site of photosynthetic water oxidation by photoactivation: Mn stoichiometry and detection of a new intermediate. *Biochemistry* **35,** 4102-4109.

Ananyev, G. M., Zaltsman, L., Vasko, G. C., and Dismukes, G. C. (2001) The inorganic biochemistry of photosynthetic oxygen evolution/water oxidation. *Biochim. Biophys. Acta* **1503,** 52-68.

Astashkin, A. V., Mino, H., Kawamori, A., and Ono, T. (1997) Pulsed EPR study of the S_3' signal in Ca^{2+}-depleted photosystem II. *Chem. Phys. Lett.* **272,** 506-516.

Babcock, G. T., Blankenship, R. E., and Sauer, K. (1976) Reaction kinetics for positive charge accumulation on the water side of chloroplast Photosystem II. *FEBS Lett.* **61,** 286-289.

Bader, K. P., Thibault, P., and Schmid, G. (1987) Study of the properties of the S_3 state by mass spectrometry in the filamentous cyanobacterium *Oscillatoria chlaybea. Biochim. Biophys. Acta* **893,** 564-571.

Baldwin, M. J., Stemler, T. L., Riggs-Gelasco, P. J., and Pecoraro, V. L. (1994) Structural and magnetic effects of successive protonations of oxo bridges in high-valent manganese dimers. *J. Am. Chem. Soc.* **116,** 11349-11356.

Baranov, S. V., Ananyev, G. M., Klimov, V. V., and Dismukes, G. C. (2000) Bicarbonate accelerates assembly of the inorganic core of the water- oxidizing complex in manganese-depleted photosystem II: a proposed biogeochemical role for atmospheric carbon dioxide in oxygenic photosynthesis. *Biochemistry* **39,** 6060-6065.

Berthold, D. A., Babcock, G. T., and Yocum, C. F. (1981) A highly resolved, oxygen-evolving Photosystem II preparation from spinach thylakoid membranes: EPR and electron-transport properties. *FEBS Lett.* **134,** 231-234.

Berthomieu, C., and Boussac, A. (1995) Histidine oxidation in the S_2 to S_3 transition probed by FTIR difference spectroscopy in the Ca(2+)-depleted photosystem II: comparison with histidine radicals generated by UV irradiation. *Biochemistry* **34,** 1541-1548.

Betts, D. D., Ross, J. R., Pichersky, E., and Yocum, C. F. (1997) Mutation Val235Ala weakens binding of the 33 kDa manganese stabilizing protein of photosystem II to one of two sites. *Biochemistry* **36,** 4047-4053.

Blankenship, R. E. (2002) in *Molecular Mechanisms of Photosynthesis*. Blackwell Science, United Kingdom.

Blankenship, R. E., and Hartmann, H. (1998) The origin and evolution of oxygenic photosynthesis. *Trends Biochem. Sci.* **23,** 94-97.

Booth, P. J., Rutherford, A. W., and Boussac, A. (1996) Location of the calcium binding site in photosystem II: a Mn^{2+} substitution study. *Biochim. Biophys. Acta* **1277,** 127-134.

Bouckaert, J., Loris, R., and Wyns, L. (2000) Zinc/calcium- and cadmium/cadmium-substituted concanavalin A: interplay of metal binding, pH and molecular packing. *Acta Crystallog.* **D56,** 1569-1576.

Boussac, A., Maison-Petteri, B., Etienne, A.-L., and Veronette, A. (1985) Reactivation of oxygen evolution of NaCl-washed photosystem II particles by Ca^{2+} and/or the 24 kDa protein. *Biochim. Biophys. Acta* **808,** 231-234

Boussac, A., and Rutherford, A. W. (1988a) Nature of the inhibition of the oxygen-evolving enzyme of photosystem II induced by sodium chloride washing and reversed by the addition of calcium(2+) or strontium(2+). *Biochemistry* **27,** 3476-3483.

Boussac, A., and Rutherford, A. W. (1988b) Ca^{2+}-binding to the oxygen evolving enzyme varies with the redox state of the Mn cluster. *FEBS Lett.* **236,** 432-436.

Boussac, A., Zimmerman, J-L., and Rutherford, A. W. (1989) EPR signals from modified charge accumulation states of the oxygen evolving enzyme in Ca^{2+}-deficient photosystem II. *Biochemistry* **28,** 8984-8989.

Boussac, A., Zimmerman, J.-L., and Rutherford, A. W. (1990a) Factors influencing the formation of modified S_2 EPR signal and the S_3 EPR signal in Ca(2+)-depleted photosystem II. *FEBS Lett.* **277,** 69-74.

Boussac, A., Zimmerman, J.-L., and Rutherford, A. W., and Lavergne, J. (1990b) Histidine oxidation in the oxygen-evolving photosystem-II enzyme. *Nature* **347,** 303-306.

Boussac, A., Sétif, P., and Rutherford, A. W. (1992) Inhibition of tyrosine Z photooxidation after formation of the S_3 state in Ca(2+)-depleted and Cl⁻-depleted photosystem II. *Biochemistry* **31,** 1224-1234.

Bowden, S. J., Hallahan, B. J., Ruffle, S. V., Evans, M. C. W., and Nugent, J. H. A. (1991) Preparation and characterization of photosystem II core particles with and without bound bicarbonate. *Biochim. Biophys. Acta* **1060,** 86-96.

Bricker, T. M., Lowrance, J., Sutton, H., and Frankel, L. K. (2001) Alterations of the oxygen-evolving apparatus in a (448)Arg → (448)S mutant in the CP47 protein of photosystem II under normal and low chloride conditions. *Biochemistry* **40,** 11483-11489.

Bricker, T. M., Morvant, J., Masri, N., Sutton, H. M., and Frankel, L. K. (1998) Isolation of a highly active photosystem II preparation from *Synechocystis* 6803 using a histidine-tagged mutant of CP 47. *Biochim. Biophys. Acta* **1409,** 50-57.

Britt, R. D., Peloquin, J. M., and Campbell, K. A. (2000) Pulsed and parallel-polarization EPR characterization of the photosystem II oxygen evolving complex. *Annu. Rev. Biophys, Biomol. Struct.* **29,** 463-495.

Brudvig, G. W., and Crabtree, R. H. (1986) Mechanism for photosynthetic oxygen evolution. *Proc. Nat. Acad. Sci. USA* **83,** 4586-4588.

Burnap, R. L., and Sherman, L. A. (1991) Deletion mutagenesis in Synechocystis sp. PCC6803 indicates that the manganese-stabilizing protein of photosystem II is not essential for oxygen evolution. *Biochemistry,* **30,** 440-446.

Burnap, R. L., Qian, M., and Pierce, C. (1996) The manganese stabilizing protein of photosystem II modifies the in vivo deactivation and photoactivation kinetics of the H_2O oxidation complex in Synechocystis sp. PCC6803. *Biochemistry* **35,** 874-882.

Campbell, K. A., Gregor, W., Pham, D. P., Peloquin, J. M., Debus, R. J., and Britt, R. D. (1998) The 23 and 17 kDa extrinsic proteins of photosystem II modulate the magnetic properties of the S_1 state Mn cluster. *Biochemistry* **37,** 5039-5045.

Carrell, T. G., Tyryshkin, A. M., and Dismukes, G. C. (2001) An evaluation of structural models for the photosynthetic water-oxidizing complex derived from spectroscopic and X-ray diffraction signatures. *J. Biol. Inorg. Chem.* **7,** 2-22.

Chen, C., and Cheniae, G. M. (1995) in *Photosynthesis: from Light to the Biosphere* (Mathis, P., Ed.) pp 329-332, Kluwer Academic Publishers, Dordrecht, The Netherlands.

Christen, G., Seeliger, A., and Renger, G. (1999) $P680^{+\bullet}$ reduction kinetics and redox transition probability of the water oxidizing complex as a function of pH and H/D isotope exchange in spinach thylakoids. *Biochemistry* **38,** 6082-6092.

Chu, H. A., Nguyen, A. P., and Debus, R. J. (1995a) Amino acid residues that influence the binding of manganese or calcium to photosystem II. 1. The lumenal interhelical domains of the D1 polypeptide. *Biochemistry,* **34,** 5839-5858.

Chu, H. A., Nguyen, A. P., and Debus, R. J. (1995b) Amino acid residues that influence the binding of manganese or calcium to photosystem II. 2. The carboxy-terminal domain of the D1 polypeptide.

Cinco, R. M., Robblee, J. H., Rompel, A., Fernandez, C., Yachandra, V. K., Sauer, K., and Klein, M. P. (1998) Strontium EXAFS reveals the proximity of calcium to the manganese cluster of oxygen-evolving photosystem II. *J. Phys. Chem. B* **102,** 8248-8256.

Clarke, S. M., and Eaton-Rye, J. J. (2000) Amino acid deletions in loop C of the chlorophyll a-binding protein CP47 alter the chloride requirement and/or prevent the assembly of photosystem II. *Plant Mol. Biol.* **44,** 591-601.

Dau, H., and Sauer, K. (1996) Exciton equilibration and the photosystem II exciton dynamics- a fluorescence study on photosystem II membrane particles of spinach. *Biochim. Biophys. Acta* **1273,** 175-190.

Dau, H., Iuzzolino, L., and Dittmer, J. (2001) The tetra-manganese complex of photosystem II during its redox cycle − X-ray absorption results and mechanistic implications. *Biochim. Biophys. Acta.* **1503,** 24-39.

Debus, R. J., Barry, B. A., Babcock, G. T., and McIntosh, L. (1988a) Site-directed mutagenesis identifies a tyrosine radical involved in the photosynthetic oxygen-evolving system. *Proc. Nat. Acad. Sci. USA* **85,** 427-430.

Debus, R. J., Barry, B. A., Sithole, I., Babcock, G. T., and McIntosh, L. (1988b) Directed mutagenesis indicates that the donor to P+680 in photosystem II is tyrosine-161 of the D1 polypeptide. *Biochemistry* **27,** 9071-9074.

Debus, R. J. (1992). The manganese and calcium ions of photosynthetic oxygen evolution. *Biochim. Biophys. Acta* **1102,** 269-352.

Debus, R. J. (2001) Amino acid residues that modulate the properties of tyrosine and the manganese cluster in the water oxidizing complex of photosystem II. *Biochim. Biophys. Acta* **1503,** 164-186.

DeRose, V. J., Yachandra, V. K., McDermott, A. E., Britt, R. D., Sauer, K., and Klein, M. P. (1991) Nitrogen ligation to the manganese in photosynthetic oxygen-evolving complex: continuous-wave and pulsed EPR studies of photosystem II particles containing 14N or 15N. *Biochemistry* **30,** 1335-1341.

DeRose, V. J., Mukerji, I., Latimer, M. J., Yachandra, V. K., Sauer, K., and Klein, M. P. (1994) Comparison of the manganese oxygen-evolving complex in photosystem II of

spinach and Synechococcus sp. with multinuclear manganese model compounds by X-ray absorption spectroscopy. *J. Am. Chem. Soc.* **116,** 5239-5249.

DeRose, V. J., Latimer, M. J., Zimmerman, J. L., Yachandra, V. K., Sauer, K., and Klein, M. P. (1995) Fluoride substitution in the Mn cluster from Photosystem II: EPR and X-ray absorption spectroscopy studies. *Chem. Phys.* **194,** 443-459.

Des Marais, D. J. (1998) Earth's early biosphere. *Gravit. Space Biol. Bull.* **11,** 22-30.

de Wijn, R and van Gorkom, H. J. (2001) Kinetics of electron transfer from Q(a) to Q(b) in photosystem II. *Biochemistry* **40,** 11912-11922.

Diner, B. A., and Petrouleas, V. (1987) Q_{400}, the non-heme iron of the photosystem II iron-quinone complex. A spectroscopic probe of quinone and inhibitor binding to the reaction center. *Biochim. Biophys. Acta* **895,** 107-125.

Diner, B. A. (2001) Amino acid residues involved in the coordination and assembly of the manganese cluster of photosystem II. Proton-coupled electron transport of redox active tyrosine residues and its relationship to water oxidation. *Biochim. Biophys. Acta* **1503,** 147-163.

Diner, B. A., and Rappaport, F. (2002) Structure, dynamics, and energetics of the primary photochemistry of photosystem II of oxygenic photosynthesis. *Annu. Rev. Plant Physiol. Plant Mol. Biol.* **53,** 551-580.

Dismukes, G. C., and Siderer, Y. (1981) Intermediates of a polynuclear manganese cluster involved in photosynthetic water oxidation. *Proc. Nat. Acad. Sci. USA* **78,** 274-278.

Dismukes, G. C. (2001) Photosynthesis. Splitting water. *Science* **292,** 447-448.

Dismukes, G. C., Klimov, V. V., Baranov, S. V., Kozlov, Y. N., DasGupta, J., and Tyryshkin, A. (2001) The origin of atmospheric oxygen on Earth: the innovation of oxygenic photosynthesis. *Proc. Nat. Acad. Sci USA* **98,** 2170-2175.

Donovan, B.,Walker, L. A., Kaplan, D., Bouvier, M., Yocum, C. F., and Sension, R. J. (1997) Structure and function in the isolated reaction center complex of photosystem II. 1. Ultrafast fluorescence measurements. *J. Phys. Chem. B* **101,** 5232-5238.

Durrant, J. R., Hastings, G., Joseph, D. M., Barber, J., Porter, G., and Klug, D. R. (1992) Subpicosecond equilibration of excitation energy in isolated photosystem II reaction centers. *Proc. Nat. Acad. Sci. USA* **89,** 11632-11636.

Dwyer, J. J., Gittis, A. G., Karp, D. A., Lattman, E. E., Spencer, D. S., Stites, W. E., and B. Garcia-Moreno, E. (2000) High apparent dielectric constants in the interior of a protein reflect water penetration. *Biophys. Journ.* **79,** 1610-1620.

Eaton-Rye, J. J., and Govindjee (1988) Electron transfer through the quinone acceptor complex of photosystem II after one or tow actinic flashes in bicarbonate-depleted spinach thylakoid membranes. *Biochim. Biophys. Acta* **935,** 237-257.

Eijckelhoff, C., van Roon, H., Groot, M. L., van Grondelle, R., and Dekker, J. P. (1996). Purification and spectroscopic characterization of photosystem II reaction center complexes isolated with or without Triton X-100. *Biochemistry* **35,** 12864-12872.

Enami, I., Kikuchi, S., Fukuda, T., Ohta, H., and Shen, J. R. (1998) Binding and functional properties of four extrinsic proteins of photosystem II from a red alga, Cyanidium caldarium, as studied by release-reconstitution experiments. *Biochemistry* **37**, 2787-2793.

Evans, M. C. W., Rich A. M., Gourovskaya, K., and Nugent, J. H. A. (1999) Investigation of the interaction of the water oxidising manganese complex of photosystem II with the aqueous solvent environment. *FEBS Lett.* **450,** 285-288.

Evans, M. C. W., Rich, A. M., and Nugent, J. H. A. (2000) Evidence for the presence of a component of the Mn complex of the photosystem II reaction centre which is exposed to water in the S_2 state of the water oxidation complex. *FEBS Lett.* **477,** 113-117.

Feyziev, Ya. M., Yoneda, D., Yoshi, T., Katsuta, N., Kawamori, A., and Watanabe, Ya. (2000) Formate induced inhibition of the water-oxidizing complex of photosystem II studied by EPR. *Biochemistry* **39,** 3848-3855.

Fierke, C. A., Calderone, T. L., and Krebs, J. F. (1991) Functional consequences of engineering the hydrophobic pocket of carbonic anhydrase II. *Biochemistry* **30,** 11054-11063.

Fischer, G., and Wydrzynski, T. (2001) Isotope effects in FTIR difference spectra of the photosynthetic oxygen-evolving catalytic site determined by ab initio calculations on model compounds. *J. Phys. Chem. B* **105,** 12894-12901.

Forbush, B., Kok, B., and McGloin, M. (1971) Cooperation of charges in photosynthetic O_2-evolution-II. Damping of flash yield oscillation, deactivation. *Photochem. Photobiol.* **14,** 307-321.

Force, D. A., Randall, D. W., and Britt, R. D. (1997) Proximity of acetate, manganese, and exchangeable deuterons to tyrosine YZ. in acetate-inhibited photosystem II membranes: implications for the direct involvement of YZ. in water-splitting. *Biochemistry* **40,** 12062-12070.

Force, D. A., Randall, D. W., Lorigan, G. A., Clemens, K. L., and Britt, R. D. (1998) ESEEM studies of alcohol binding to the manganese cluster of the oxygen evolving complex of photosystem II. *J. Am. Chem. Soc.* **120,** 13321-13333.

Förster, V., and Junge, W. (1985) Stoichiometry and kinetics of proton release upon photosynthetic water oxidation. *Photochem. Photobiol.* **41,** 183-190.

Fowler, C. F. (1977) Proton evolution from photosystem II. Stoichiometry and mechanistic implications. *Biochim. Biophys. Acta* **462,** 414-421.

George, G. N., Prince, R. C., and Cramer, S. P. (1989) The manganese site of the photosynthetic water-splitting enzyme. *Science* **243,** 789-791.

Ghanotakis, D. F., Topper, J. N., Babcock, G. T., and Yocum, C. F. (1984) Water-soluble 17 and 23 kDa polypeptides restore oxygen evolution activity by creating a high affintity binding site for Ca^{2+} on the oxidizing side of photosystem II. *FEBS Lett.* **170,** 169-173.

Ghanotakis, D. F., Babcock, G. T., and Yocum, C. F. (1985) On the role of water-soluble polypeptides (17, 23 kDa), calcium and chloride in photosynthetic oxygen evolution. *FEBS Lett* **192,** 1-3.

Ghanotakis, D. F., and Yocum, C. F. (1990) Photosystem II and the oxygen evolving complex. *Annu. Rev. Plant Physiol. Mol. Plant Biol.* **41,** 255-276.

Gilchrist, M. L., Ball, J. A., Randall, D. W., and Britt, R. D. (1995) Proximity of the manganese cluster of photosystem II to the redox active tyrosine Y_Z. *Proc. Nat. Acad. Sci. USA* **92,** 9545-9549.

Goodin, D. B., Yachandra, V. K., Britt, R. D., Sauer, K., and Klein, M. P. (1984) The state of manganese in the photosynthetic apparatus 3. Light induced changes in X-ray absorption [K-edge] energies of manganese in photosynthetic membranes. *Biochim. Biophys. Acta* **767,** 209-216.

Gounaris, K., Chapman, D. J., Booth, P., Crystall, B., Giorgi, L. B., Klug, D. R., Porter, G., and Barber, J. (1990) Comparison of the D1/D2/cytochrome b559 reaction centre complex of photosystem two isolated by two different methods. *FEBS Lett.* **265,** 88-92.

Grätzel, M. (2001) Photoelectronchemical cells. *Nature* **414,** 338-344.

Greenfield, S. R., Seibert, M., Govindjee, and Wasielewski, M. R. (1997) Direct measurement of the effective rate constant for primary charge separation in isolated photosystem II reaction centers. *J. Phys. Chem. B* **101,** 2251-2255.

Grove, G. N., and Brudvig, G. W. (1998) Clacium binding studies of photosystem II using a calcium-sensitive electrode. *Biochemistry* **37,** 1532-1539.

Guy, R. D., Fogel, M. L., and Berry, J. A. (1993) Photosynthetic fractionation of stable isotopes of oxygen and carbon. *Plant Physiol.* **101,** 37-47.

Haddy, A., Aasa, R., and Andreasson, L. –E. (1989) S-band EPR studies of the S2 state multiline signal from the photosynthetic oxygen evolving complex. *Biochemistry* **28,** 6954-6959.

Hallahan, B. J., Nugent, J. H. A., Warden, J. T., and Evans, M. C. W. (1992) Investigation of the origin of the "S3" EPR signal from the oxygen-evolving complex of photosystem 2: the role of tyrosine Z. *Biochemistry* **31,** 4562-4573.

Han, K.-C., and Katoh, S. (1993) Different localization of two Ca^{2+} in spinach oxygen-evolving photosystem II membranes. Evidence for involvement of only one in oxygen evolution. *Plant Cell Physiol.* **34,** 585-593.

Han, K.-C., and Katoh, S. (1995) Different binding affinity sites of Ca2+ for reactivation of oxygen evolution in NaCl-washed photosystem II membranes represent differently modified states of a single binding site. *Biochim. Biophys. Acta* **1232,** 230-236.

Hankamer, B., Morris, E., Nield, J., Gerle, C., and Barber, J. (2001a) Three-dimensional structure of the photosystem II core dimer of higher plants determined by electron microscopy. *J. Struct. Biol.* **135,** 262-269.

Hankamer, B., Morris, E., Nield, J., Carne, A., and Barber, J. (2001b) Subunit positioning and transmembrane helix organization in the core dimer of photosystem II. *FEBS Lett.* **504,** 142-151.

Hansson, Ö., Andréasson, L.–E., and Vänngård, T. (1986) Oxygen from water is coordinated to manganese in the S_2 state of photosystem II. *FEBS Lett.* **195,** 151-154.

Harris, E. H. (1989) in *The Chlamydomonas Sourcebook*: *A Comprehensive Guide to Biological and Laboratory Use.* Academic Press, San Diego.

Hasegawa, K., Ono, T.-A., Inoue, Y., and Kusunoki, M. (1999) Spin-exchange interactions in the S_2-state manganese tetramer in photosynthetic oxygen-evolving complex deduced from g=2 multiline EPR signal. *Chem. Phys. Lett.* **300,** 9-19.

Haumann, M., and Junge, W. (1994) Extent and rate of proton release by photosynthetic water oxidation in thylakoids: electrostatic relaxation versus chemical production. *Biochemistry* **33,** 864-872.

Haumann, M., and Junge, W. (1996) in *Oxygenic Photosynthesis: The Light Reactions* (Ort, D. R., and Yocum, C. F., Ed.) Kluwer Academic Publishers, Dordrecht, The Netherlands.

Haumann, M., Mulkidjanian, A. Y., and Junge, W. (1997) Electrogenicity of electron and proton transfer at the oxidizing side of photosystem II. *Biochemistry,* **36,** 9304-9315.

Haumann, M., and Junge, W. (1999) Photosynthetic water oxidation: a simplex-scheme of its partial reactions. *Biochim. Biophys. Acta* **1411,** 86-91.

Hendry, G., and Wydrzynski, T. (2002) The two substrate-water molecules are already bound to the oxygen evolving complex in the S_2 state of photosystem II. Biochemistry, in press.

Hienerwadel, R., and Berthomieu, C. (1995) Bicarbonate binding to the non-heme iron of photosystem II investigated by Fourier transform infrared difference spectroscopy and ^{13}C-labeled bicarbonate. *Biochemistry* **34,** 146-148.

Hillier, W., Messinger, J., and Wydrzynski, T. (1998) Kinetic determination of the fast exchanging substrate water molecule in the S_3 state of photosystem II. *Biochemistry* **37,** 16908-16914.

Hillier, W. (1999) Substrate exchange in the water-oxidizing complex of photosystem II. *PhD Thesis, The Australian National University.*

Hillier, W., and Babcock, G. T. (2001) Photosynthetic reaction centers. *Plant Physiol.* **125,** 33-37.

Hillier, W., and Wydrzynski, T. (2000) The affinities for the two substrate water binding sites in the O2 evolving complex of photosystem II vary independently during S-state turnover. *Biochemsitry* **39,** 4399-4405.

Hillier, W., Hendry, G., Burnap, R. L., and Wydrzynski, T. (2001) Substrate water exchange in photosystem II depends on the peripheral proteins. *J. Biol. Chem.* **276,** 46917-46924.

Hillier, W., and Wydrzynski, T. (2001) Oxygen ligand exchange at metal sites – implications for the O_2 evolving mechanism of photosystem II. *Biochim. Biophys. Acta* **1503,** 197-209.

Hoganson, C. W., and Babcock, G. T. (1997) A metalloradical mechanism for the generation of oxygen from water in photosynthesis. *Science* **277,** 1953-1956.

Hulsebosch, R. J., Allakhverdiev, S. I., Klimov, V. V., Picorel, R., and Hoff, A. J. (1998) Effect of bicarbonate on the S2 multiline EPR signal of the oxygen-evolving complex in photosystem II membrane fragments. *FEBS Lett.* **424,** 146-148.

Iuzzolino, L., Dittmer, J., Dorner, W., Meyer-Klaucke, W., and Dau, H. (1998) X-ray absorption spectroscopy on layered photosystem II membrane particles suggests manganese centered oxidation of the oxygen-evolving complex for the S_0-S_1, S_1-S_2 and S_2-S_3 transitions of the water oxidation cycle. *Biochemistry* **37,** 17112-17119.

Joliot, P., Barieri, G., and Chabaud, R. (1969) Un nouveau modéle des centres photochimique du systém II. *Photochem. Photobiol.* **10,** 309-329.

Kalosaka, K., Beck, W. F., Brudvig, G., and Cheniae, G. (1990) Coupling of the PS2 reaction center to the O_2-evolving center requires a very high affinity Ca^{2+} site. *Curr. Res. Photosynth.* **1,** 721-724.

Ke, B. (2001) in *Photosynthesis: Photochemistry and Photobiophysics*. Kluwer Academic Publishers, Dordrecht, The Netherlands.

Kelly, P. M., and Izawa, S. (1978) The role of the chloride ion in photosystem II: I. Effects of chloride ion of photosystem II electron transport and on hydroxylamine inhibition. *Biochim. Biophys. Acta* **502,** 198-210.

Kimura, Y., Hasegawa, K., and Ono, T.–A. (2002) Characteristic changes of the S_1/S_2 difference FTIR spectrum induced by Ca^{2+} depletion and metal cation substitution in the photosynthetic oxygen-evolving complex. *Biochemistry* **41,** 5844-5853.

Klein, M. P., Sauer, K., and Yachandra, V. K. (1993) Perspectives on the structure of the photosynthetic oxygen evolving manganese complex and its relation to the S-state cycle. *Photosynth. Res.* **38,** 265-277.

Klimov, V. V., Allakhverdiev, S. I., Demeter, S., and Kransnovskii, A. (1979) Photoreduction of pheophytin in photosystem 2 (Russian). *Dokl. Akad. Nauk. SSSR* **249,** 227-230.

Klimov, V. V., Allakhverdiev, S. I., Feyziev, Ya. M., and Baranov, S. V. (1995a) Bicarbonate requirement for the donor side of photosystem II. *FEBS Lett.* **363,** 251-255.

Klimov, V. V., Allakhverdiev, S. I., Baranov, S. V., Ya. M., and Feyziev, Ya. M. (1995b) Effects of bicarbonate and formate on the donor side of photosystem 2. *Photosynth. Res.* **46,** 219-225.

Klimov, V. V., Hulesbosch, R. J., Allakhverdiev, S. I., Wincencjusz, H., van Gorkom, H. J., and Hoff, A. J. (1997a) Bicarbonate may be required for ligation of manganese in the oxygen-evolving complex of photosystem II. *Biochemistry,* **36,** 16277-16281.

Klimov, V. V., Baranov, S. V., and Allakhverdiev, S. I. (1997b) Bicarbonate protects the donor side of photosystem II against photoinhibition and thermoinactivation. *FEBS Lett.* **418,** 243-246.

Klimov, V. V., and Baranov, S. V. (2001) Bicarbonate requirement for the water-oxidizing complex of photosystem II. *Biochim. Biophys. Acta* **1503,** 187-196.

Klug, D. R., Rech, T., Joseph, D. M., Barber, J., Durrant, J. R., and Porter, G. (1995) Primary processes in isolated photosystem II reaction centers probed by magic angle transient absorption spectroscopy. *Chem. Phys.* **194,** 433-442.

Kok, B., Forbush, B., and McGloin M. (1970) Cooperation of charges in photosynthetic O_2-evolution-1. A linear four step mechanism. *Photochem. Photobiol.* **11,** 457-475.

Kozlov, Yu. N., Kazakova, A. A., and Klimov, V. V. (1997) in *Biol. Membr.* (Moscow) **14,** 93-97.

Kühlbrandt, W., Wang, D. N., and Fujiyoshi, Y. (1994) Atomic model of plant light-harvesting complex by electron crystallography. *Nature* **367,** 614-621.

Kusunoki, M. (1992) A new paramagnetic hyperfine structure effect in manganese tetramers. The origin of "multiline" EPR signals from an S_2 state of a photosynthetic water-splitting. *Chem. Phys. Lett.* **197,** 108-116.

Kusunoki, M., Takano, T., Ono, T., Noguchi, T., Yamaguchi, Y., Oyanagi, H., and Inoue, Y. (1995) in *Photosynthesis: From Light to Biosphere* (Mathis, P., Ed.) pp 251-254, Kluwer Academic Publishers, Dordrecht, The Netherlands.

Kuwabara, T., and Murata, N. (1983) Inactivation of photosynthetic oxygen evolution and concomitant release of three polypeptides in photosystem II particles of spinach chloroplasts. *Plant Cell Physiol.* **24,** 741-747.

Kuzek, D., and Pace, R. J. (2001) Probing the Mn oxidation states in the OEC. Insights from spectroscopic, computational and kinetic data. *Biochim. Biophys. Acta* **1503,** 123-137.

Laemmli, U. K. (1970) Cleavage of structural proteins during the assembly of the head of bacteriophage T4. *Nature* **227,** 680-685.

Latimer, M. J., DeRose, V. J., Mukerji, I., Yachandra, V. K., Sauer, K., and Klein, M. P. (1995) Evidence for the proximity of calcium to the manganese cluster of photosystem II: Determination by X-ray absorption spectroscopy. *Biochemistry* **34,** 10898-10909.

Latimer, M. J., DeRose, V. J., Yachandra, V. K., Sauer, K., and Klein, M. P. (1998) Structural effects of calcium depletion on the manganese cluster of photosystem II: determination by X-ray absorption spectroscopy. *J. Phys. Chem. B* **102,** 8257-8265.

Lavergne, J., and Junge, W. (1993) Proton release during the redox cycle of the water oxidase. *Photosynth. Res.* **38,** 279-296.

Leuschner, C., and Bricker, T. M. (1996) Interaction of the 33 kDa extrinsic protein with photosystem II: rebinding of the 33 kDa extrinsic protein to photosystem II membranes which contain four, two, or zero manganese per photosystem II reaction center. *Biochemsitry* **35,** 4551-4557.

Liang, W., Roelofs, T. A., Cinco, R. M., Rompel, A., Latimer, M. J., Yu, W. O., Sauer, K., and Klein, M. P. (2000) Structural change of the Mn cluster during the $S_2 \rightarrow S_3$ state transition of the oxygen-evolving complex of photosystem II. Does it reflect the onset of water/substrate oxidation? Determination by Mn X-ray absorption spectroscopy. *J. Am. Chem. Soc.* **122,** 3399-3412.

Limburg, J., Szalai, V. A., and Brudvig, G. W. (1999) A mechanistic and structural model for the formation and reactivity of a Mn^V=O species in photosynthetic water oxidation. *J. Chem. Soc., Dalton Trans.* 1353-1361.

Lincoln, S. F., and Merbach, A. E. (1995) Substitution reactions of solvated metal ions. *Adv. Inorg. Chem.* **42,** 1-88.

Lindberg, K., Vänngård, T., and Andréasson, L. (1993) Studies of the slowly exchanging chloride in photosystem II membranes. *Photosynth. Res.* **38,** 401-408.

Lu, Y.-K., and Stemler, A. J. (2002) Extrinsic photosystem II carbonic anhydrase in Maize mesophyll chloroplasts. *Plant Physiol.* **128,** 643-649.

MacLachlan, D. J., Hallahan, B. J., Ruffle, S. V., Nugent, J. H. A., Evans, M. C. W., Strange, R. W., and Hasnain, S. S. (1992) An e.x.a.f.s. study of the manganese O_2-evolving complex in purified photosystem II membrane fractions. *Biochem. J.* **285,** 569-576.

Matysik, J., Nachtegaal, G., van Gorkom, H. F., Hoff, A. J., and de Groot, H. J. M. (2000) Exploring the calcium-binding site in photosystem II membranes by solid-state ^{113}Cd NMR. *Biochemistry* **39,** 6751-6755.

McDermott, A. E., Yachandra, V. K., Guiles, R. D., Cole, J. L., Dexhiemer, S. L., Britt, R. D., Sauer, K., and Klein, M. P. (1988) Characterization of the manganese oxygen-evolving complex and the iron-quinone acceptor complex in photosystem II from a thermophilic cyanobacterium by electron paramagnetic resonance and x-ray absorption spectroscopy. *Biochemistry* **27,** 4021-4031.

Merry, S. A., Nixon, P. J., Barter, L. M., Schilstra, M., Porter, G., Barber, J., Durrant, J. R., and Klug, D. R. (1998) Modulation of quantum yield of primary radical pair formation in photosystem II by site-directed mutagenesis affecting radical cations and anions. *Biochemistry* **37,** 17439-17447.

Messinger, J., Wacker, U., and Renger, G. (1991) Unusual low reactivity of the water oxidase in redox state S_3 toward exogenous reductants. Analysis of the NH_2OH- and NH_2NH_2-induced modifications of flash-induced oxygen evolution in isolated spinach thylakoids. *Biochemistry* **30,** 7852-7862.

Messinger, J., Badger, M., & Wydrzynski, T. (1995) Detection of one *slowly* exchanging substrate water molecule in the S3 state of photosystem II. *Proc. Nat. Acad. Sci* **92,** 3209-3213.

Messinger, J., Robblee, J. H., Bergmann, U., Fernandez, C., Glatzel, P., Visser, H., Cinco, R. M., McFarlane, K. L., Bellacchio, E., Pizarro, S. A., Cramer, S. P., Sauer, K., Klein, M. P., and Yachandra, V. K. (2001) Absence of Mn-centered oxidation on the $S_2 \rightarrow S_3$ transition : implications for the mechanism of photosynthetic water oxidation. *J. Am. Chem. Soc.* **123,** 7804-7820.

Metz, J. G., Nixon, P. J., Rogner, M., Brudvig, G. W., and Diner, B. A. (1989) Directed alteration of the D1 polypeptide in photosystem II: evidence that tyrosine-161 is the redox component , Z, connecting the oxygen-evolving complex to the primary electron donor, P680. *Biochemistry* **28,** 6960-6969.

Metzner, H. (1978) in *Photosynthetic Oxygen Evolution* pp 59-76, Academic Press, New York.

Metzner, H., Fischer, K., and Bazlen, O. (1981) in *Photosynthesis* (Akoynoglou, G., ed.) pp 375-387, Balaban, Philadelphia.

Miller, A.-F., and Brudvig, G. (1990) Electron transfer events leading to reconstitution of oxygen evolving-activity in manganese-depleted photosystem II membranes. *Biochemistry* **29,** 1385-1392.

Miller, A. G., Salon, C., Espie, G. S., and Canvin, D. T. (1997) Measurement of the amount and isotopic composition of the CO_2 release from the cyanobacterium *Synechococcus* UTEX 625 after rapid quenching of the active CO_2 transport system. *Can. J. Bot.* **75,** 981-997.

Mino, H., Kawamori, A., Matsukawa, T., and Ono, T.-A. (1998) Light-induced high-spin signals from the oxygen evolving center in Ca^{2+}-depleted photosystem II studied by dual mode electron paramagnetic resonance spectroscopy. *Biochemistry* **37,** 2749-2799.

Miyao, M., and Murata, N. (1984) Calcium ions can be substituted for the 24-kDa polypeptide in photosynthetic oxygen evolution. *FEBS Lett.* **168,** 118-120.

Mulkidjanian, A. Y., Cherepanov, D. A., Haumann, M., and Junge, W. (1996) Photosystem II of green plants: topology of core pigments and redox cofactors as inferred from electrochromic difference spectra. *Biochemistry,* **35,** 3093-3107.

Murata, N., and Miyao, M. (1985) Extrinsic membrane proteins in the photosynthetic oxygen evolving complex. *Trends Biochem. Sci.* **10,** 122-124.

Nixon, P. J., Gounaris, K., Coomber, S. A., Hunter, C. N., Dyer, T. A., and Barber, J. (1989) psbG is not a photosystem two gene but may be an ndh gene. *J. Biol. Chem.* **264,** 14129-14135.

Nixon, P. J., and Diner, B. A. (1992) Aspartate 170 of the photosystem II reaction center polypeptide D1 is involved in the assembly of the oxygen-evolving manganese cluster. *Biochemistry* **31,** 942-948.

Nixon, P. J., and Diner, B. A. (1994) Analysis of water-oxidation mutants constructed in the cyanobacterium Synechocystis sp. PCC 6803. *Biochem. Soc. Trans.* **22,** 338-343.

Noguchi, T., Ono, T.-A., and Inoue, Y. (1995) Direct detection of a carboxylate bridge between Mn and Ca^{2+} in the photosynthetic oxygen-evolving center by means of Fourier transform infrared spectroscopy. *Biochim. Biophys. Acta* **1228,** 189-200.

Noghchi, T., and Sugiura, M. (2000) Structure of an active water molecule in the water-oxidizing complex of photosystem II as studied by FTIR spectroscopy. *Biochemsitry* **39,** 10943-10949.

Noguchi, T., and Sugiura, M. (2002) Flash-induced FTIR difference spectra of the water oxidizing complex in moderately hydrated photosystem II core films: effect of hydration extent on S-state transitions. *Biochemistry* **41,** 2322-2330.

Nugent, J. H. A. (1987) Water binding to the oxygen evolving system of chloroplasts; effects of isotope substitution on the S_2 state of the EPR spectrum. *Biochim. Biophys. Acta* **893,** 184-189.

Nugent, J. H. A., Corrie, A. R., Demetriou, C., Evans, M. C. W., and Lockett, C. J. (1988) Bicarbonate binding and the properties of photosystem II electron acceptors. *FEBS Lett.* **235,** 71-75.

Nugent, J. H. A., Rich, A. M., and Evans, M. C. W. (2001) Photosynthetic water oxidation: towards a mechanism. *Biochim. Biophys. Acta* **1503,** 138-146.

Ono, T-A., and Inoue, Y. (1983) Mn-preserving extraction of 33- 24- and 16-kDa proteins from O_2-evolving PSII particles by divalent salt-washing. *FEBS Lett.* **164,** 255-260.

Ono, T., and Inoue, Y. (1984) Reconstitution of photosynthetic oxygen evolution activity by rebinding of the 33 kDa protein to CaCl2-extracted PSII particles. *FEBS Lett.* **166,** 381-384.

Ono, T., Zimmerman, J. L., Inoue, Y., and Rutherford, A. W. (1986) EPR evidence for a modified S-state transition in chloride-depleted photosystem II. *Biochim. Biophys. Acta* **851,** 193-201.

Ono, T.-A., and Inoue, Y. (1988) Discrete extraction of the Ca atom functional for O_2 evolution in higher plant photosystem II by a simple low pH treatment. *FEBS Lett.* **227,** 147-152.

Ono, T., and Inoue, Y. (1989) Roles of Ca^{2+} in O_2 evolution in higher plant photosystem II: effects of replacement of Ca^{2+} site by other metal cations. *Arch. Biochem. Biophys.* **275,** 440-448.

Ono, T., and Inoue, Y. (1990) Abnormal redox reactions in photosynthetic O_2-evovling centers in NaCl/EDTA-washed PSII; a dark-stable EPR multiline signal and an unknown positive charge accumulator. *Biochim. Biophys. Acta* **1020,** 269-277.

Ono, T., Noguchi, T., Inoue, Y., Kosunoki, M., Matsushita, T., and Oyanagi, H. (1992) X-ray detection of the period-four cycling of the manganese cluster in the photosynthetic water oxidizing enzyme. *Science,* **258,** 1335-1337.

Ono, T.-A., Rompel, A., Mino, H., and Chiba, N. (2001) Ca^{2+} function in photosynthetic oxygen evolution studied by alkali metal cations substitution. *Biophys. J.* **81,** 1831-1840.

Oprea, T. I., Hummer, G., and Garcia, A. E. (1995) Identification of a functional water channel in cytochrome P450 enzymes. *Proc. Nat. Acad. Sci USA* **94,** 2133-2138.

Pandolfino, E. R., Christie, R. J., Munske, G. R., Fry, J., and Magnuson, J. A. (1980) Activation of concanavalin A by Cd^{2+}. *J. Biol. Chem.* **255,** 8772-8775.

Pecoraro, V. L., Baldwin, M. J., Cuadle, M. T., Hsieh, W-Y., and Law, N. A. (1998) A proposal for water oxidation in photosystem II. *Pure & Appl. Chem.* **70,** 925-929.

Penner-Hahn, J. E., Fronko, R. M., Pecoraro, V. L., Yocum, C. F., Betts, S. D., and Bowlby, N. R. (1990) Structural characterization of the manganese sites in the photosynthetic oxygen-evolving complex using x-ray absorption spectroscopy. *J. Am. Chem. Soc.* **112,** 2549-2557.

Peloquin, J. M., Campbell, K. A., Randall, D. W., Evanchik, M. A., Pecoraro, V. L., Armstrong, W. H. and Britt, R. D. (2000) ^{55}Mn ENDOR of the S_2-state multiline EPR signal of photosystem II: Implications on the structure of the tetranuclear Mn cluster. *J. Am. Chem. Soc.* **122,** 10926-10942.

Peloquin, J. M., and Britt, R. D. (2001) EPR/ENDOR characterization of the physical and electronic structure of the OEC Mn cluster. *Biochim. Biophys. Acta* **1503,** 96-111.

Perrin, D. D. (1969) in *IUPAC Dissociation Constants of Inorganic Acids and Bases in Aqueous Solution*. Butterworth and Co., London.

Peterson, S., Åhrling, K. A., Hogblom, J., and Styring, S. (2001) EPR studies of the oxygen-evolving complex reveal a light-adaptation process in photosystem II. 12th International Congress on Photosynthesis, CSIRO Publishers. www.publish.csiro.au/PS2001, S10-003.

Peterson, S., Åhrling, K. A., Hogblom, J. P. E., and Styring, S. (2002) Single turnover light-adaptation of photosystem II involves the appearance of a paramagnetic species near the oxygen-evolving comples. *Submitted*.

Petrouleas, V., Deligiannakis, Y., and Diner, B. A. (1994) Binding of carboxylate anions at the non-heme Fe(II) of PSII. 2. Competition with bicarbonate and effects on the QA/QB electron transfer rate. *Biochim. Biophys. Acta* **1188,** 271-277.

Pitera, J. W., Falta, M., and van Gunsteren, W. F. (2001) Dielectric properties of proteins from simulation: the effects of solvent, ligands, pH and temperature. *Biophys. Journ.* **80,** 2546-2555

Porra, R. J., Thompson, W. A., and Kriedemann, P. E. (1989) Determination of accurate extinction coefficients and simultaneous equations for assaying chlorophylls *a* and *b* extracted with four different solvents: verification of the concentration of chlorophyll standards by atomic absorption. *Biochim. Biophys. Acta* **975,** 384-394.

Radmer, R., and Ollinger, O. (1980) Isotopic composition of the photosynthetic O_2 flash yields in the presence of $H_2^{18}O$ and $HC^{18}O_3^-$. *FEBS Lett.* **110,** 57-61.

Radmer, R., and Ollinger, O. (1986) Do the higher oxidation states of the photosynthetic O_2-evolving system contain bound H_2O? *FEBS Lett.* **195,** 285-289.

Rappaport, F., and Lavergne, J. (1991) Proton release during successive oxidation steps of the photosynthetic oxidation process: stoichiometries andpH dependence. *Biochemistry* **30,** 10004-10012.

Rappaport, F., and Lavergne, J. (2001) Coupling of electron and proton transfer in the photosynthetic water oxidase. *Biochim. Biophys. Acta* **1503,** 246-259.

Razeghifard, M. R., Klughammer, C., and Pace, R. J. (1997) Electron paramagnetic resonance kinetic studies of the S states in spinach thylakoids. *Biochemistry* **36,** 86-92.

Razeghifard, M. R., and Pace, R. J. (1999) EPR kinetic studies of oxygen release in thylakoids and PSII membranes: an intermediate in the S_3 to S_0 transition. *Biochemistry* **38,** 1252-1257.

Rhee, K. H., Morris, E. P., Barber, J., and Kühlbrandt, W. (1998) Three-dimensional structure of the plant photosystem II reaction centre at 8 Å resolution. *Nature* **396,** 283-286.

Richens, D. T. (1997) in *The Chemistry of Aqua Ions.* John Wiley and Sons, West Sussex, England.

Riggs-Gelasco, P.,Mei, R., Gahnotakis, D. F., Yocum, C. F., and Penner-Hahn, J. E. (1996) X-ray absorption spectroscopy of calcium-substituted derivatives of the oxygen-evolving complex of photosystem II. *J. Am. Chem. Soc.* **118,** 2400-2410.

Robblee, J. H., Cinco, R. M., and Yachandra, V. K. (2001) X-ray spectroscopy-based structure of the Mn cluster and mechanism of photosynthetic oxygen evolution. *Biochim. Biophys. Acta* **1503,** 7-23.

Roelofs, T. A., Lee, C. H., and Holzwarth, A. R. (1992) Global target analysis of picosecond chlorophyll fluorescence kinetics from pea chloroplasts: a new approach to the characterization of the primary processes in photosystem II a and b units. *Biophys. J.* **61,** 1147-1163.

Roelofs, T. A., Liang, W., Latimer, M. J., Cinco, R. M., Rompel, A., Andrews, J. C., Sauer, K., Yachandra, V. K., and Klein, M. P. (1996) Oxidation states of the manganese cluster during the flash-induced S-state cycle of the photosynthetic oxygen-evolving complex. *Proc. Nat. Acad. Sci. USA* **93,** 3335-3340.

Ruettinger, W., and Dismukes, G. C. (2000) Protonation and dehydration reactions of the $Mn_4O_4L_6$ cubane and synthesis and crystal structure of the oxidized cubane $[Mn_4O_4L_6]^+$: new models for the photosynthetic water oxidizing complex. *Inorg. Chem.* **38,** 1036-1037.

Rutherford, A. W. (1989) Photosystem II, the water splitting enzyme. *Trends Biochem. Sci.* **14,** 227-232.

Sandusky, P. O., and Yocum, C. F. (1984) The chloride requirement for photosynthetic oxygen evolution. Analysis of the effects of chloride and other anions on amine inhibition of the oxygen-evolving complex. *Biochim. Biophys. Acta* **766,** 603-611.

Saphon, S., and Crofts, A. R. (1977) Protolytic reactions in photosystem II: a new model for the release of protons accompanying the photooxidation of water. *Z. Naturforsch.* **32C,** 617-626.

Saygin, Ö., and Witt, H. T. (1985) Evidence for the electrochromic identification of the change of charges in the four oxidation steps of the photoinduced water cleavage in photosynthesis. *FEBS Lett.* **187,** 224-226.

Schelvis, J. P. M., van Noort, P. I., Aartsma, T. J., and van Gorkom, H. J. (1994) Energy transfer, charge separation and pigment arrangement in the reaction center of photosystem II. *Biochim. Biophys. Acta* **1184,** 242-250.

Schilstra, M. J., Rappaport, F., Nugent, J. H. A., Barnett, C. J., and Klug, D. R. (1998) Proton/hydrogen transfer affects the S-state-dependent microsecond phases of P680$^+$ reduction during water splitting. *Biochemistry* **37,** 3974-3981.

Schlodder, E., and Witt, H. T. (1999) Stoichiometry of proton release from the catalytic center in photosynthetic water oxidation: reexamination by a glass electrode study at pH 5.5-7.2. *J. Biol. Chem.* **274,** 30387-30392.

Schubert, W. D., Klukas, O., Saenger, W., Witt, H. T., Fromme, P., and Krauss, N. (1998) Acommon ancestor for oxygenic and anoxygenic photosynthetic systems: a comparison based on the structural model of photosystem I. *J. Mol. Biol.* **280,** 297-314.

Seidler, A. (1996) The extrinsic polypeptides of photosystem II. *Biochim. Biophys. Acta* **1277,** 35-60.

Shi, L. X., Kim, S. J., Marchant, A., Robinson, C., and Schroder, W. P. (1999) Characterisation of the PsbX protein from Photosystem II and light regulation of its gene expression in higher plants. *Plant Mol. Biol.* **40,** 737-744.

Shopes, R. J., Blubaugh, D., Wraight, C., and Govindjee (1989) Absence of a bicarbonate-depletion effect in electron transport between quinones and reaction centers of *Rhodobacter sphaeriodes. Biochim. Biophys. Acta* **974,** 114-118.

Siegbahn, P. E. (2000) Theoretical models for the oxygen radical mechanism of water oxidation and of the water oxidizing complex of photosystem II. *Inorg. Chem.* **39,** 2923-2935.

Sivaraja, M., Tso, J., and Dismukes, G. C. (1989) A calcium-specific site influences the structure and activity of the manganese cluster responsible for photosynthetic water oxidation. *Biochemsitry* **28,** 9459-9464.

Steinberg-Yfrach, G., Riguad, J-L., Durantini, E. N., Moore, A., Gust, D., and Moore, T. A. (1998) Light-driven production of ATP catalysed by F_0F_1-ATP synthase in an artificial photosynthetic membrane. *Nature* **392,** 479-482.

Stemler, A. J., and Govindjee (1973) Bicarbonate ion as a critical factor in photosynthetic oxygen evolution. *Plant Physiol.* **52,** 146-150.

Stemler, A. J. (1980) Inhibition of photosystem II by formate: possible evidence for a direct role of bicarbonate in photosynthetic oxygen evolution. *Biochim. Biophys. Acta* **593,** 103-112.

Stemler, A. J., and Lu, Y.-K. (2001) PSII carbonic anhydrase activity and the bicarbonate effect. PS2001 Proceedings. 12th International Congress on Photosynthesis, CSIRO Publishers. www.publish.csiro.au/PS2001, S13-003.

Stumm, W., and Morgan, J. J. (1970) in *Aquatic Chemistry: An Introduction to Emphasizing Chemical Equilibria in Natural Waters.* John Wiley and Sons, West Sussex, England.

Tamura, N., and Cheniae, G. M. (1987) Photoactivation of the water-oxidizing complex in photosystem II membranes depleted of Mn and extrinsic proteins. I. Biochemical and kinetic characterization. *Biochim. Biophys. Acta* **890,** 179-194.

Tang, X. S., and Diner, B. A. (1994) Biochemical and spectroscopic characterization of a new oxygen-evolving photosystem II core complex from the cyanobacterium *Synechocystis* sp. PCC 6803. *Biochemistry* **33,** 4594-4603.

Tang, X. S., Diner, B. A., Larsen, B. S., Gilchrist, M. L., Lorigan, G. A., and Britt, R. D. (1994) Identification of histidine at the catalytic site of the photosynthetic oxygen-evolving complex. *Proc. Nat. Acad. Sci. USA* **91,** 704-708.

Tang, X. S., Randall, D. W., Force, D. A., Diner, B. A., and Britt, R. D. (1996) Manganese-tyrosine interaction in photosystem II oxygen-evolving complex. *J. Am. Chem. Soc.* **118,** 7638-7639.

Tommos, C., and Babcock, G. T. (1998) Oxygen production in nature: a light-driven metalloradical enzyme process. *Acc. Chem. Res.* **31,** 18-25.

Tomo, T., Enami, I., and Satoh, K. (1993) Orientation and nearest neighbor analysis of psbI gene product in the photosystem II reaction center complex using bifunctional cross-linkers. *FEBS Lett.* **323,** 15-18.

Tripp, B. C., Smith, K., and Ferry, J. G. (2001) Carbonic Anhydrase: New insights for an ancient enzyme. *Journ. Biol. Chem.* **276,** 48615-48618.

Turconi, S., MacLachlan, D. J., Bratt, P. J., Nugent, J. H. A., and Evans, M. C. W. (1997) Analysis of the interaction of water with the manganese cluster of photosystem II using isotopically labeled water. *Biochemistry* **36,** 879-885.

Van Gorkom, H. J., and Schelvis, J. P. M. (1993) Kok's oxygen clock: what makes it tick? The structure of P_{680} and consequences of its oxidizing power. *Photosynth. Res.* **38,** 297-301.

Vander Meulen, K. A., Hobson, A., and Yocum, C. F. (2002) Calcium depletion modifies the structure of the photosystem II O_2-evolving complex. *Biochemistry* **41,** 958-966.

van Rensen, J. J. S., Xu, C., and Govindjee. (1999) Role of bicarbonate in photosystem II, the water-plastoquinone oxidoreductase of plant photosynthesis. *Physiol. Plant.* **105,** 585-592.

Vermaas, W. F. J., and Rutherford, A. W. (1984) EPR measurements on the effect of bicarbonate and triazine resistance on the acceptor side of photosystem II. *FEBS Lett.* **175,** 243-248.

Vermaas, W. F. J., Rutherford, A. W., and Hansson, O. (1988) Site-directed mutagenesis in photosystem II of the cyanobacterium *Synechcocystis* sp. PCC 6803; donor D is a tyrosyl residue in the D2 protein. *Proc. Nat. Acad. Sci. USA* **85,** 8477-8481.

Visser, H. M., Groot, M-L., van Mourik, F., van Stokkum, I. H. M., Dekker, J. P., and van Grondelle, R. (1995) Subpicosecond transient absorption difference spectroscopy on the reaction center of photosystem II: radical pair formation at 77K. *J. Phys. Chem.* **99,** 15304-15309.

Vrettos, J. S., Stone, D. A., and Brudvig, G. W. (2001a) Quantifying the ion selectivity of the Ca^{2+} site in photosystem II: evidence for direct involvement of Ca^{2+} in O_2 formation. *Biochemistry* **40,** 7937-7945.

Vrettos, J. S., Limburg, J., and Brudvig, G. W. (2001b) Mechanism of photosynthetic water oxidation: combining biophysical studies of photosystem II with inorganic model chemistry. *Biochim. Biophys. Acta* **1503,** 229-245.

Wang, X., Cao, J., Maroti, P., Stilz, H. U., Finkele, U., Lauterwasse, Zinth, W., Oesterhelt, D., Govindjee, Wraight, C. A. (1992) Is bicarbonate in photosystem II the equivalent of the glutamate ligand to the iron atom in bacterial reaction centers? *Biochim. Biophys. Acta* **1100,** 1-8.

Warburg, O., and Krippahl, G. (1958) Hill-Reaktionen. *Z Naturforsch* **13b,** 509-514.

Westphal, K. L., Lydakis-Simantris, N., Cukier, R. I., and Babcock, G. T. (2000) Effects of Sr^{2+}-substitution on the reduction rates of Y_Z in PSII membranes-evidence for a concerted hydrogen-atom transfer in oxygen evolution. *Biochemistry* **39,** 16220-16229.

Wincencjusz, H., Allakhverdiev, S. I., Klimov, V. V., and van Gorkom, H. J. (1996) Bicarbonate-reversible formate inhibition at the donor side of photosystem II. *Biochim. Biophys. Acta* **1273,** 1-3.

Wincencjusz, H., Yocum, C. F., and van Gorkom, H. J. (1997) The photosynthetic oxygen evolving complex requires chloride for its redox state $S_2 \rightarrow S_3$ and $S_3 \rightarrow S_0$ transitions but not for $S_0 \rightarrow S_1$ or $S_1 \rightarrow S_2$ transitions. *Biochemistry* **36,** 3663-3670.

Wincencjusz, H., Yocum, C. F., and van Gorkom, H. J. (1998) S-state dependence of chloride binding affinities and exchange dynamics in the intact and polypeptide-depleted O_2 evolving complex of photosystem II. *Biochemistry* **37,** 8595-8604.

Wincencjusz, H., Yocum, C. F., and van Gorkom, H. J. (1999) Activating anions that replace Cl⁻ in the O_2-evolving complex of photosystem II slow the kinetics of the terminal step in water oxidation and destabilize the S2 and S3 states. *Biochemistry,* **38,** 3719-3725.

Wydrzynski, T., and Govindjee (1975) A new site of bicarbonate effect in photosystem II of photosynthesis: evidence from chlorophyll fluorescence transients in spinach chloroplasts. *Biochim. Biophys Acta* **387,** 403-408.

Wydrzynski, T., Hillier, W., and Messinger, J. (1996) On the functional significance of substrate accessibility in the photosynthetic water oxidation mechanism. *Physiol. Plant.* **96,** 342-350.

Xiong, J., Subramaniam, S., and Govindjee (1996) Modeling of the D1/D2 proteins and cofactors of the photosystem II reaction center: implications for herbicide and bicarbonate binding. *Protein Sci.* **5,** 2054-2073.

Xu, C., Taoka, S., Crofts, A. R., and Govindjee (1991) Kinetic characteristics of formate/formic acid binding at the plastoquinone reductase site in spinach thylakoids. *Biochim. Biophys. Acta* **1098,** 32-40.

Yachandra, V. K., Guiles, R. D., Sauer, K., and Klein, M. P. (1986) The state of the manganese in the photosynthetic apparatus. 5. The chloride effect in photosynthetic oxygen evolution. Is halide coordinated to the EPR-active manganese in the O_2-evolving complex? Studies of the substructure of the low temperature multiline EPR signal. *Biochim. Biophys. Acta* **850,** 333-342.

Yachandra, V. K., DeRose, V. J., Latimer, M. J., Mukerji, I., and Klein, M. P. (1991) A structural model of the oxygen evolving manganese cluster. *Photochem. Photobiol.* **53,** Suppl. 98S.

Yachandra, V. K., DeRose, V. J., Latimer, M. J., Mukerji, I., Sauer, K., and Klein, M. P. (1993). Where plants make oxygen: a structural model for the photosynthetic oxygen-evolving manganese cluster. *Science* **260,** 675-679.

Yamamoto, Y., Shinkai, H., Isogai, Y., Matsuura, K., and Nishimura, M. (1984) Isolation of a Mn-carrying 33-kDa protein from an oxygen evolving photosystem II preparation by phase partitioning in butanol. *FEBS Lett.* **175,** 429-432.

Yocum, C. F. (1991) Calcium activation of photosynthetic water oxidation. *Biochim. Biophys. Acta* **1059,** 1-15.

Yreula, I., Allakhverdiev, S. I., Ibarra, J. V., and Klimov, V. V. (1998) Bicarbonate binding to the water-oxidizing complex in the photosystem II. A Fourier transform infrared spectroscopy study. *FEBS Lett.* **425,** 396-400.

Zheng, M., Khangulov, S. V., Dismukes, G. C., and Barynin, V.V. (1994) Electronic structure of dimanganese(II,III) and dimanganese(III,IV) complexes and dimanganese catalase enzyme: a general EPR spectral simulation approach. *Inorg. Chem.* **33,** 382-387.

Zheng, M., and Dismukes, G. C. (1996) Orbital configuration of the valence electrons, ligand field symmetry, and manganese oxidation states of the photosynthetic water oxidizing complex: analysis of the S_2 state multiline EPR signals. *Inorg. Chem.* **35,** 3307-3319.

Zouni, A., Witt, H. T., Kern, J., Fromme, P., Krauss, N., Saenger, W., and Orth, P. (2001) Crystal structure of photosystem II from Synechococcus elongatus at 3.8 Å resolution. *Nature* **409,** 739-743.